UNIVERSIDADE FEDERAL DO CEARÁ
CENTRO DE TECNOLOGIA
DEPARTAMENTO DE ENGENHARIA DE TELEINFORMÁTICA
PROGRAMA DE PÓS-GRADUAÇÃO EM ENGENHARIA DE TELEINFORMÁTICA
DOUTORADO EM ENGENHARIA DE TELEINFORMÁTICA

YURI VICTOR LIMA DE MELO

DYNAMIC E-ICIC STRATEGIES BASED ON FINANCIAL TECHNIQUES

FORTALEZA

2020

YURI VICTOR LIMA DE MELO

DYNAMIC E-ICIC STRATEGIES BASED ON FINANCIAL TECHNIQUES

Tese apresentada ao Programa de Pós-Graduação em Engenharia de Teleinformática do Centro de Tecnologia da Universidade Federal do Ceará, como requisito parcial à obtenção do título de doutor em Engenharia de Teleinformática. Área de Concentração: Sinais e Sistemas

Orientador: Prof. Dr. Tarcisio Ferreira Maciel

Coorientador: Prof. Dr. Vicente Angelo de Sousa Junior

FORTALEZA

2020

YURI VICTOR LIMA DE MELO

DYNAMIC E-ICIC STRATEGIES BASED ON FINANCIAL TECHNIQUES

> Tese apresentada ao Programa de Pós-Graduação em Engenharia de Teleinformática do Centro de Tecnologia da Universidade Federal do Ceará, como requisito parcial à obtenção do título de doutor em Engenharia de Teleinformática. Área de Concentração: Sinais e Sistemas

Aprovada em:

BANCA EXAMINADORA

―――――――――――――――――――
Prof. Dr. Tarcisio Ferreira Maciel (Orientador)
Universidade Federal do Ceará (UFC)

―――――――――――――――――――
Prof. Dr. Vicente Angelo de Sousa
Junior (Coorientador)
Universidade Federal do Rio Grande do Norte
(UFRN)

―――――――――――――――――――
Prof. Dr. Diego Aguiar Sousa
Instituto Federal do Ceará (IFCE)

―――――――――――――――――――
Prof. Dr. José Cândido Silveira Santos Filho
Universidade Estadual de Campinas
(UNICAMP)

―――――――――――――――――――
Prof. Dr. Yuri Carvalho Barbosa Silva
Universidade Federal do Ceará (UFC)

To my family.

ACKNOWLEDGEMENTS

"Acknowledging the good that you already have
in your life is the foundation for all abundance."
(Eckhart Tolle)

RESUMO

As comunicações móveis estão se preparando para incríveis mudanças da quarta geração (4G) para quinta geração (5G). Nesta nova geração, a interferência co-canal é um dos desafios críticos a serem enfrentados devido à densificação da rede a fim de fornecer altas taxas de dados por meio de várias macrocélulas e células pequenas trabalhando juntas, configurando a chamada Rede Heterogênea. O 3GPP (do inglês, 3rd Generation Partnership Project) especifica o ABS (do inglês, Almost Blank Subframe) como um esquema da Coordenação de Interferência Intercelular aprimorada (do inglês, enhanced Inter-Cell Interference Coordination (e-ICIC)) para mitigar a interferência entre células. O ABS silencia algumas transmissões da macrocélula em subframes selecionados a fim de diminuir a interferência sofrida pelas células pequenas, ortogonalizando transmissões no domínio do tempo. Diante do exposto, esta tese usa técnicas baseadas no conhecimento prático de negociação para propor um algoritmo de tempo real para ABS a fim de melhorar a capacidade do sistema, ou seja, estratégias financeiras são usadas para receber informações do sistema e fornecer um resultado célere para gerenciar o ABS enquanto a Rede Heterogênea está em operação. Em relação às estratégias financeiras, esta tese usa o MAC (do inglês, Moving Average Crossover) e MACD (do inglês, Moving Average Convergence / Divergence) que geram o sinal de negociação, compra ou venda, quando eles identificam tendências de subida ou descida. A propósito, MAC é uma estratégia baseada na subtração de duas RAMAs (do inglês, Right Aligned Moving Averages), enquanto MACD é uma estratégia que considera a volatilidade histórica. Os resultados numéricas do MAC e MACD são comparados com outros algoritmos existentes na literatura por meio de simulações em nível de sistema que têm algumas diretrizes do 3GPP. Os resultados obtidos por estratégias em tempo real de compra e venda têm se mostrado promissores para reconhecer boas oportunidades de alocar ABS, pois mostraram ganhos relativos mínimo e máximo de 12% e 112%, respectivamente. Levando tudo isso em consideração, a viabilidade depende de uma combinação precisa do conhecimento prático financeiro com o comportamento do sistema de comunicação sem fio.

Palavras-chave: Rede Heterogênea. e-ICIC. ABS. Tendência. Negociação. MAC. MACD.

ABSTRACT

Mobile communications are preparing for the incredible changes from 4th Generation (4G) to 5th Generation (5G) in the coming years. In this new generation, co-channel interference is one of the critical challenges to be tackled due to network densification by providing high data rates through several macro and small cells working together, configuring the so-called Heterogeneous Network (HetNet). The 3rd Generation Partnership Project (3GPP) provides the Almost Blank Subframe (ABS) as a scheme of the enhanced Inter-Cell Interference Coordination (e-ICIC) framework to mitigate interference among macro and small cells. The ABS mutes some of the macro cell transmissions in selected subframes to decrease interference to small cells, thus orthogonalizing macro and small cell transmissions in the time-domain. In view of the above, this thesis uses techniques based on trading know-how to propose a real-time algorithm for ABS to improve the system capacity, that is, financial strategies are used to receive system information and provide a quick result to manage ABS while HetNet is in operation. Regarding financial strategies, this thesis uses Moving Average Crossover (MAC) and Moving Average Convergence / Divergence (MACD) that generate the trading signal, buy or sell, when they identify trends upward or downward. By the way, MAC is a strategy based on the subtraction of two Right Aligned Moving Averages (RAMAs), while MACD is a strategy that considers the historical volatility. The numerical results of MAC and MACD are compared with other algorithms in the literature by way of system-level simulations that follow some 3GPP guidelines. The results obtained by real-time strategies to buy and sell have been shown to be promising in recognizing good opportunities to allocate ABS, because they showed minimum and maximum relative gains of 12% and 112%, respectively. All in all, feasibility depends on a precise merge of the financial know-how with the wireless communication system.

Keywords: Heterogeneous network. e-ICIC. ABS. Trend. Trading. MAC. MACD.

LIST OF FIGURES

LIST OF TABLES

LIST OF ABBREVIATIONS AND ACRONYMS

3GPP	3rd Generation Partnership Project
4G	4th Generation
5G	5th Generation
ABS	Almost Blank Subframe
ACK	Acknowledgement
ADX	Average Directional Index
B3	Brasil, Bolsa, Balcão
BS	Base Station
CD	Classical Decomposition
CDMA	Code-Division Multiple Access
CMA	Centered Moving Average
CR	Cognitive Radio
CRS	Common Reference Signal
D2D	Device-to-Device
DEMA	Double Exponential Moving Average
DL	Downlink
DMA	Double Moving Average
DMI	Directional Movement Index
e-ICIC	enhanced Inter-Cell Interference Coordination
ECO	Efficient Coordination of ABS with Coupling Macro Cells
EMA	Exponential Moving Average
eNB	Evolved Node B
FDD	Frequency Division Duplex
GSM	Global System for Mobile Communications
HARQ	Hybrid Automatic Repeat Request
HetNet	Heterogeneous Network
HMA	Hull Moving Average
ICI	Inter-Cell Interference
ICIC	Inter-Cell Interference Coordination
KF	Kalman Filter
LMA	Linear Moving Average

LOS	Line of Sight
LTE	Long Term Evolution
LTE-A	Long Term Evolution-Advanced
LTE-U	Long Term Evolution-Unlicensed
MA	Moving Average
MAC	Moving Average Crossover
MACD	Moving Average Convergence / Divergence
MBSFN	Multimedia Broadcast multicast service Single Frequency Network
MIMO	Multiple-Input Multiple-Output
mmWave	Millimeter Wave
MOM	Momentum
NACK	Negative acknowledgement
NLOS	Non-Line of Sight
OFDM	Orthogonal Frequency Division Multiplexing
P-MA	Price Minus Moving Average Rule
PC	Power Control
PDSCH	Physical Downlink Shared Channel
PF	Proportional Fair
QoS	Quality of Service
RAMA	Right Aligned Moving Average
RAT	Radio Access Technology
RR	Round Robin
RRM	Radio Resource Management
SFR	Strict Frequency Reuse
SINR	Signal to Interference-plus-Noise Ratio
SMA	Simple Moving Average
SoftFR	Soft Frequency Reuse
SSA	Singular Spectrum Analysis
STL	Seasonal Trend Decomposition Procedure Based on Local Regression
SVD	Singular Value Decomposition
TMA	Triangular Moving Average
TVWS	TV White Space

UE	User Equipment
UL	Uplink
UMa	Urban Macro Model
UMi	Urban Micro Model
UMTS	Universal Mobile Telecommunications System
VoD	Video on Demand
VoIP	Voice over IP

LIST OF SYMBOLS

n	Moving average window size
t	Time
Y_t	Time series
ω	Weight data
ψ	Weighting function
κ	Average lag time
ΔY_t	Change time series
ϕ	Value-change weighting function
λ	Decay factor
TS	Trading signal
f_c	Frequency carrier
B	Bandwidth
R	Macro cell radius
p_m	Macro cell transmit power
p_s	Small cell transmit power
r	Small cell radius
E_f	Edge scale factor
G	Pathloss
d_m	Distance between the macro cell and a UE
ρ_{LOS}^m	Probability of LOS in the urban macro
d_s	Distance between the small cell and UE
ρ_{LOS}^p	Probability of LOS in the urban micro
η	Noise power
C	Capacity (bps)
u	Macro UE index
U	Number of macro UE

k	Subframe index
N_{sf}	Number of subframe
γ	SINR
g	Macro channel coefficient
h	Small channel coefficient
o	Small cell index
O	Number of small cell
j	Small cell UE index
J	Number of small cell UE
m	Center small cell UE index
M	Number of center small cell UE
l	Edge small cell UE index
L	Number of edge small cell UE

CONTENTS

1 INTRODUCTION

Currently, the lifestyle of the world population is the driving force for the rapid growth of mobile data traffic that is supported by services such as Video on Demand (VoD) and Voice over IP (VoIP). Such services can be materialized through the megacorporations that hold the majority of mobile data traffic. For instance, YouTube had a worldwide traffic share of 37% in 2019, so it is called the Mobile King (CULLEN; CANTOR, 2019), as shown in Figure 1. Day after day, new applications are developed for smartphones, increasing the demand for mobile traffic. The forecast is for a growth rate of 170% in the global mobile data traffic between 2019 and 2022, reaching approximately 78 exabytes per month by 2022 (CISCO, 2019).

Figure 1 – Global mobile application traffic share.
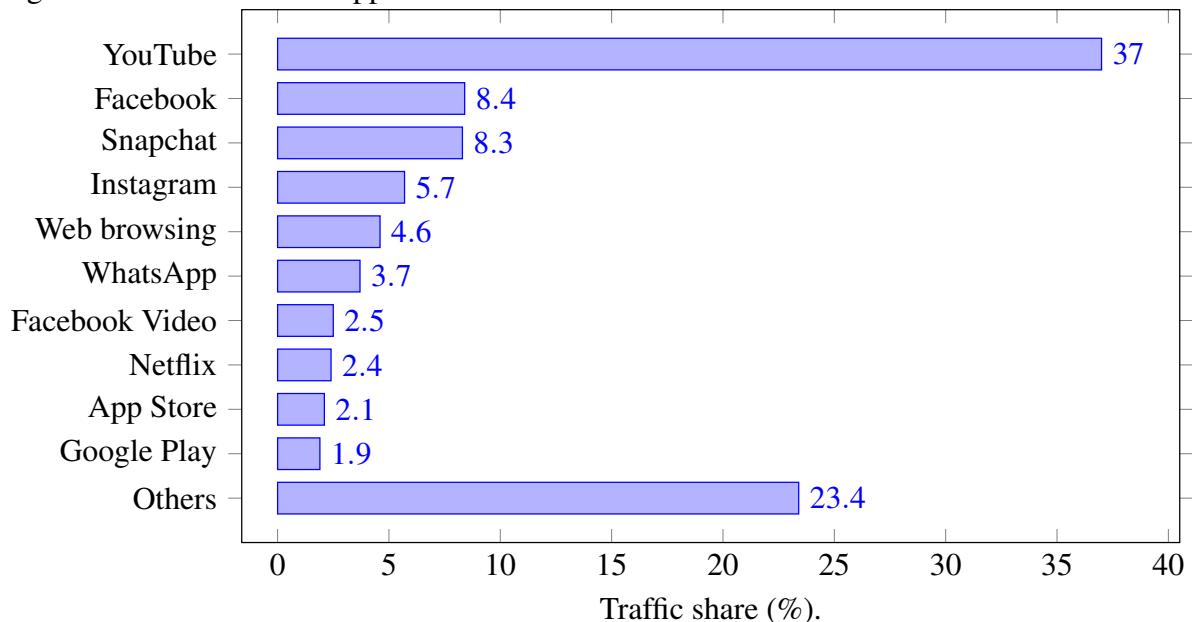
Source: (CISCO, 2019).

In view of the panorama mentioned above, technical requirements are necessary for proper operation of services, such as: low latency, high coverage, and high capacity. With this in mind, one of the 3GPP recommendations to deal with such needs is the use of multi-connectivity across different Radio Access Technologys (RATs) which can be called HetNets (3GPP, 2018c).

HetNets are multiple tiers of networks of different cell sizes (e.g. small cells, femto-cells, pico-cells, and relays) and/or of multiple RATs (e.g. Bluetooth, Wi-Fi, Global System for Mobile Communications (GSM), Universal Mobile Telecommunications System (UMTS), and Long Term Evolution (LTE)) acting together (YEH et al., 2011). Incidentally, the main reasons for HetNets to be able to potentially meet these technical requirements are:

- **Latency:** HetNets can provide low latency due to close proximity between User Equipment (UE) and RATs (CLAUSSEN *et al.*, 2016). In addition, other strategies can be used to decrease latency, and Millimeter Wave (mmWave) is a case in point (YANG *et al.*, 2018);
- **Coverage:** Multiple tiers and RATs can be used to improve coverage, acting in places where the signal of the macro cell is insufficient to provide a good UE connection or where the macro cell is at its capacity limit (YANG *et al.*, 2019). In other words, HetNets cope with the problems of blind spots in coverage (LIANG *et al.*, 2018);
- **Capacity:** The multiples tiers and RATs can simultaneously reuse the available bandwidth, thus increasing network capacity (CLAUSSEN *et al.*, 2016).

Figure 2 – Simplified HetNet scenario.
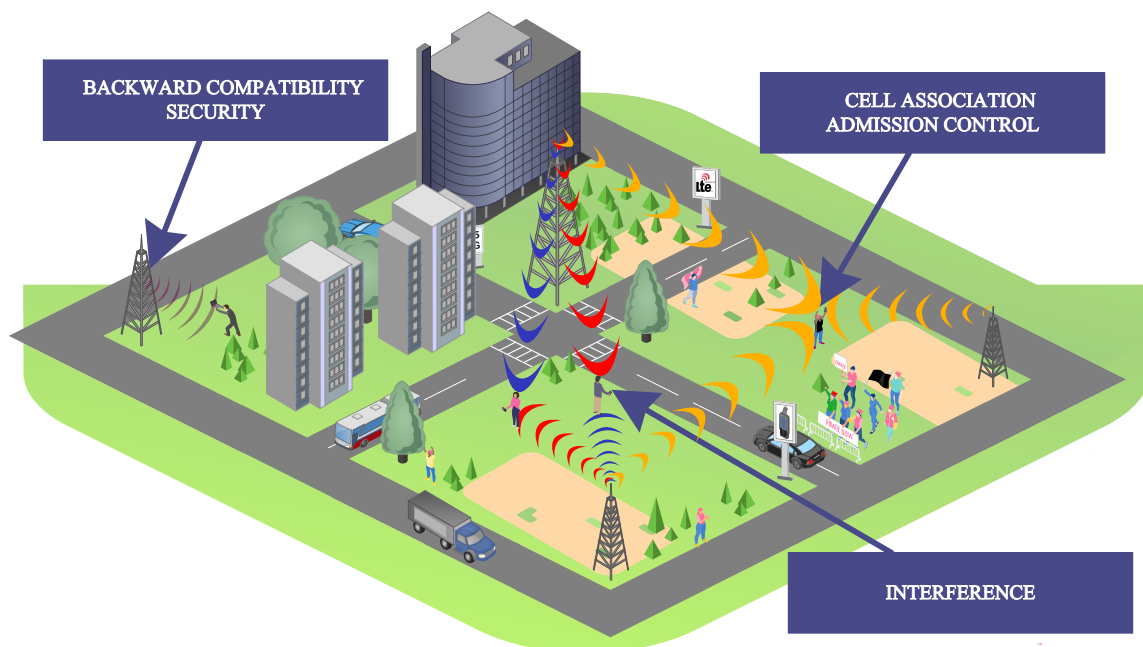
Source: elaborated by the author (2020).

However, for a HetNet to work properly, it is necessary to offer solutions to some challenges, such as cell association, admission control, backward compatibility, security, and interference management, which are illustrated in Figure 2 and described as follows:

- **Cell association:** In a HetNet with dense deployment of the RATs, the number of potential RATs with which a UE can be associated is increased. In this case, it is necessary to design a cell association (RATs assignment to UEs) scheme to prevent UEs from being associated with inappropriate RATs, which could result in reduced capacity, increased interference, inefficient energy consumption, and load imbalance (HOSSAIN *et al.*, 2017; LEE *et al.*,

2020);

- **Admission control:** This mechanism is used to decide whether or not an incoming service request will be accepted according to an admission constraint as well as determining to which RAT among the available ones it will be connected. In other words, it manages the access to network resources to ensure a certain level of Quality of Service (QoS) in a HetNet (OMHENI *et al.*, 2014; HOSSAIN *et al.*, 2015);

- **Backward compatibility:** In order for several RATs and UEs with different technological characteristics to work in concert, it is necessary to solve problems such as: different backhaul systems, essential control signals, and spectrum utilization (GORSHE *et al.*, 2014);

- **Security:** HetNets bring a number of additional security challenges which are physical in nature as well as related to information. Small cells can easily be tampered with and potentially compromised by unauthorized people since these are primarily deployed in public areas. Thus strong security measures need to be placed to prevent misuse of units (ASIF, 2018);

- **Interference:** One of the consequences of using HetNets is the increased interference because of multiple tiers and RATs working in concert, resulting in an environment dominated by interference. Thus, UEs and RATs hold off transmissions, which causes delay and reduces capacity. Besides, it can degrade wireless backhaul[1] and coverage, hampering the expansion of the HetNets (CLAUSSEN *et al.*, 2016).

Concerning interference, it must be clarified that techniques to mitigate it have evolved over time. Originally, 3GPP introduced in Release 8 a technique to decrease Inter-Cell Interference (ICI) called Inter-Cell Interference Coordination (ICIC), which basically uses the frequency domain to reduce the interference created by two or more cells. For example, the frequency resource blocks from multiple neighboring cells are allocated so that they do not overlap in frequency. However, in the midst of the expansion of LTE networks and rapid development of LTE technologies, new network topologies have emerged, and ICIC has also been enhanced.

As a result, the 3GPP introduced in Release 10 a technique called e-ICIC, which exploits the time domain to reduce interference in new topologies composed by multiple tiers and RATs. Particularly, e-ICIC uses subframes that contain only some essential signals with low

---

[1] Technology used to provide backhaul connectivity to a large number of small cells simultaneously (HUQ; RODRIGUEZ, 2016).

power called ABSs and which reduce interference in HetNets due to the orthogonalization of RAT transmissions.

At this time, it is important to provide a quick overview of ABSs before presenting the technical terms and specific features, which will be covered in more depth in Chapter 2. Basically, the use of ABS depends on the definition of three areas (as illustrated in Figure 3). The first area is formed by macro cell coverage, where macro cell users are affected by small cells interference. Regarding the small cells, they are divided into two areas. A center area, that is close to the small cell Base Station (BS) and an area that surrounds the center area, called the edge area. In a situation without any interference management, users located at the edge area suffer not only with the high transmission power from the macro cell (interference), but also with the low reception power from the serving small cell BS. So, they are the main victims of the system.

In order to protect the main victims, the macro cell can mute parts of its transmission, called ABSs, and give the small cell an opportunity to transmit with lower interference. During ABSs, the macro cell transmits only control signaling, such as Common Reference Signal (CRS) (3GPP, 2011). In particular for Long Term Evolution-Advanced (LTE-A), the ABS functionality is defined by the ABS ratio, which is the ratio between the number of ABSs and non-ABSs within a duty-cycle period of 40 ms (3GPP, 2011). This process is also illustrated in Figure 3.

Figure 3 – Illustration of HetNet deployment and temporal behavior of ABS.
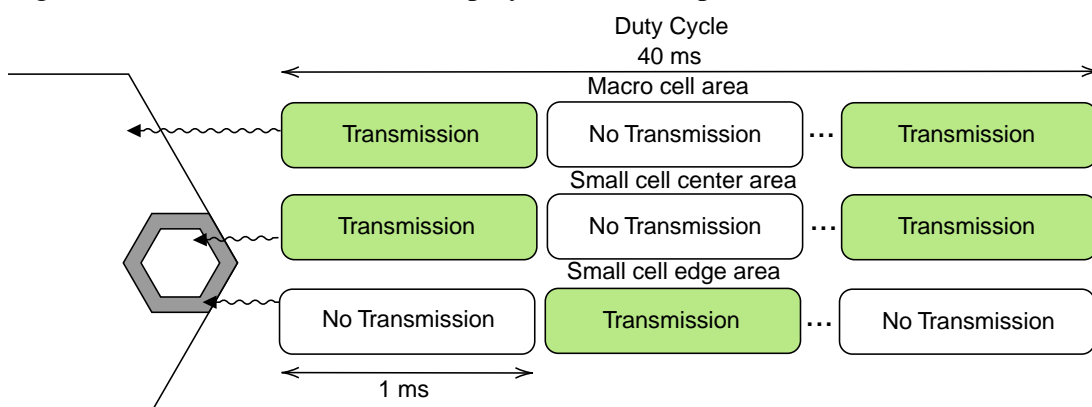
Source: elaborated by the author (2020).

1.1 Motivation and Thesis Scope

In general, the problem addressed in this thesis consists of:

How to recognize a good opportunity to allocate ABSs in a HetNet?

In an effort to answer this question, the scientific community goes on two fronts. The first one sets a fixed ABS ratio; that is, it does not change over time. Therefore, it is categorized as static. The second front is called dynamic; in this case, the ABS ratio changes over time, generally depending on some characteristics of the system such as network load, fairness or capacity.

Concerning the algorithms, they can be classified as real-time (online) or non-real-time (offline). A non-real-time algorithm considers a frozen picture of the system to provide a solution; in other words, the system information cannot change during data processing performed by the algorithm. In contrast, a real-time algorithm can provide a solution without stopping the system. Based on the above considerations, the fixed ABS ratio algorithms are classified as real-time, since they can be easily implemented in the system, whereas dynamic ABS ratio algorithms can be classified as real-time or non-real-time.

In order to treat the ABS problem, in this thesis we formulate three Research Questions (RQs) that serve as guides. Such RQs are listed below:

- **RQ 1:** What is the sensitivity of the system gain to the use of ABSs in different layouts?
- **RQ 2:** Is there any circumstance in which the use of ABSs impairs the system capacity?
- **RQ 3:** Is it feasible to develop a real-time dynamic ABS ratio algorithm using financial strategies?

To discuss the RQs mentioned above, we performed a numerical simulation capable of verifying the performance of different algorithms in twelve HetNet layouts.

In view of the RQs, we elaborate hypotheses for each one of them, as seen below:

- **Hypothesis related to RQ 1:** We hypothesize that the sensitivity of the system gain is directly proportional to the level of interference suffered by the small cell's edge user. For example, in layouts that present a high level of interference to the edge user, the sensitivity of the system gain will be higher than in layouts with a low level.
- **Hypothesis related to RQ 2:** We hypothesize that the algorithms are not able to provide good results or can even harm the system in layouts where the interference of the edge and center small cell users are similar. In this case, the opportunity to allocate ABSs is not only rare but also extremely damaging if used inappropriately.
- **Hypothesis related to RQ 3:** We hypothesize that real-time financial strategies used to buy and sell stocks can be applied to recognize good opportunities to allocate ABSs, thus

improving system's capacity. However, feasibility depends on a precise merge of the financial know-how and the wireless communication system behaviors.

At the end of the thesis, it will be mentioned whether the hypotheses were confirmed or refuted.

1.2 State of the Art and Thesis Contributions

This thesis developed a state of the art around three pillars and their intersections, as illustrated in Figure 4.

Figure 4 – Venn diagram of the state of the art.
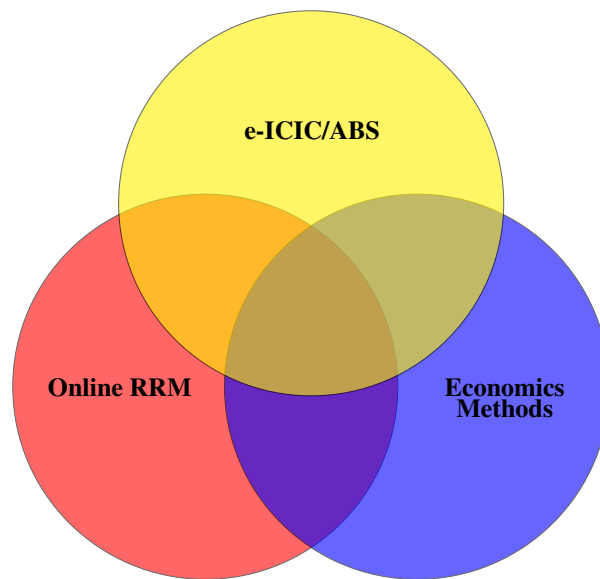
Source: elaborated by the author (2020).

Online Radio Resource Management (RRM) will be the starting point of the state of the art in this thesis. There are several studies in the literature that involve strategies and algorithms for controlling radio resources to make the radio network infrastructure as efficiently as possible. In Muhammad e Mohammed (2010), Lee *et al.* (2015), Melo *et al.* (2015) a dynamic Power Control (PC) was used to set output power levels of BS and UE to Downlink (DL) and Uplink (UL), respectively. This way, it was possible to decrease the system interference levels. Basically, in these articles, the algorithm needs to satisfy a request (e.g., minimum Signal to Interference-plus-Noise Ratio (SINR)); for this, it alters the values of the network resources (e.g., transmit power) based on feedback to converge.

Traditional e-ICIC/ABS researches are the second pillar of the state of the art. Such studies use classical optimization theory, which generally is executed offline, to solve the ABS problem. In Moreira *et al.* (2020), the authors propose ABS optimization based on game theory

that has a modified utility function based on past throughput and data statistics. According to the authors, the game achieved a throughput gain around 51% for cell edge users, when compared to ABS optimization without modified utility functions.

Motivated by the Long Term Evolution-Unlicensed (LTE-U) proposed by Qualcomm, Chatterjee *et al.* (2017) proposed to increase the capacity of existing LTE networks through WiFi. However, this scenario creates several potential challenges for managing the activities of these two different technologies in the same band. Thus, the authors developed an adaptive coexistence scheme between LTE and WiFi by utilizing ABSs, where they allow WiFi to access the spectrum. The scheme is based on quorum, which are subsets of a given set where each pair of subsets has a non-empty intersection.

Mishra *et al.* (2014) proposed to optimize the ABS ratio for a given macro cell user association. According to the authors, ABS ratio is a critical parameter, where a higher ABS ratio benefits small cell users and a lower ABS ratio benefits macro cell users. Thus, the challenge is to determine ABS ratios for two-tier cellular networks consisting of a set of small cells. The authors formulated and solved a joint optimization based on combinatorial optimization using the Hungarian algorithm (JUNGNICKEL, 2007). The results validated that the associations made by the algorithm really increase the system capacity.

Metaheuristic was the artifice used by Daeinabi *et al.* (2015), which proposes a dynamic ABS scheme based on genetic algorithms to find the best ABS ratio to mitigate interference between macro cell and pico cells in a scenario with video streaming traffic. After an exhaustive numerical simulation, the authors concluded that the proposed solution improved the system throughput. Additionally, Jiang *et al.* (2019) used ant colony (DORIGO *et al.*, 2004) optimization to define ABS ratios in HetNets. Simulation results show that the proposed solution improved the total system throughput significantly, when compared with a fixed ABS ratio.

The third pillar of the state of the art is developed around research focused on the economic and financial area. Surely, this research will be useful for a better understanding of economic methods. Kolkova (2018) applied technical analysis indicators to the prediction of prices in the food industry. The analysis was carried out using Moving Average (MA) such as Simple Moving Average (SMA), Exponential Moving Average (EMA), and Double Exponential Moving Average (DEMA) in the time series of raw materials of the food industry such as wheat food, wheat forage, malting barley, milk, apples and potatoes. According to the author, the effectiveness of the MA was confirmed, namely in a short period of time on the monthly data

of prices of basic agricultural commodities. The proposal of Wang e Kim (2018) is to develop a new indicator to compete with MACD, which is the indicator most used by investors. The proposed indicator is called MACD-HVIX because it is based on the change index of historical volatility. It is worth mentioning that historical volatility is a statistical measure of the dispersion of returns for a given market index over a given period of time. In other words, it reflects the panic of the market to a certain extent. According to the authors, the MACD-HIXV achieved a 12% gain in terms of price accuracy, when compared to MACD for the Shanghai stock market.

Henceforth, one can find works based on the union between two pillars. To begin with, the authors Li *et al.* (2013), Maglogiannis *et al.* (2018), Santana *et al.* (2019), Bajracharya *et al.* (2019), and Simsek *et al.* (2012) made the union between online RRM and ABS.

Li *et al.* (2013) focused on developing an e-ICIC strategy that uses Q-learning. Specifically, the system is designed to learn an optimal ABS ratio by repeatedly interacting with the environment. The proposed solution yielded substantial gains in terms of user throughput compared to using a fixed ABS ratio. Additionally, reinforcement learning strategies were employed to automatically set the ABS ratio, providing a way to dynamically track the optimum system operation point over varying offered data traffic (MAGLOGIANNIS *et al.*, 2018; SANTANA *et al.*, 2019; BAJRACHARYA *et al.*, 2019; SIMSEK *et al.*, 2012). It is worth noting that the online solutions mentioned above are complex and very dependent on the training stage of the learning strategies.

Some articles stood out for the development of online RRM algorithms based on economics methods. Bourdena *et al.* (2014) developed a research in which an RRM based on economic transactions was applied to Cognitive Radio (CR) networks. The aim of the proposed RRM is to enable an opportunistic lease of unused TV White Space (TVWS), by secondary systems, respecting constraints and QoS requirements. The proposed RRM estimates a spectrum-unit price and creates a portfolio to act as spectrum broker, which is an entity that orchestrates the available portions of radio spectrum. Numerical simulations showed that the proposed RRM reached good levels of average spectrum utilization.

In the context of a Code-Division Multiple Access (CDMA) scenario with the increasing demand for wireless data services at the time, Saraydar *et al.* (2002) proposed the need for establishing PC algorithms for information sources other than voice. Thus, a UL PC was investigated in wireless data networks using a concept from microeconomics called pricing via a non-cooperative game. Pricing has been used as an effective tool by both economists and

researchers in the field of computer networks because it generates revenue for the system and encourages players to use system resources more efficiently. This way, the pricing function used was a linear function, which was simply the product of a pricing factor and the transmit power. According to the authors, the proposed algorithm attains good transmitting power equilibrium among users near and far from the BS.

A way to increase spectral and energy efficiency can be achieved through Device-to-Device (D2D) communication, which takes advantage of proximity of two close users to communicate directly without passing through the BS. In D2D underlay, no subchannels are dedicated, causing interference among D2D pairs and cellular users. Thus, Yin *et al.* (2015) proposed a decentralized joint power and channel allocation among D2D pairs using pricing and game theory to guarantee the data rate requirements of both cellular users and D2D pairs. Basically, the idea of the proposed algorithm is to monitor the interference incurred by the D2D communications on each subchannel through the BS. If it violates the QoS of any cellular user, the prices on the corresponding subchannels will be raised. The authors attest that the proposed solution provided effectiveness on interference coordination to guarantee the QoS of both the cellular users and the D2D pairs.

Finally, the next articles involve economics methods and e-ICIC. Li *et al.* (2018) decided to merge economic artifacts with e-ICIC to propose a pricing framework with ABS scheme. Within the proposed framework, each small cell BS mutes a portion of the whole frame in time domain and the macro cell BS announces a price for these ABSs and offers a certain amount of revenue to each small cell BS according to the length of its ABS. Thus, the authors created an economic strategic game in which the leader firm moves first and then the follower firms move sequentially (i.e., a Stackelberg game) to optimize the use of ABS. It is worth to highlight that the authors consider one small cell user per small cell BS, which is scheduled for transmission during a whole frame. Additionally, all channels involved are considered to be block-fading, that is, the channel gains remain constant during each frame but may change from one frame to another. Numerical results validated the proposed framework when Stackelberg equilibrium is achieved.

In view of the above, this thesis contributes through the development of a method that uses mathematical tools of **financial area** as an alternative solution for **online RRM** strategies in **e-ICIC**. It is worth emphasizing that no studies with such characteristics were found in the literature, as illustrated in Figure 5.

Figure 5 – Venn diagram of the state of the art with references.

e-ICIC/ABS
Moreira *et al.* (2020)
Jiang *et al.* (2019)
Huang *et al.* (2018)
Chatterjee *et al.* (2017)
Daeinabi *et al.* (2015)
Mishra *et al.* (2014)

Santana *et al.* (2019)
Bajracharya *et al.* (2019)
Maglogiannis *et al.* (2018)
Li *et al.* (2013)
Simsek *et al.* (2012)

Li *et al.* (2018)

Online RRM
Melo *et al.* (2015)
Lee *et al.* (2015)
Muhammad e Mohammed (2010)

Yin *et al.* (2015)
Bourdena *et al.* (2014)
Saraydar *et al.* (2002)

Economics Methods
Kolkova (2018)
Wang e Kim (2018)
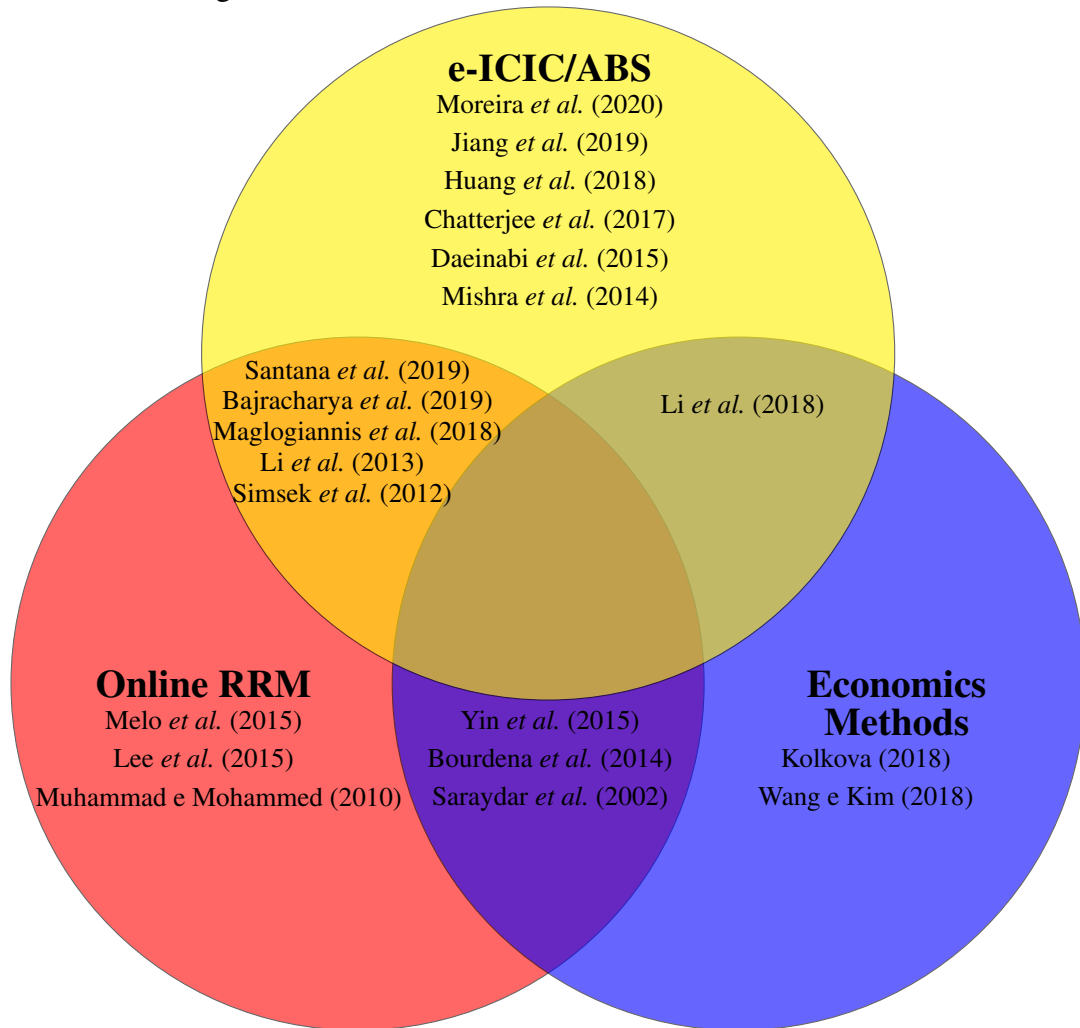
Source: elaborated by the author (2020).

The main contributions of this thesis can be summarized as follows:

- Propose a mathematical formulation for the ABS problem based on finance models;

- Propose a real-time solution that considers this finance-based formulation;

- Provide a real-time solution that combines low complexity and practical parameter configuration.

The main works that were developed during the doctoral course are listed below:

- Journal Papers

  - **Yuri Victor L. de Melo**, Vicente A. de Sousa Junior, and Tarcisio F. Maciel, *MACD e-ICIC: a Dynamic LTE Interference Coordination Method based on Trend and Trading Know-how*, in Telecommunication Systems, 2020.

  - **Yuri Victor L. de Melo**, Vicente A. de Sousa Junior, and Tarcisio F. Maciel, *Dynamic e-ICIC using Moving Average Crossover*, in Journal of Communication and

Information Systems, vol. 34, pp. 87- 91, 2019.

- Conference Papers

  – **Yuri Victor L. de Melo**, Tarcisio F. Maciel, and Kadmo T. H. L. Ponte, *Bernoulli Distribution Effects on ABS Pattern in Heterogeneous Networks*, in XXXVI Simpósio Brasileiro de Telecomunicações e Processamento de Sinais SBrT 2018, pp. 291- 295, 2018.

  – Kadmo T. H. L. Ponte, **Yuri Victor L. de Melo**, and Tarcisio F. Maciel, *Generation of Optimal Almost Blank Frames using Genetic Algorithm*, in XXXV Simpósio Brasileiro de Telecomunicações e Processamento de Sinais SBrT 2017, pp. 22- 26, 2017.

- Dissertation (using the tool developed by this thesis)

  – Kádmo Thadeu Hardy Lima Ponte, *Genetic Algorithms and Particle Swarm Optimization Applied to Almost Blank Subframe Allocation in Heterogeneous Networks*, in Federal University of Ceará, 2018.

- Monograph (advised by the PhD candidate)

  – Heberlano Liberato de Carvalho Barrozo, *Redução de Interferência em Redes Heterogêneas utilizando a técnica Almost Blank Subframes*, in Federal University of Ceará, 2019.

  – Carolina Magalhães de Sousa, *Otimização da Técnica Almost Blank Subframes para Redes Heterogêneas utilizando Metaheurísticas*, in Federal University of Ceará, 2018.

1.3 Thesis Outline

This thesis is divided into five chapters, including this introductory chapter. A brief description of the four remaining chapters is presented as follows.

Chapter 2: It provides a theoretical basis for the methods developed in this thesis. It introduces the challenge of interference management with the advancement of new communications standards, and the importance of ABS in HetNet systems. Next, it presents time series, MA and the main trading rules used in this thesis, known as MAC and MACD.

Chapter 3: It presents the integration of the ABS problem with MAC. Afterwards, MAC parametrization and performance are presented and discussed for twelve layouts. In addition, it delineates the system model and the main measures.

Chapter 4: It addresses the ABS problem with MACD. Through a detailed variation of the MACD parameters, the best performances were collected and compared with the MAC.

Chapter 5: It concludes the thesis by summarizing the obtained results and answering the questions formulated in Chapter 2.

2 THEORETICAL REVIEW

This chapter addresses the main subjects that compose the theoretical basis of this thesis. Initially, it presents the evolution of the interference management challenges for the techniques shown by 3GPP. Next, it shows the vocabularies, concepts, mathematical formulations, peculiarities, advantages, and disadvantages of economic methods used in the financial market. The importance of the time series is presented, which can be used to recognize and explain a temporal pattern of a variable, even when the variable does not appear to vary significantly over time. Then, it presents some strategies to extract trend, putting a focus on MA, which are used to develop the proposed trading rules. Finally, the pullback concept is defined, which basically consists of a loss caused by a move against the trend.

2.1 3GPP Evolution

In order to offer a high-quality of experience for the user's demand, 3GPP introduced the LTE, which uses unity frequency reuse to improve the system capacity (HOLMA; TOSKALA, 2012; DAHLMAN *et al.*, 2013). However, this frequency reuse leads to high ICI because the interference level of cell edge UEs increases sharply when adjacent cells use the same channel (XIAO *et al.*, 2012). Figure 6 illustrates two cells that use the same frequency channel, and each cell has a UE that uses the same frequency resource. So, if the two UEs are located at the edge of their cells, a substantial interference is caused because they are far from the cell of interest and close to the interfering one.

Figure 6 – DL ICI between two macro cells in a homogeneous network.
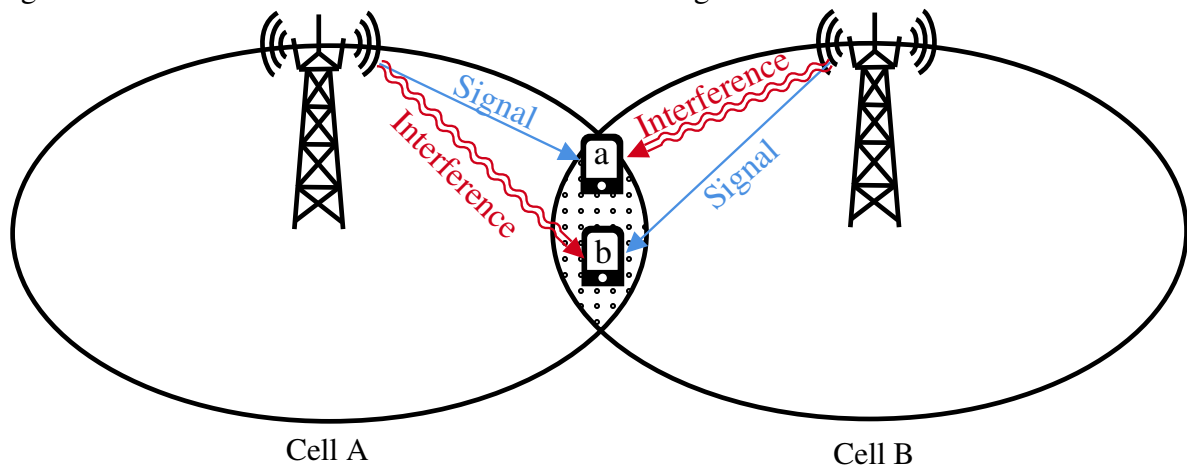
Source: elaborated by the author (2020).

In this context, 3GPP defines specific features in Release 8 to deal with interference problems at the edge of a cell. For this reason, ICIC emerged as a set of techniques responsible for managing interference such as Strict Frequency Reuse (SFR) and Soft Frequency Reuse (SoftFR) (DöTTLING *et al.*, 2009).

In SFR, the cell center users share a common sub-band of frequencies, while the bandwidth of cell edge users is partitioned based on a different one. It is worth noting that SFR does not allow that interior users share any spectrum with edge users, which reduces interference for both center and cell edge users (GHOSH *et al.*, 2010), as illustrated in Figure 7a. SoftFR employs a similar partitioning strategy, where the exception is that center users can share the same bandwidth of edge users in adjacent cells, as illustrated in Figure 7b. As a result, macro cell transmits lower power levels to center users than the edge users in order to reduce interference to neighboring cells (GHOSH *et al.*, 2010).

Figure 7 – ICIC specified in Release 8.
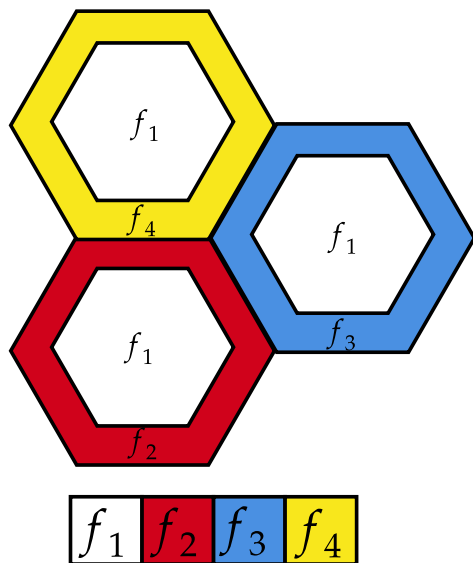
(a) Strict Frequency Reuse.   (b) Soft Frequency Reuse.
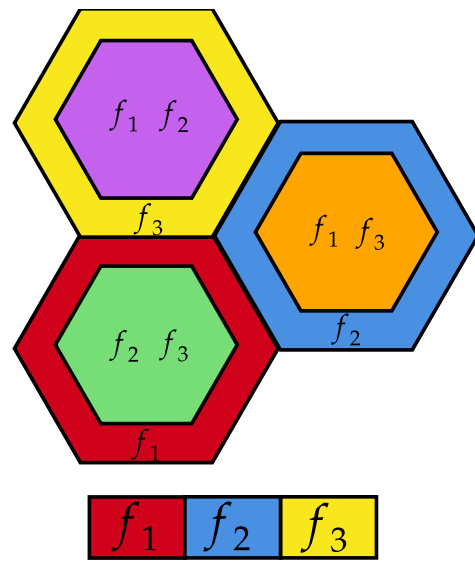
Source: elaborated by the author (2020).

In the meantime, there has been a massive development of new small cells as a means to increase system coverage and meet the growing demand for mobile traffic without adding extra frequency spectrum, in other words, the system became densified (DHILLON *et al.*, 2012). The densification can be performed through HetNets, which consist of multiple tiers (or layers) of networks of different cell sizes/footprints and/or of multiple radio access technologies (YEH *et al.*, 2011). For instance, one LTE-A macro cell overlaying another LTE-A small cell is a good example of HetNet (HU, 2013).

It is important to highlight that HetNets will lead to a network severely limited by interference due to the transmission of different users over the same frequency band limiting capacity. In view of current discussions, the 3GPP in Release 10 proposes e-ICIC to reduce the interference caused by network densification in the LTE-A system (SAUTER, 2017).

2.2 Enhanced Inter-Cell Interference Coordination

Concerning Release 10, the LTE-A exploits the time-domain to manage interference through ABS, where a macro Evolved Node B (eNB) stops data transmission to protect the UEs at the borders of small cells. Figure 8 illustrates HetNet deployment, identifying three important areas: macro cell area, small cell center area, and small cell edge area. It also illustrates the temporal behavior of ABS (exclusive transmission to UE at small cell's edge) and non-ABS (simultaneous transmission to UE at macro cell and small cell's center areas) situations. In fact,

Figure 8 – ABS operation mode when small cell is deployed under the macro cell coverage.
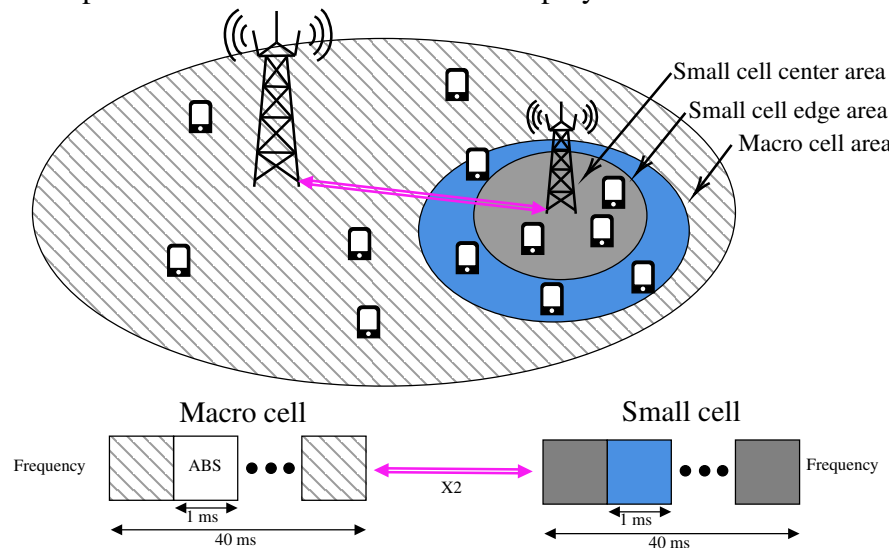
Source: elaborated by the author (2020).

the macro cell does not transmit the Physical Downlink Shared Channel (PDSCH)[1], but for compatibility with previous versions, specific signals must be transmitted in all subframes, even if silenced.

It is important to mention that in Frequency Division Duplex (FDD), 3GPP defines ABS in a bitmap[2] format of 40 subframes lasting for 40 ms, which is the least common multiplier

---

[1] This is the downlink transport channel which carries user data between the mobile device and the eNB.
[2] In computing, bitmap is an array data structure that compactly stores bits. It is also called as bit string, bit array, bit vector or bitmap index.

of Hybrid Automatic Repeat Request (HARQ)[3] with periodicity of 8 ms and Multimedia Broadcast multicast service Single Frequency Network (MBSFN)[4] with a period of 10 ms (3GPP, 2018).

The progress of e-ICIC in the scientific community has led to defining some aspects, such as **ABS Ratio**, **ABS Pattern**, **ABS Information**, and **ABS Status**. Regarding the **ABS Ratio**, it is the number of ABSs during the macro cell duty-cycle time (40 ms) (CLAUSSEN *et al.*, 2016). For instance, an ABS Ratio equal to 0.4 means that the macro cell gates off 40% of duty-cycle time (40 ms) and transmits in the rest (simultaneously with small cell's center area). The **ABS Pattern** is a bitmap, for which the value 1 indicates the subframe that has been designated as protected from ICI by the macro eNB, and available to serve this purpose for DL scheduling in the small eNB edge area, while the value 0 is used to indicate that macro eNB and small eNB center are transmitting (3GPP, 2018).

With regard to the **ABS Information**, it groups information such as ABS Pattern, number of antenna ports for cell-specific reference signals and DL channel quality measurements. This information is conveyed in messages for global procedures called **LOAD INFORMA-TION** (3GPP, 2018). The **ABS Status** is used to aid the macro eNB to evaluate the need for modification of the ABS pattern, in order to assess whether the small eNB needs more or less ABSs (3GPP, 2018). The macro eNB requests **ABS Status** from the small eNB via a **RESOURCE STATUS REQUEST**, and the small eNB replies via a **RESOURCE STATUS UPDATE** (3GPP, 2018).

Figure 9 presents all the concepts mentioned above in a logical way, that is, it illustrates the coordination through the X2 interface between macro eNB and small eNB. In general, the ABS X2 coordination starts with the small eNB requesting **ABS Information** from the macro eNB by sending invoke. The macro eNB provides information about which subframes are configured as ABSs within the **LOAD INFORMATION** message. Subsequently, the macro eNB requests **ABS Status** via **RESOURCE STATUS REQUEST** to evaluate the need for modification of the ABS and small eNB replies via **RESOURCE STATUS UPDATE**. Finally, macro eNB defines ABS or non-ABS based on the **ABS Status** via **LOAD INFORMATION**.

---

[3] It is a stop-and-wait protocol, where the transmitter sends a packet and waits until it receives an Acknowledgement (ACK) or Negative acknowledgement (NACK) from the destination (RUMNEY, 2013).

[4] It is a transmission mode which exploits Orthogonal Frequency Division Multiplexing (OFDM) radio interface to send multicast or broadcast data as a multicell transmission over a synchronized single-frequency network (LESCUYER, 2008).

Figure 9 – ABS X2 coordination.
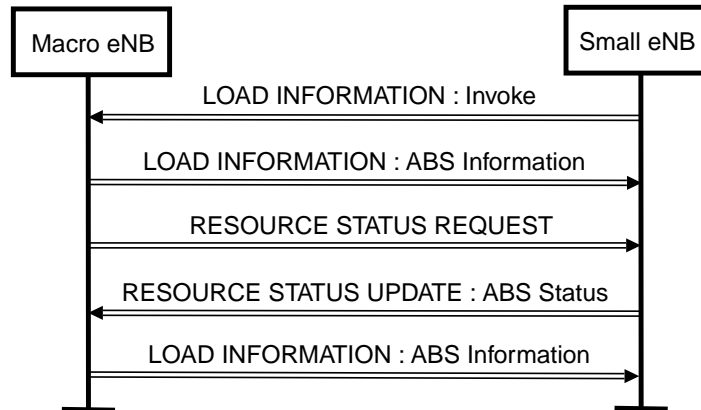
2.3 Time Series

Chatfield (1975) describes a time series as "... a collection of observations made sequentially in time". Many years after this publication, time series are still present in several areas of knowledge. In economics, time series can arise as prices on successive days, incomes in consecutive months, and yearly sales figures (GHYSELS, 2018). For social sciences, time series can be created from the observations of monthly violent crime rates, yearly early pregnancy, or political corruption (BOX-STEFFENSMEIER *et al.*, 2015). In biological sciences, the electrical activity of the heart at millisecond or electroencephalogram at seconds intervals are examples of time series (SAALASTI, 2003). So, it shall consist of data collected regularly over time, for example, millisecond, second, minute, hour, day, month, year, and so on (SHIN, 2017).

A time series consists of at least three essential components known as the trend, seasonality, and irregular fluctuations. First of all, the irregular fluctuations are composed of a sequence of uncorrelated random values that have zero mean and constant variance (CRYER, 2009). Secondly, the seasonality can be interpreted as a change of time series at a fixed period or the repeating short-term cycle in the series (YAFFEE; MCGEE, 2000). Last but not least, trend is defined by Chatfield (1975) as "long term change in the mean", in other words, a direction in which the dependent variable is developing or changing over a time interval.

It is worth noting that among the three components, the trend draws attention because it contains information about global change, which can be used to recognize or predict oscillations useful for decision making (ALEXANDROV, 2009).

Concerning the trend extraction, there are countless methods in the literature. To start with the classics, they separate the time series into subpatterns that identify each compo-

nent (HYNDMAN; ATHANASOPOULOS, 2018). Specifically, the Classical Decomposition (CD) method originated in the 1920s, where the trend is extracted using a Centered Moving Average (CMA) (HYNDMAN; ATHANASOPOULOS, 2018). On the other hand, the Seasonal Trend Decomposition Procedure Based on Local Regression (STL) is an enhancement of CD in which the trend is estimated and refined by two loops, one nested within the other. In the loops several procedures are performed, such as cycle-subseries smoothing, low-pass filtering of smoothed cycle-subseries, detrending of smoothed cycle-subseries, and post-smoothing of the seasonal (CLEVELAND *et al.*, 1990). In general, the CD and STL are useful for a better understanding of the behavior of the series, which facilitates improved accuracy in forecasting. However, they are not recommended to real-time problems because there are better methods such as Kalman Filter (KF) and Singular Spectrum Analysis (SSA) (HYNDMAN; ATHANA-SOPOULOS, 2018).

The KF was proposed by KALMAN (1960) and used to estimate the positioning on the Apollo 11 mission. Basically, the KF combines the measurement and statistical noise to find optimal estimates (NIELSEN, 2019). The SSA is a method originated between the late 70s and early 80s, mainly in the area of dynamical systems (ALEXANDROV *et al.*, 2008), which consists of two parts: decomposition and reconstruction. With regard to decomposition, it sets the window length and creates a matrix with portions of the time series on which it performs the Singular Value Decomposition (SVD). Then, the reconstruction extracts the trend from the Hankelization (i.e, averaging through anti-diagonals) of the matrix created by selected SVD components (ALEXANDROV *et al.*, 2008). The disadvantage of KF and SSA is their high complexity and computational cost (NIELSEN, 2019; ALEXANDROV *et al.*, 2008).

The trend extraction methods, so far, have disadvantages such as not being suitable for real-time problems or presenting high computational costs. With this in mind, this thesis uses MA to extract trend because it can be used in real-time problems and has low complexity (MAKRIDAKIS; WHEELWRIGHT, 1997). It is worth noting that the accuracy of MA depends on adequate parameterization. In this thesis, parameter sweeping was adopted for this purpose. Lastly, it should be pointed out that the next sections will delve deeper into MA.

2.4 Moving Average

MA[5] is a very popular trend extraction method that has been used in several areas of knowledge. For example, it is used in civil engineering to filter random variables such as vehicle speed and path location to reduce the damage on a steel truss bridge (CASPEELE *et al.*, 2018). Moreover, it is used to predict traffic flow, providing an improvement in transportation planning (LV *et al.*, 2015).

Medicine uses MA to provide noise reduction in image processing (BOVIK, 2009) and smoothed curves of neural signature of brain-computer interfaces (LOPES-DIAS *et al.*, 2019). Besides that, it is used in real-time processes to monitor the quality assurance framework in the clinical laboratory (DURANT *et al.*, 2017) and to improve the synchronization between neural activity and changes in the cutaneous peripheral microcirculation (HODGES *et al.*, 2018). Finally, the biologists use MA to estimate evapotranspiration and for improving numerical weather forecasting (ACTON, 2013).

After this brief introduction about MA popularization, the next subsections will address the mathematical formulation, advantages, and disadvantages of this versatile method.

2.4.1 Centered Moving Average

There are several types of MAs in the literature, which have been developed over time. For this reason, we believe that the appropriate starting point for better assimilation of this mathematical tool is CMA.

In general, MA adopts a data of a length n commonly referred to as a window that moves through time in order to extract trends. Concerning CMA, it has a window with a center and two halves of size k; therefore, $n = 2k + 1$. This way, CMA at time t of the time series Y_t is written as (ZAKAMULIN, 2017):

$$CMA_t(n) = \frac{Y_{t-k} + \cdots + Y_t + \cdots + Y_{t+k}}{n} = \frac{1}{n} \sum_{i=-k}^{k} Y_{t+i}. \tag{2.1}$$

With the purpose of illustrating the CMA, fictitious data were used in Figures 10a and 10b. Both figures are composed of three curves:

1. The upward and downward trend;
2. The trend with disturbance;
3. The $CMA_t(n)$ using $n = 11$ or $n = 41$.

Figure 10 – CMA response for different window sizes (n).

(a) CMA with $n = 11$.   (b) CMA with $n = 41$.
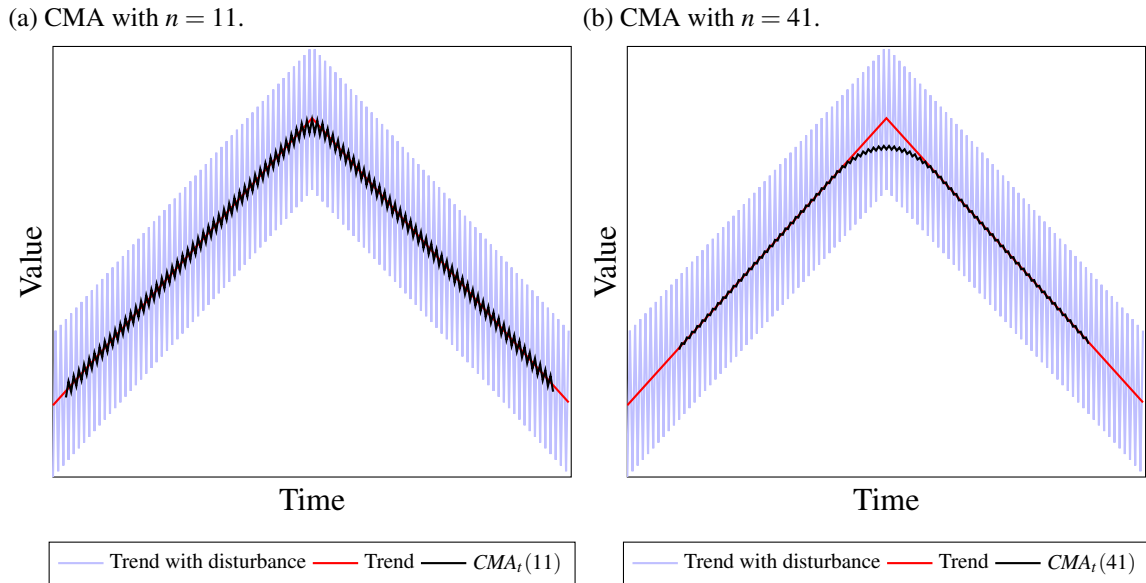
Source: adapted from (ZAKAMULIN, 2017).

It is noted that $CMA_t(11)$ and $CMA_t(41)$ detect a trend, however, $CMA_t(41)$ compared to $CMA_t(11)$ provides a curve closer to the trend; on the other hand, $CMA_t(11)$ computes the first value before $CMA_t(41)$. As a rule, CMA with a larger window size provides a smoother curve. By the way, it was mentioned in Section 2.3 that CMA is not suitable for real-time problems. Now, this statement makes more sense because it can be observed that CMA depends on future data Y_{t+k} (ZAKAMULIN, 2017).

2.4.2 Right Aligned Moving Average

Differently from the CMA, the RAMA is suitable for real-time problems because it does not depend on future data. This way, RAMA at time t of the time series Y_t is written as (ZAKAMULIN, 2017):

$$RAMA_t(n) = \frac{\omega_0 Y_t + \omega_1 Y_{t-1} + \omega_2 Y_{t-2} + \cdots + \omega_{n-1} Y_{t-n+1}}{\omega_0 + \omega_1 + \omega_2 + \cdots + \omega_{n-1}} = \frac{\sum\limits_{i=0}^{n-1} \omega_i Y_{t-i}}{\sum\limits_{i=0}^{n-1} \omega_i}, \tag{2.2}$$

where ω_i is a weight that distinguishes the importance of one data against another. Thus, the RAMA value over time is computed using the current data (Y_t) with weight (ω_0) and lagged data (Y_{t-i}) with weights (ω_i), $i \in [1, n-1]$.

Observing the RAMA equation, it is possible to group useful terms for comparison

---

[5]   MA, also called rolling average, rolling mean, or running average.

between different types of RAMAs. For instance:

$$\psi_i = \frac{\omega_i}{\sum_{j=0}^{n-1} \omega_j}, \tag{2.3}$$

is defined as weighting function, and each type of RAMA has its own distinct weighting function. Basically, it measures the influence of the weight of a sample in relation to the entire window (ZAKAMULIN, 2017).

In addition to ψ_i, the lag time can be used to compare RAMAs. The general equation shows that each weight acts at a different time instant; for example, ω_1 and ω_3 have a lag time $t-1$ and $t-3$, respectively. Thus, κ was defined as a single lag time, which behaves as if all the lag time of RAMA were concentrated on it. In other words, it is the ratio of the weighted sum of delays of individual observations by the sum of all weights (ZAKAMULIN, 2017). This way:

$$\kappa = \frac{\sum_{i=1}^{n-1} \omega_i\, i}{\sum_{i=0}^{n-1} \omega_i} = \sum_{i=1}^{n-1} \psi_i\, i. \tag{2.4}$$

In general, an alternative representation of (2.2) is used for dynamic processes in time. Basically, it considers:

$$\Delta Y_{t-i} = Y_{t-i+1} - Y_{t-i}, \tag{2.5}$$

which is the change in the time series over the interval; in other words, it can be interpreted as the sizes of the steps taken (forward or backward) over the interval, as illustrated in Figure 11.

Figure 11 – Dynamics of changes in time series over the interval from $t-i$ to t.
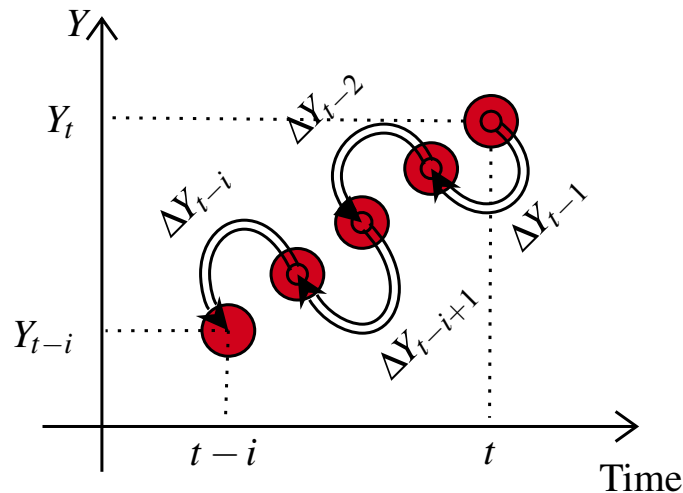
Source: elaborated by the author (2020).

In doing so, it is possible to write (ZAKAMULIN, 2017):

$$Y_{t-i} = Y_t - \Delta Y_{t-1} - \Delta Y_{t-2} - \Delta Y_{t-i+1} - \Delta Y_{t-i} = Y_t - \sum_{j=1}^{i} \Delta Y_{t-j}, \quad i \geq 1, \tag{2.6}$$

and rewrite (2.2) as:

$$
\begin{aligned}
RAMA_t(n) &= \frac{\sum_{i=0}^{n-1} \omega_i Y_{t-i}}{\sum_{i=0}^{n-1} \omega_i} = \frac{\sum_{i=0}^{n-1} \omega_i \left(Y_t - \sum_{j=1}^{i} \Delta Y_{t-j} \right)}{\sum_{i=0}^{n-1} \omega_i} = \frac{\omega_0 Y_t + \sum_{i=1}^{n-1} \omega_i \left(Y_t - \sum_{j=1}^{i} \Delta Y_{t-j} \right)}{\sum_{i=0}^{n-1} \omega_i} \\[2em]
&= \frac{\omega_0 Y_t + \sum_{i=1}^{n-1} \omega_i Y_t - \sum_{i=1}^{n-1} \omega_i \sum_{j=1}^{i} \Delta Y_{t-j}}{\sum_{i=0}^{n-1} \omega_i} = \frac{\sum_{i=0}^{n-1} \omega_i Y_t - \sum_{i=1}^{n-1} \omega_i \sum_{j=1}^{i} \Delta Y_{t-j}}{\sum_{i=0}^{n-1} \omega_i} \\[2em]
&= Y_t - \frac{\sum_{i=1}^{n-1} \omega_i \sum_{j=1}^{i} \Delta Y_{t-j}}{\sum_{i=0}^{n-1} \omega_i} = Y_t - \frac{\sum_{j=1}^{n-1} \left(\sum_{i=j}^{n-1} \omega_i \right) \Delta Y_{t-j}}{\sum_{i=0}^{n-1} \omega_i}.
\end{aligned}
\tag{2.7}
$$

In this alternative representation, it is noted that RAMA is equal to the current value minus the weighted sum of the previous time-series changes. Indeed, the weighted sum is called a value-change weighting function:

$$\phi_j = \frac{\sum_{i=j}^{n-1} \omega_j}{\sum_{i=0}^{n-1} \omega_i}, \tag{2.8}$$

that is, RAMA can be written as:

$$RAMA_t(n) = Y_t - \sum_{j=1}^{n-1} \phi_j \Delta Y_{t-j}. \tag{2.9}$$

Up to now, only the generic formula of RAMA was presented in this thesis, but there are several types of RAMA in the literature, such as Linear Moving Average (LMA), Triangular Moving Average (TMA), Double Moving Average (DMA), DEMA, Hull Moving Average (HMA), among others. For this reason, this thesis is limited to SMA and EMA because they are widely used in several areas of knowledge and easy to implement in real-time problems.

2.4.2.1 Simple Moving Average

RAMA is classified as SMA when all weights (ω_i) are equal to one. Therefore (ZA-KAMULIN, 2017):

$$SMA_t(n) = \frac{Y_t + Y_{t-1} + Y_{t-2} + \cdots + Y_{t-n+1}}{n} = \frac{\sum\limits_{i=0}^{n-1} Y_{t-i}}{n}, \qquad (2.10)$$

having $\psi_i = \frac{1}{n} \; \forall i \in [0, n-1]$ and $\kappa = \frac{n-1}{2}$.

With a view to illustrate SMA, Figure 12 presents SMA with window size equal to 11 and 41. It is noted that the turning point[6] of $SMA_t(41)$ occurs later than $SMA_t(11)$ because they have $k = 21$ and $k = 5$, respectively. However, $SMA_t(41)$ has a greater smoothness than $SMA_t(11)$. So, proper configuration between smoothness and lag is essential for an efficient strategy of identifying turning points in real-time problems to avoid fake turning points (ZAKAMULIN, 2017).

Figure 12 – Right aligned moving average response for different window sizes (n).
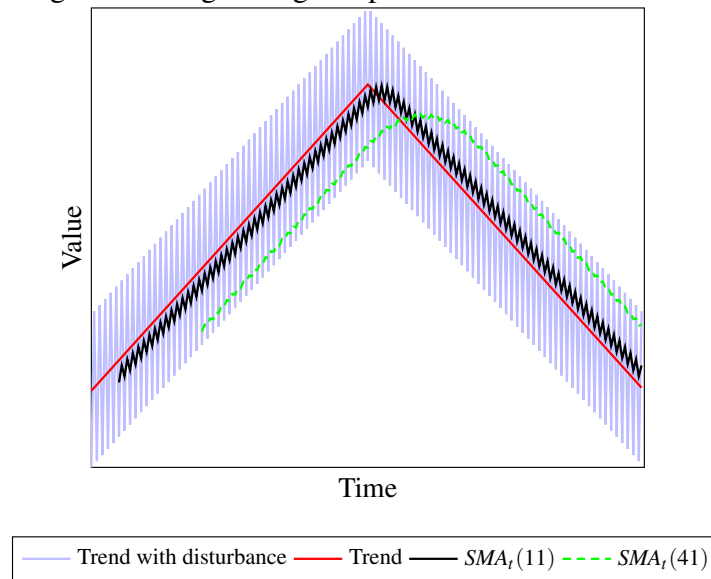
Source: adapted from (ZAKAMULIN, 2017).

Figure 13 shows the behavior of ψ_i and ϕ_j for different lags of $SMA_t(11)$. The ψ_i values inform that the influence of each sample is equal in the window because $\psi_i = 1/11 \; \forall i \in [0, n-1]$. In contrast, the value-change weighting function ϕ_j shows that the most recent price changes have a higher weight, in this case the sequence of weights ϕ_j is decreasing with increasing j. This way, ψ_i shows the contribution of each lag to the value of MA, while ϕ_j represents the dynamic properties of MA.

---

[6] A time instant when a situation starts to change.

Figure 13 – Weighting function (ψ) and value-change weighting function (ϕ) of $SMA_t(11)$.

(a) Behavior of ψ as function of lag i.

(b) Behavior of ϕ as function of lag j.
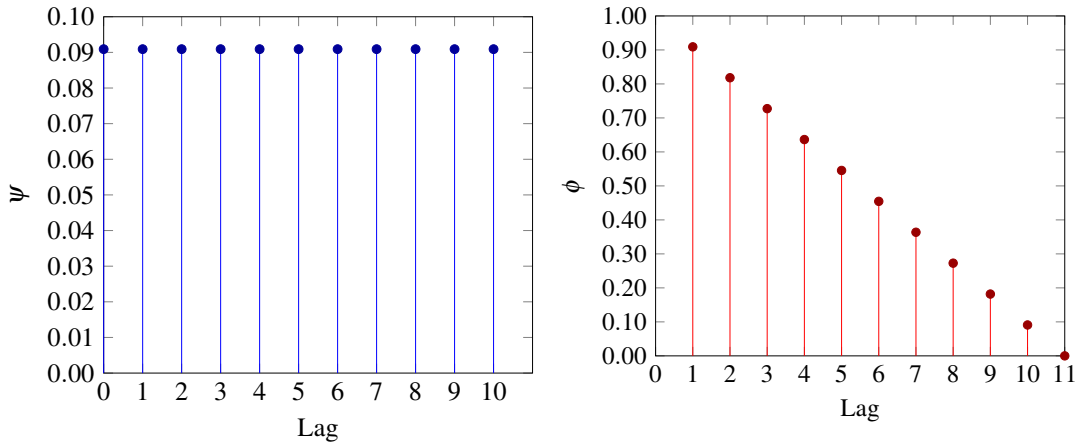
Source: adapted from (ZAKAMULIN, 2017).

2.4.2.2 Exponential Moving Average

The EMA is a versatile RAMA because it allows to increase or decrease the weight of recent data through the decay factor, that is, $\omega_i = \lambda^i$. Thus, EMA is written as (ZAKAMULIN, 2017):

$$EMA_t(\lambda, n) = \frac{\lambda^0 Y_t + \lambda^1 Y_{t-1} + \lambda^2 Y_{t-2} + \cdots + \lambda^{n-1} Y_{t-n+1}}{\lambda^0 + \lambda^1 + \lambda^2 + \cdots + \lambda^{n-1}} = \frac{\sum_{i=0}^{n-1} \lambda^i Y_{t-i}}{\sum_{i=0}^{n-1} \lambda^i}, \tag{2.11}$$

where λ ($0 < \lambda < 1$). When λ approaches one, the value of EMA converges to SMA, $\lim_{\lambda \to 1} EMA_t(\lambda, n) = SMA_t(n)$. Otherwise, if λ approximates zero, the value of EMA becomes the current value of the time series, $\lim_{\lambda \to 0} EMA_t(\lambda, n) = Y_t$. In addition, $\kappa = \frac{\lambda - \lambda^n}{(1-\lambda)(1-\lambda^n)} - \frac{(n-1)\lambda^n}{1-\lambda^n}$.

Concerning $EMA_t(\lambda, n)$ and κ, it can be noticed that there exists a dependence on λ and n, which allows many combinations with similar results. In order to standardize and reduce these combinations, the EMA and κ can be rewritten as (ZAKAMULIN, 2017):

$$EMA_t(\lambda) = \frac{\lambda^0 Y_t + \lambda^1 Y_{t-1} + \lambda^2 Y_{t-2} + \cdots}{\lambda^0 + \lambda^1 + \lambda^2 + \cdots} = \frac{\sum_{i=0}^{\infty} \lambda^i Y_{t-i}}{\sum_{i=0}^{\infty} \lambda^i} = \frac{\sum_{i=0}^{\infty} \lambda^i Y_{t-i}}{(1-\lambda)^{-1}} = (1-\lambda)\sum_{i=0}^{\infty} \lambda^i Y_{t-i},$$

$$\tag{2.12}$$

and

$$\kappa = \lim_{n \to \infty} \left(\frac{\lambda - \lambda^n}{(1-\lambda)(1-\lambda^n)} - \frac{(n-1)\lambda^n}{1-\lambda^n} \right) = \frac{\lambda}{(1-\lambda)}. \tag{2.13}$$

As a rule, κ of SMA[7] is used as reference to other RAMAs. As a result, λ is obtained from the equality with SMA, that is:

$$\lambda = \frac{n-1}{n+1}. \tag{2.14}$$

At last, in practice, $EMA_t(n)$ can be expressed as (ZAKAMULIN, 2017):

$$EMA_t(n) = (1-\lambda) \sum_{i=0}^{\infty} \lambda^i Y_{t-i}, \quad \lambda = \frac{n-1}{n+1}. \tag{2.15}$$

Figure 14 – Weighting function (ψ) and value-change weighting function (ϕ) of $EMA_t(11)$.

(a) Behavior of ψ as function of lag i. (b) Behavior of ϕ as function of lag j.
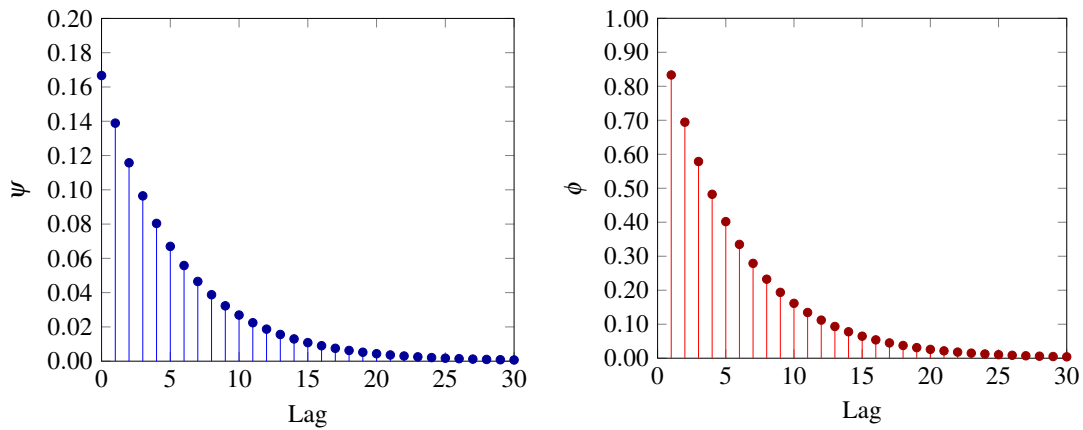
Source: adapted from (ZAKAMULIN, 2017).

Figure 14 shows the behavior of ψ_i and ϕ_i for different lags of an $EMA_t(11)$. It is interesting to remark that both ψ_i and ϕ_j have a smooth fall that goes beyond lag equal to 11, that is, EMA registers all data history.

For this reason, the advantage of EMA over SMA is to achieve the turning point sooner, as illustrated in Figure 15. It is possible to see that $SMA_t(n)$ and $EMA_t(n)$ have the same lag time, however, when the trend is changing, $EMA_t(n)$ follows the trend more closely than $SMA_t(n)$.

2.5 Trading Rules

Typically, the finance literature adopts technical analysis as a methodology of predicting future stock returns from past stock prices and patterns in price dynamics. By the

---

[7] SMA is considered a primary RAMA, so it serves as a reference for several metrics.

Figure 15 – Comparison between $SMA_t(n)$ and $EMA_t(n)$ with a focus on turning point.
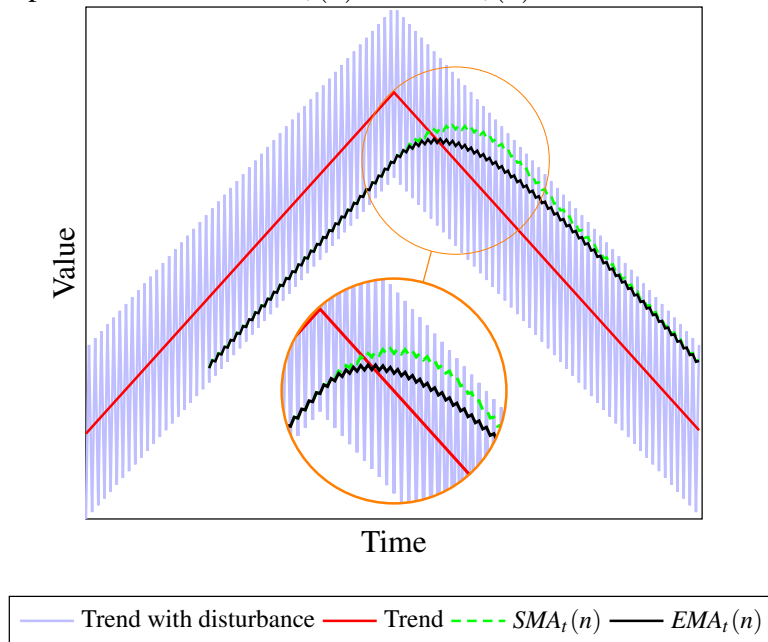
Source: adapted from (ZAKAMULIN, 2017).

way, technical analysis through MA is very popular and is also used in this thesis. The next sections present the trading rules called Price Minus Moving Average Rule (P-MA), MAC and MACD. Furthermore, the pullback concept will be detailed, which is a situation harmful to the performance of MAC and MACD.

2.5.1 Trading Signal

Fist of all, it is essential to mention that a trading signal, buy or sell, is the key element of any trading rule because it must be able to identify changes in the financial market to provide good returns on investment. For instance, Figure 16 shows a sample of the stock price change of the Brazilian company Positivo Tecnologia S.A. from november to december. Using this historical data, an analyst would easily choose to buy stocks on november 1, 2019, and sell on december 12, 2019, getting after 42 days a gain of 166.74% minus taxes. Any other choice of buying or selling would result in a lower gain or even a loss of investment.

It is important to note that in the real world, future stock values are not available; this way, financial market elaborates methodologies that provide trading signal with past stock values. So, a trading signal at time $t + 1$ can be defined as:

$$TS_{t+1} = \begin{cases} \text{Buy}, & \text{if } Indicator_t > 0, \\ \text{Sell}, & \text{if } Indicator_t \leq 0, \end{cases} \qquad (2.16)$$

Figure 16 – The stock price of Positivo Tecnologia S.A. obtained at B3.
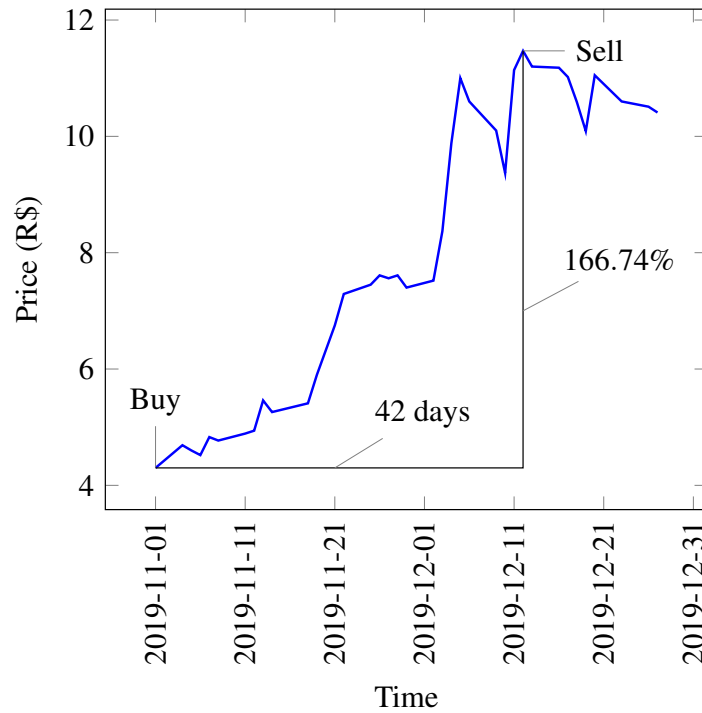
Source: elaborated by the author (2020).

where *Indicator$_t$* is the result of a function that identifies changes in time series. This way, *Indicator$_t$* $= f(Y_t, Y_{t-1}, \dots)$.

2.5.2 Main Trading Rules

This section presents concepts about trading rules. By the way, the trading nomenclature rule represents a verbal description of the trading signal generation process in a specific strategy such as Momentum (MOM), Average Directional Index (ADX), Directional Movement Index (DMI), among others. However, this thesis addresses classic trading rules such as P-MA, MAC, and MACD.

2.5.2.1 Price Minus Moving Average

The best way to understand more sophisticated trading rules is through P-MA. Basically, it determines the trading signal from the subtraction between the current data Y_t and the $RAMA_t(n)$. A Buy signal occurs when the current data is above the RAMA. Otherwise, if the current data is below the RAMA, a Sell signal is generated. This way, the P-MA is computed as:

$$P - MA_t(n) = Y_t - RAMA_t(n), \tag{2.17}$$

and trading signal is:

$$TS_{t+1} = \begin{cases} \text{Buy}, & \text{if } P - MA_t(n) > 0, \\ \text{Sell}, & \text{if } P - MA_t(n) \leq 0. \end{cases} \tag{2.18}$$

In order to visualize behavior of the P-MA, Figure 17 presents only essential information, that is, trend, trend with disturbance, $SMA_t(n)$, turning point line, P-MA using SMA (i.e., $P - SMA_t(n)$) and trading signal. It is noted that the difference between trend with disturbance and the SMA provides a buying region in the upward trend because $Y_t - SMA_t(n)$ is a positive value. During a downward trend, $Y_t - SMA_t(n)$ is a negative value, creating a selling region. In the period of transition between the buy and sell signal, false signals appear in the region of buy (such signals recommend buying, causing loss to the investor). Analogously, false signals will be in the selling region if there is a downward trend followed by an upward trend.

2.5.2.2 *Moving Average Crossover*

MAC was proposed by Gartley (1935) in which a trading sinal is generated from the subtraction of two RAMAs, that is:

$$MAC_t(n_1, n_2) = RAMA_t(n_1) - RAMA_t(n_2), \tag{2.19}$$

with $n_2 > n_1$. After the calculated MAC, the trading signal is defined as:

$$TS_{t+1} = \begin{cases} \text{Buy}, & \text{if } MAC_t(n_1, n_2) > 0, \\ \text{Sell}, & \text{if } MAC_t(n_1, n_2) \leq 0. \end{cases} \tag{2.20}$$

The MAC dynamic is illustrated in Figure 18, which consists of trend with and without disturbance, SMA using n_1 and n_2, turning point line, MAC using SMA (i.e., $SMAC_t(n_1, n_2)$) and trading signal. The illustration shows that the MAC provides a buying region in the upward trend because the result of $SMA_t(n_1) - SMA_t(n_2)$ is a positive value. In contrast, the result of $SMA_t(n_1) - SMA_t(n_2)$ is a negative value during a downward trend, causing a selling region. Incidentally, the financial market uses the nomenclature crossover when the shorter RAMA (i.e., $RAMA_t(n_1)$) crosses either above or below the longer RAMA (i.e., $RAMA_t(n_2)$). Thus, buy or sell signals are generated from the Bullish crossover/Golden cross or Bearish crossover/Death cross, respectively.

It is worth noting that during the period of transition between the buy and sell signal, false signals appear in the region of buy (such signals recommends buying), causing loss to the

Figure 17 – P-MA using $SMA_t(n)$.
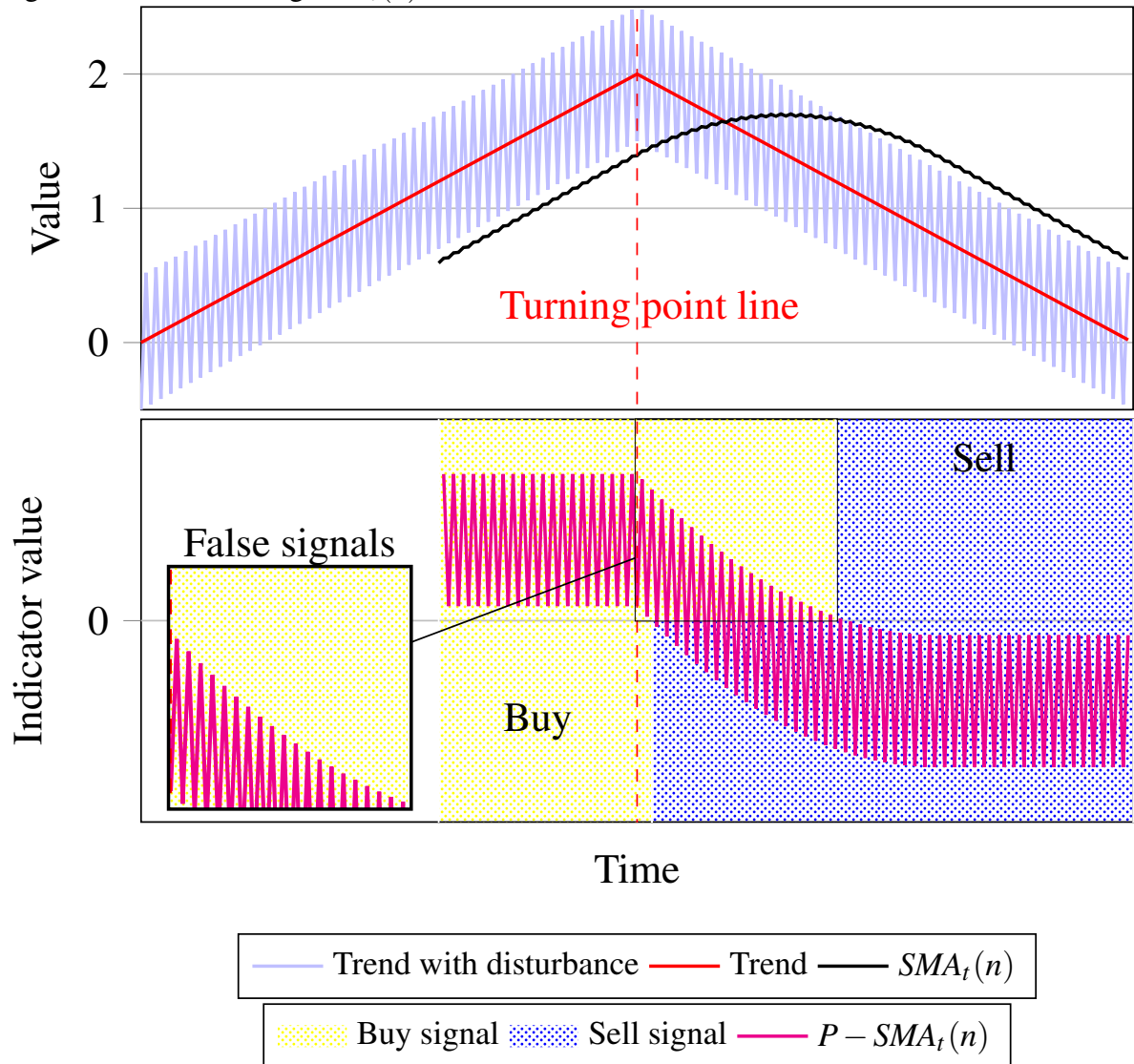
Source: elaborated by the author (2020).

investor. In addition, the false signals from $SMAC_t(n_1, n_2)$ have a smaller width and amplitude than $P - SMA_t(n_2)$, resulting in better financial returns.

From now on, an alternative equation to reduce the number of math operations is developed, that is, a shorter equation. With this in mind, Equation 2.9 is used with Equation 2.19, resulting in (ZAKAMULIN, 2017):

$$MAC_t(n_1, n_2) = Y_t - \sum_{j=1}^{n_1-1} \phi_j^{n_1} \Delta Y_{t-j} Y_t - Y_t + \sum_{j=1}^{n_2-1} \phi_j^{n_2} \Delta Y_{t-j} \qquad (2.21)$$

$$= \sum_{j=1}^{n_2-1} \phi_j^{n_2} \Delta Y_{t-j} - \sum_{j=1}^{n_1-1} \phi_j^{n_1} \Delta Y_{t-j},$$

where $\phi_j^{n_1} = \dfrac{\sum\limits_{i=j}^{n_1-1} \omega_j^{n_1}}{\sum\limits_{i=0}^{n_1-1} \omega_i^{n_1}}$, $\phi_j^{n_2} = \dfrac{\sum\limits_{i=j}^{n_2-1} \omega_j^{n_2}}{\sum\limits_{i=0}^{n_2-1} \omega_i^{n_2}}$ use weights $\omega_i^{n_1}$ and $\omega_i^{n_2}$ for short and long RAMA, respec-

Figure 18 – MAC using $SMA_t(n_1)$ and $SMA_t(n_2)$.
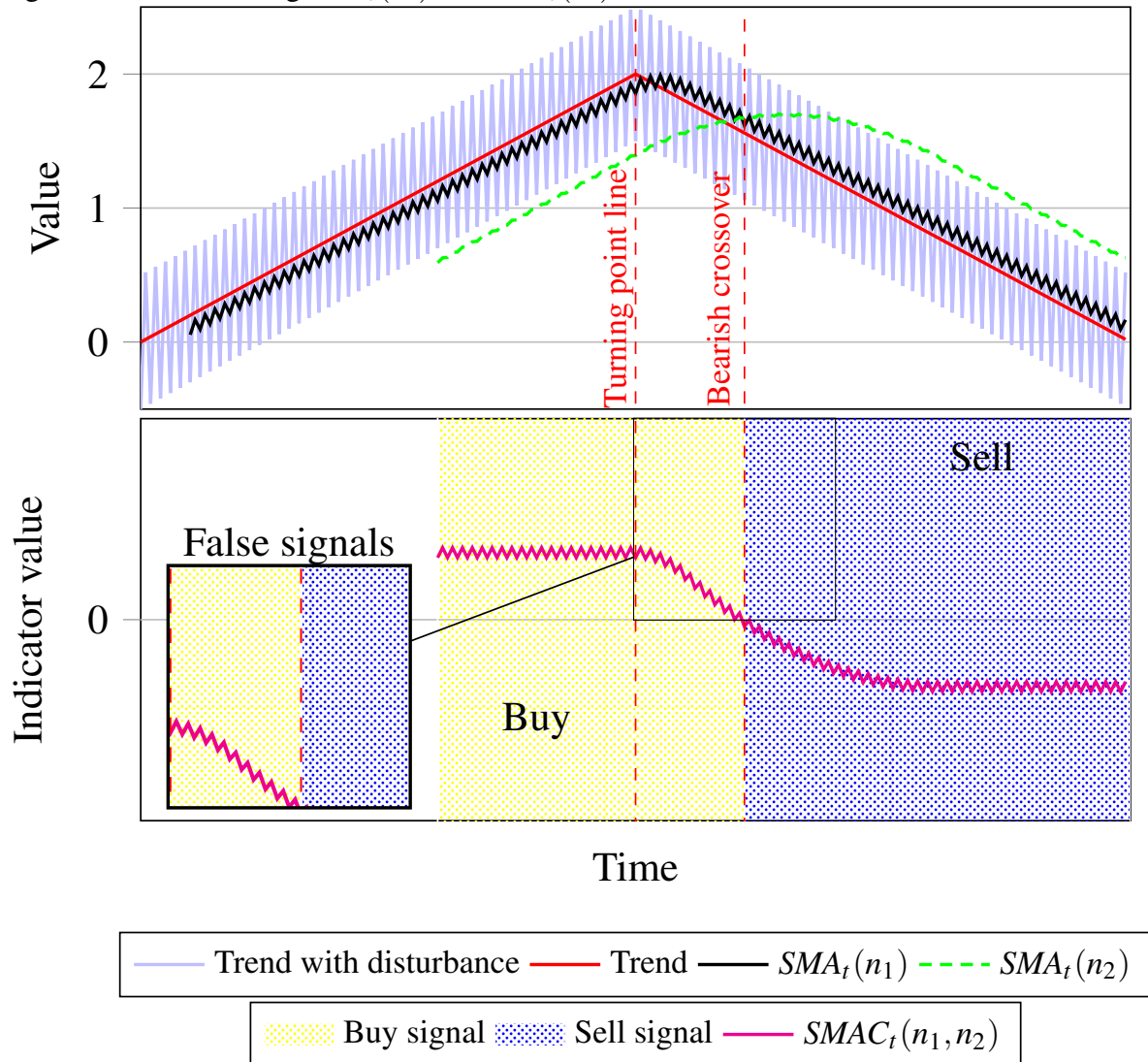
Source: elaborated by the author (2020).

tively.

As ΔY_{t-j} is identical during the n_1 values of both RAMA, it is possible to rewrite Equation 2.21 as (ZAKAMULIN, 2017):

$$MAC_t(n_1,n_2) = \sum_{j=1}^{n_1-1} (\phi_j^{n_2} - \phi_j^{n_1})\Delta Y_{t-j} + \sum_{j=n_1}^{n_2-1} \phi_j^{n_2} \Delta Y_{t-j}. \qquad (2.22)$$

With regard to the SMAC, Equation 2.22 can be written as (ZAKAMULIN, 2017):

$$
\begin{aligned}
SMAC_t(n_1, n_2) &= Y_t - \frac{\sum_{j=1}^{n_1-1}\left(\sum_{i=j}^{n_1-1}\omega_i^{n_1}\right)\Delta Y_{t-j}}{\sum_{i=0}^{n_1-1}\omega_i^{n_1}} - Y_t + \frac{\sum_{j=1}^{n_2-1}\left(\sum_{i=j}^{n_2-1}\omega_i^{n_2}\right)\Delta Y_{t-j}}{\sum_{i=0}^{n_2-1}\omega_i^{n_2}} \\[2ex]
&= \frac{\sum_{j=1}^{n_2-1}\left(\sum_{i=j}^{n_2-1}\omega_i^{n_2}\right)\Delta Y_{t-j}}{\sum_{i=0}^{n_2-1}\omega_i^{n_2}} - \frac{\sum_{j=1}^{n_1-1}\left(\sum_{i=j}^{n_1-1}\omega_i^{n_1}\right)\Delta Y_{t-j}}{\sum_{i=0}^{n_1-1}\omega_i^{n_1}} \\[2ex]
&= \frac{\sum_{j=1}^{n_2-1}\left(\sum_{i=j}^{n_2-1}1\right)\Delta Y_{t-j}}{\sum_{i=0}^{n_2-1}1} - \frac{\sum_{j=1}^{n_1-1}\left(\sum_{i=j}^{n_1-1}1\right)\Delta Y_{t-j}}{\sum_{i=0}^{n_1-1}1} \\[2ex]
&= \frac{\sum_{j=1}^{n_2-1}(n_2-j)\Delta Y_{t-j}}{n_2} - \frac{\sum_{j=1}^{n_1-1}(n_1-j)\Delta Y_{t-j}}{n_1} \\[2ex]
&= \sum_{j=1}^{n_1-1}\left(\frac{n_2-j}{n_2}-\frac{n_1-j}{n_1}\right)\Delta Y_{t-j} + \sum_{j=n_1}^{n_2-1}\frac{(n_2-j)}{n_2}\Delta Y_{t-j} \\[2ex]
&= \sum_{j=1}^{n_1-1}\frac{(n_2-n_1)j}{n_1 n_2}\Delta Y_{t-j} + \sum_{j=n_1}^{n_2-1}\frac{(n_2-j)}{n_2}\Delta Y_{t-j}.
\end{aligned}
\tag{2.23}
$$

Regarding EMAC, that is, when both RAMAs are EMA with $\omega_i^{n_1} = \lambda_{n_1}^i = \frac{n_1-1}{n_1+1}$ and $\omega_i^{n_2} = \lambda_{n_2}^i = \frac{n_2-1}{n_2+1}$, it can be written (ZAKAMULIN, 2017):

$$
\begin{aligned}
EMAC_t(n_1, n_2) &= \frac{\sum_{j=1}^{\infty}\left(\sum_{i=j}^{\infty}\omega_i^{n_2}\right)\Delta Y_{t-j}}{\sum_{i=0}^{\infty}\omega_i^{n_2}} - \frac{\sum_{j=1}^{\infty}\left(\sum_{i=j}^{\infty}\omega_i^{n_1}\right)\Delta Y_{t-j}}{\sum_{i=0}^{\infty}\omega_i^{n_1}} \\[2ex]
&= \frac{\sum_{j=1}^{\infty}\left(\sum_{i=j}^{\infty}\lambda_{n_2}^i\right)\Delta Y_{t-j}}{\sum_{i=0}^{\infty}\lambda_{n_2}^i} - \frac{\sum_{j=1}^{\infty}\left(\sum_{i=j}^{\infty}\lambda_{n_1}^i\right)\Delta Y_{t-j}}{\sum_{i=0}^{\infty}\lambda_{n_1}^i} \\[2ex]
&= \frac{\sum_{j=1}^{\infty}(1-\lambda_{n_2})^{-1}\lambda_{n_2}^j\Delta Y_{t-j}}{(1-\lambda_{n_2})^{-1}} - \frac{\sum_{j=1}^{\infty}(1-\lambda_{n_1})^{-1}\lambda_{n_1}^j\Delta Y_{t-j}}{(1-\lambda_{n_1})^{-1}} \\[2ex]
&= \sum_{j=1}^{\infty}\left(\lambda_{n_2}^j - \lambda_{n_1}^j\right)\Delta Y_{t-j}.
\end{aligned}
\tag{2.24}
$$

Actually, it is not obligatory to use the same RAMA with different values of n to perform the MAC; another strategy is to mix different RAMAs. Remember that $SMA_t(n)$ and

$EMA_t(n)$ have the same lag time, however, when the trend is changing, $EMA_t(n)$ follows the trend more closely than $SMA_t(n)$. This way, it is possible to reduce the number of parameters using (ZAKAMULIN, 2017):

$$MAC_t(n) = EMA_t(n) - SMA_t(n) = \sum_{j=1}^{\infty} \lambda_n^j \Delta Y_{t-j} - \frac{\sum_{j=1}^{n-1} (n-j) \Delta Y_{t-j}}{n}. \tag{2.25}$$

2.5.2.3 Moving Average Convergence/Divergence

MACD generates a trading signal from three RAMAs, which is divided into three steps (TURNER, 2006). The first step uses MAC, that is:

$$MAC_t(n_1, n_2) = RAMA_t(n_1) - RAMA_t(n_2), \tag{2.26}$$

with $n_1 < n_2$. The second step computes an EMA from the MAC in order to create a delayed and smoothed MAC version, called Signal, and written as:

$$Signal_t(n_{\text{sig}}) = EMA_t^{\text{MAC}}(n_{\text{sig}}), \tag{2.27}$$

where n_{sig} is the signal window size, and EMA_t^{MAC} is the EMA over $MAC_t(n_1, n_2)$. The last step combines MAC with Signal, this way:

$$MACD_t(n_1, n_2, n_{\text{sig}}) = MAC_t(n_1, n_2) - Signal_t(n_{\text{sig}}). \tag{2.28}$$

Thus, the trading signal can be expressed as:

$$TS_{t+1} = \begin{cases} \text{Buy}, & \text{if } MACD_t(n_1, n_2, n_{\text{sig}}) > 0, \\ \text{Sell}, & \text{if } MACD_t(n_1, n_2, n_{\text{sig}}) \leq 0. \end{cases} \tag{2.29}$$

Figure 19 shows the MACD dynamics at specific time instants numbered as points 1 to 8. In **point 1**, the divergence between $EMA_t(n_1)$ and $EMA_t(n_2)$ begins, causing $MAC_t(n_1, n_2)$ to move away from zero. In **point 2**, $Signal_t(n_{\text{sig}})$ and $MACD_t(n_1, n_2, n_{\text{sig}})$ curves are generated, indicating a sell signal. The delay between MAC and MACD depends on the n_{sig} value. In **point 3**, $EMA_t(n_1)$ and $EMA_t(n_2)$ stop diverging, and the behavior of convergence between EMAs begins, causing $MAC_t(n_1, n_2)$ to move towards zero. In **point 4**, the first crossing between $MAC_t(n_1, n_2)$ and $Signal_t(n_{\text{sig}})$ occurs, causing $MACD_t(n_1, n_2, n_{\text{sig}})$ to be positive and indicating a buy signal. In **point 5**, $EMA_t(n_1)$ and $EMA_t(n_2)$ stop converging, and the behavior of divergence between EMAs begins, causing $MAC_t(n_1, n_2)$ to become positive and move away

Figure 19 – MACD dynamics using fictitious trend and disturbance data.
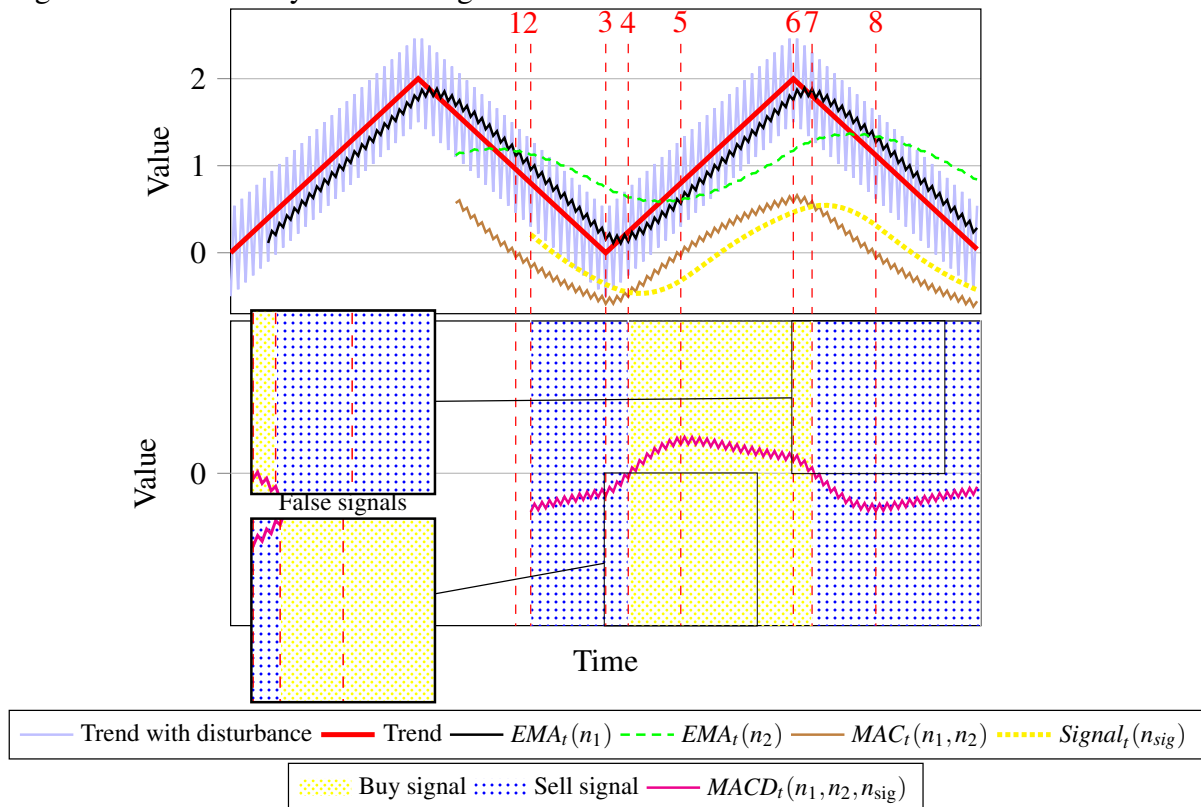
Source: elaborated by the author (2020).

from zero. In **point 6**, EMAs stop diverging and begin to converge, causing the $MAC_t(n_1, n_2)$ to move towards zero. In **point 7**, $MAC_t(n_1, n_2)$ and $Signal_t(n_{sig})$ cross for a second time, causing $MACD_t(n_1, n_2, n_{sig})$ to become negative and indicating a sell signal. In **point 8**, EMAs stop converging and begin to diverge, causing $MAC_t(n_1, n_2)$ to become negative and move away from zero.

It is worth noting that $Signal_t(n_{sig})$ acts as a trigger, postponing, or delaying the trading signal; therefore, an inappropriate $Signal_t(n_{sig})$ impairs MACD performance due to the use of improper trading signal, called false signals.

2.5.3 *Pullbacks*

The pullback is a response of the new information coming into the market, or it can simply be a result of a random price movement stimulating movement in the same direction. For instance, the pullback in a downtrend is an increase, while pullback in an uptrend is a decline (BULKOWSKI, 2002).

Figure 20 presents a pullback in an uptrend, where it is possible to note that Point A has the lowest value, and Point B has a significant high. In the move from A to B, there can be

Figure 20 – Typical behavior of a pullback.
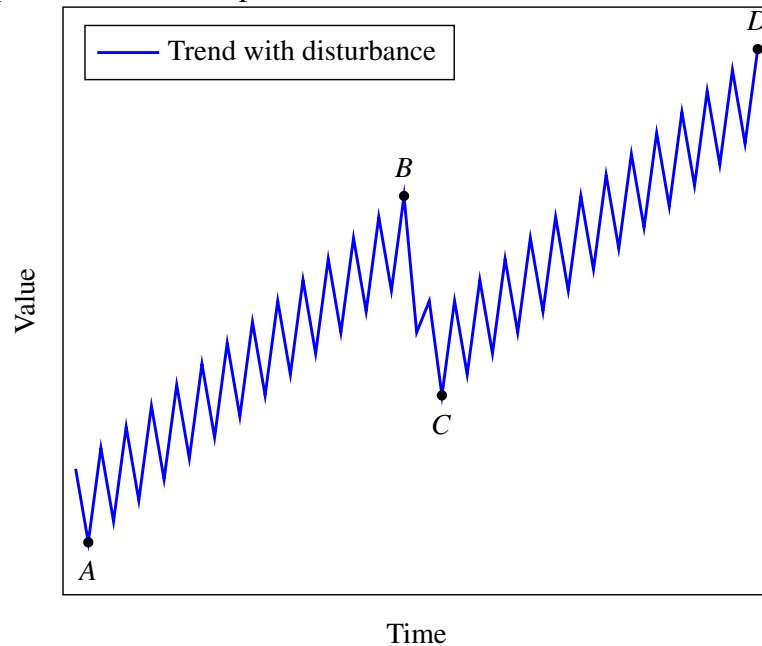
Source: elaborated by the author (2020).

no lows below Point A and no highs above Point B. The Point C must be higher than Point A, and when moving from B up to C, there can be no highs above Point B, and no lows bellow Point C. Finally, it is necessary to ensure that the Point D must be higher than Point B and in the move from C to D there can be no lows bellow Point C, and no highs above Point D (BULKOWSKI, 2002).

In the case of a pullback in a downtrend, Point A has the highest value, and Point B has a significant low. In the change from A up to B, there can be no lows below Point B, and no highs above Point A. Point C must be higher than Point B, and when changing from B to C, there can be no highs above Point C, and no lows below Point B. The Point D must be lower than Point B and the change from C up to D there can be no lows below Point D, and no highs above Point C (BULKOWSKI, 2002).

In general, the performance of trading rules decreases when a pullback occurs. Figure 21 shows the effect of the pullback on the $MAC(n_1, n_2)$ using fictitious data. An uptrend starts in Point 1, then in Point 2 appears a buy signal. The uptrend is sustained until Point 3, where the pullback begins. In Point 4, a second trading signal appears, indicating a sell. In Point 5, a third trading signal appears, indicating a buy (BULKOWSKI, 2002).

Numerically, it can be evidence that $MAC(n_1, n_2)$ provides a profit of 8 due to a buy of 1.25 and a sell of 4, followed by a buy and sell of 4.75 and 10, respectively. In contrast, it is possible to profit 8.75, when the pullback does not occur. In relative terms, a pullback caused a

profit loss of 8.6%. It is worth mentioning that the pullback detector algorithms are detailed in Appendix B. Such algorithms are useful for pullback count in the layouts that will be presented in the next chapter.

Figure 21 – Numerical example of a pullback.
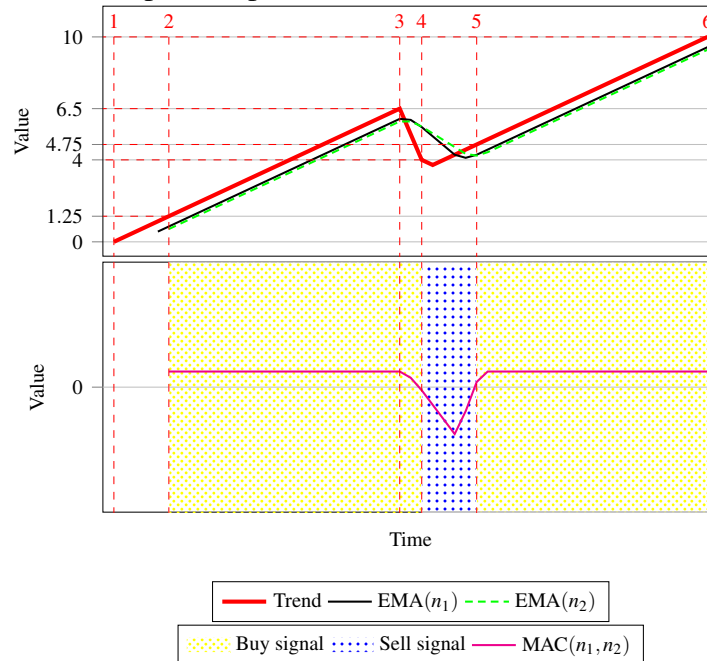
Source: elaborated by the author (2020).

2.6   Chapter Summary

In this chapter, techniques for the interference management applied in heterogeneous networks were presented. In addition, the chapter presents useful techniques for extracting trends from time series. Highlighting the advantages and disadvantages in the face of problems. Finally, financial techniques (e.g. MAC and MACD) that use trends to make decisions have been described and illustrated.

3 DYNAMIC E-ICIC USING MAC

This chapter presents the system features adopted in this thesis, which was performed using simulation (by an in-house built simulator), where it is possible to simulate a wireless network based on some 3GPP guidelines because they are widely used within industry and academia, and thus facilitate the comparison of the results from distinct parties. Moreover, the ABS problem formulation and the reference e-ICIC algorithms modeling are presented. A proposal for dynamic e-ICIC based on MAC is introduced as well as results and discussion of its added value on system performance.

3.1 System Modeling

The system modeling of this thesis to analyze HetNets is composed of one macro cell and a number of small cells using a frequency carrier f_c and bandwidth B of 2 GHz and 1.4 MHz, respectively (3GPP, 2018). The macro cell has a radius R of 1500 m (3GPP, 2018b) and a transmit power p_m of 46 dBm (3GPP, 2018), while the small cells use a transmit power p_s of 36 dBm (3GPP, 2018) to cover a radius r of 200 m (3GPP, 2018b). In addition, all BSs and UEs are equipped with a single omnidirectional antenna. Regarding the UEs, they have a speed of 3 km/h (3GPP, 2013a) and are uniformly distributed over the cells' coverage areas, with 10 UEs in the macro cell area and 20 UEs in each small cell. As a side note, this thesis does not use a mobility model, that is, the users do not move over the HetNet coverage area. Instead, the mobile speed is assigned to the small scale fading model.

In an effort to evaluate the DL behavior, this thesis performs system-level simulations considering the main propagation effects on the wireless channel, that is, pathloss, shadowing, and small scale fading. Basically, the macro and small cell models with Line of Sight (LOS) and Non-Line of Sight (NLOS) propagation conditions are based on Urban Macro Model (UMa) and Urban Micro Model (UMi) (3GPP, 2009; CLAUSSEN *et al.*, 2016). This way, the macro cell LOS pathloss is modeled as:

$$G_{\text{LOS}}^m(d_m) = -22\log_{10}(d_m) - 34.02, \tag{3.1}$$

while the macro cell NLOS pathloss is:

$$G_{\text{NLOS}}^m(d_m) = -39.01\log_{10}(d_m) - 21.56, \tag{3.2}$$

where d_m is the distance between the macro cell transmitter and a UE in meters.

Concerning system-level simulations, 3GPP proposes a smooth transition between LOS and NLOS propagation based on the probability of LOS occurrence (CLAUSSEN *et al.*, 2016), which is modeled as:

$$\rho_{LOS}^m(d_m) = \min\left(\frac{18}{d_m}, 1\right) \cdot \left(1 - e^{\frac{-d_m}{63}}\right) + e^{\frac{-d_m}{63}}. \tag{3.3}$$

This way, the macro cell pathloss $G^m(d_m)$ is calculated as:

$$G^m(d_m) = \rho_{LOS}^m(d_m)\, G_{\text{LOS}}^m(d_m) + [1 - \rho_{LOS}^m(d_m)]\, G_{\text{NLOS}}^m(d_m). \tag{3.4}$$

The small cell LOS pathloss is modeled as follows:

$$G_{\text{LOS}}^p(d_s) = -22\log_{10}(d_s) - 34.02, \tag{3.5}$$

while the small cell NLOS pathloss is modeled as:

$$G_{\text{NLOS}}^p(d_s) = -36.7\log_{10}(d_s) - 30.5, \tag{3.6}$$

where d_s is the distance between the small cell transmitter and UE in meters. The probability of LOS occurrence in the UMi is modeled as (CLAUSSEN *et al.*, 2016):

$$\rho_{LOS}^p(d_s) = \min\left(\frac{18}{d_s}, 1\right) \times (1 - e^{\frac{-d_s}{36}}) + e^{\frac{-d_s}{36}}, \tag{3.7}$$

which is used to provide a smooth transition between LOS and NLOS propagation, that is:

$$G^p(d_s) = \rho_{LOS}^p(d_s)\, G_{\text{LOS}}^p(d_s) + [1 - \rho_{LOS}^p(d_s)]\, G_{\text{NLOS}}^p(d_s). \tag{3.8}$$

In addition, it is important to mention that the equations above were developed using the average building height, average street width, macro cell height, small cell height and receiver height equal to 20 m, 20 m, 25 m, 10 m and 1.5 m, respectively (3GPP, 2009). Shadowing is modeled as lognormal distribution of zero mean and standard deviation of 8 dB and 10 dB for macro and small cells, respectively (3GPP, 2006), while the small scale fading is modeled as complex gaussian channel coefficients by Clarke/Gans model (CHO *et al.*, 2010).

After presenting the propagation models, the next step is to describe equations that measure the link quality using the received power. From the standpoint of the macro cell, the SINR of a UE u, with $u \in \{1, 2, \ldots, U\}$ in the macro cell, using the subframe of index k can be calculated as:

$$\gamma_{u,k}^{\text{macro}} = \frac{|g_{u,k}|^2 p_m}{\sum\limits_{o=1}^{O} |h_{u,k}^{(o)}|^2 p_s + \eta}, \tag{3.9}$$

where $o \in \{1, 2, \ldots, O\}$ is the index for small cells; $g_{u,k}$ and $h_{u,k}$ are channel coefficients for macro and small cells, respectively (comprising pathloss, shadowing, and small scale fading); and η is the thermal noise power, whose corresponding value in logarithmic scale is equal to -112 dBm (3GPP, 2006). Given the SINR, the Shannon-Hartley formulation is used to compute the DL capacity, that is:

$$C_{u,k}^{\text{macro}} = B \log_2 \left(1 + \gamma_{u,k}^{\text{macro}} \right). \tag{3.10}$$

All things considered, the macro cell mean capacity is computed as:

$$C_{\text{mean}}^{\text{macro}} = \frac{1}{N_{sf}} \sum_{k=1}^{N_{sf}} \sum_{u=1}^{U} C_{u,k}^{\text{macro}}, \tag{3.11}$$

where N_{sf} is the total number of subframes. In addition, it is important to mention that the macro cell capacity during ABS subframes is equal to zero because there is no macro cell payload transmission.

From the standpoint of the small cell, the SINR can be computed in two ways: it employs or does not employ ABS e-ICIC. First, if the small cell does not employ ABS e-ICIC, then SINR of a UE $j \in \{1, 2, \ldots, J\}$ connected in the small cell o and allocated in the subframe k is calculated as:

$$\gamma_{j,k}^{(o),\text{small}} = \frac{|h_{j,k}^{(o)}|^2 p_s}{|g_{j,k}^{(o)}|^2 p_m + \sum_{o'=1, o' \neq o}^{O} |h_{j,k}^{(o')}|^2 p_s + \eta}, \tag{3.12}$$

where $o' \in \{1, 2, \ldots, O\}$ is the index for small cell that causes interference. This way, the capacity can be defined as $C_{j,k}^{(o),\text{small}} = B \log_2 \left(1 + \gamma_{j,k}^{(o),\text{small}} \right)$, and the small cell mean capacity is computed as:

$$C_{\text{mean}}^{\text{small}} = \frac{1}{N_{sf} \cdot O} \sum_{o=1}^{O} \sum_{k=1}^{N_{sf}} \sum_{j=1}^{J} C_{j,k}^{(o),\text{small}}. \tag{3.13}$$

Second, if the small cell employs ABS e-ICIC, UEs of small cells are split into two sets: (i) UEs $m \in \{1, 2, \ldots, M\}$ located at small cell's center area, and (ii) UEs $l \in \{1, 2, \ldots, L\}$ located at small cell's edge area. Thus, the SINR of user l connected to small cell o in subframe k during ABSs is:

$$\gamma_{l,k}^{(o),\text{small}} = \frac{|h_{l,k}^{(o)}|^2 p_s}{\sum_{o'=1, o' \neq o}^{O} |h_{l,k}^{(o')}|^2 p_s + \eta}, \tag{3.14}$$

and the capacity is calculated as:

$$C_{l,k}^{(o),\text{small}} = B \log_2 \left(1 + \gamma_{l,k}^{(o),\text{small}} \right). \tag{3.15}$$

For non-ABSs, the SINR is formulated as:

$$\gamma_{m,k}^{(o),\text{small}} = \frac{|h_{m,k}^{(o)}|^2 p_s}{|g_{m,k}^{(o)}|^2 p_m + \sum\limits_{o'=1,o'\neq o}^{O} |h_{m,k}^{(o')}|^2 p_s + \eta}, \tag{3.16}$$

because UEs located at the center area experience macro cell interference. In doing so, the capacity is computed as:

$$C_{m,k}^{(o),\text{small}} = B \log_2 \left(1 + \gamma_{m,k}^{(o),\text{small}} \right). \tag{3.17}$$

Finally, the small cell mean capacity is:

$$C_{\text{mean}}^{\text{small}} = \frac{1}{N_{sf} \cdot O} \sum_{o=1}^{O} \sum_{k=1}^{N_{sf}} \left(\sum_{m=1}^{M} C_{m,k}^{(o),\text{small}} + \sum_{l=1}^{L} C_{l,k}^{(o),\text{small}} \right). \tag{3.18}$$
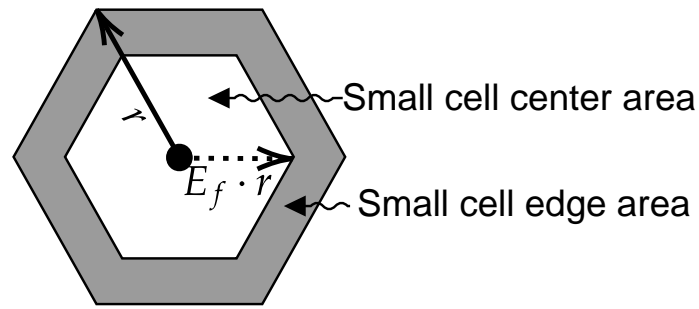
Concerning the dynamic behavior of HetNets, the system model uses Round Robin (RR) scheduling policy to provide a fair basis for sharing resources (3GPP, 2018a) and FDD. Besides, the full buffer traffic model is adopted, which refers to a case when there is a fixed number of UEs in the network whose data buffers are constantly full. It is typically used to test the air interface in the sense of "worst-case traffic scenario", and is useful to measure the system capacity (SADIQ *et al.*, 2009).

Based on this system model, twelve layouts were developed to analyze different interference conditions. Table 1 and Figure 22 show the network layout to macro cell and small cell. As a side note, it is important to highlight that the value of 1126m is due to the apothem of the hexagons located to the north and south of the macro cell transmitter.

3.1.1 Small Cell's Edge Area Analysis: Choosing the Edge Scale Factor

An essential requirement for the LTE system is to improve cell edge throughput, that is, to provide some level of service consistency in geographical terms within the coverage area. In the cellular system, however, the SINR disparity between cell-center and cell-edge users can achieve the order of 20 dB (KHAN, 2009). As a UE moves away from the cell-center, SINR degrades due to two factors. Firstly, the received signal goes down as the pathloss increases with distance from the serving eNB. Secondly, the ICI goes up because when a UE moves away from

Table 1 – Layouts parameters.

Layout	Dist. from macro to small cells (m)	O	Small index	Number of users
1	1300	1	1	30
2	1300 and ≈ 1126	2	1-2	50
3	1300 and ≈ 1126	3	1-2-3	70
4	1300 and ≈ 1126	4	1-2-3-4	90
5	$d_2 \approx 726$	1	5	30
6	$d_2 \approx 726$	2	5-6	50
7	$d_2 \approx 726$	3	5-6-7	70
8	$d_2 \approx 726$	4	5-6-7-8	90
9	$d_1 \approx 326$	1	9	30
10	$d_1 \approx 326$	2	9-10	50
11	$d_1 \approx 326$	3	9-10-11	70
12	$d_1 \approx 326$	4	9-10-11-12	90

Source: elaborated by the author (2020).

Figure 22 – Illustration of twelve evaluation layouts: location of the small cell in each layout.

Source: elaborated by the author (2020).

one eNB, it is generally getting closer to another eNB. In this thesis, the small cell edge area comprises a region similar to a hexagonal shape ring that starts from $E_f \cdot r$ up to r, where E_f is a factor that scales the size of the edge, as illustrated in Figure 23.

In an effort to define E_f, the small cell SINR behavior was simulated and analyzed for 3 layouts with high interference levels (i.e., layouts 4, 8, and 12) adopting $E_f \in [0.8, 0.85, 0.90, 0.95]$ without ABS e-ICIC, as illustrated in Figure 24. It can be seen in all layouts that two sets of curves are formed, that is, cell-center and cell-edge curves. Regarding E_f, it is noticed that both sets move to the left when E_f increases due to the users getting closer to the macro cell transmitter and getting farther away from the small cell transmitter.

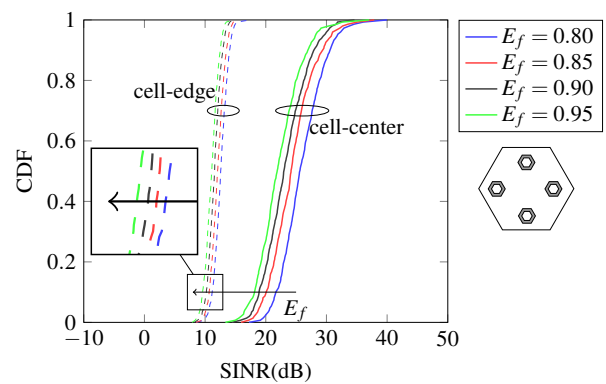Figure 23 – Detail of the small cell layout.

Source: elaborated by the author (2020).

Figure 24 – Small cell SINR for different E_f values.
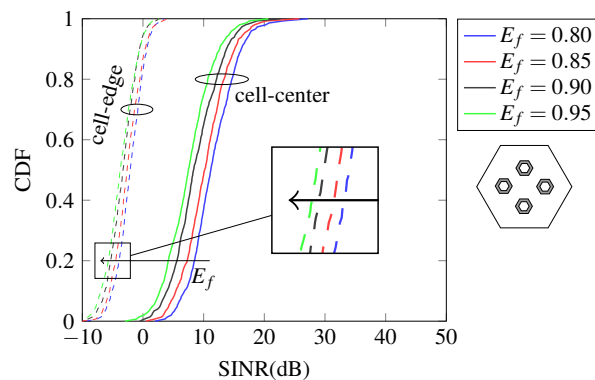
(a) Small cell SINR for Layout 4.
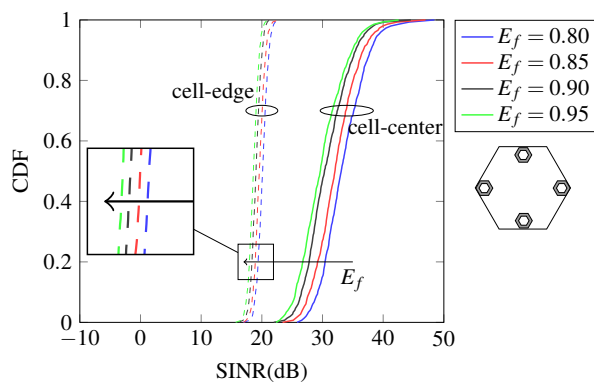
(b) Small cell SINR for Layout 8.

(c) Small cell SINR for Layout 12.
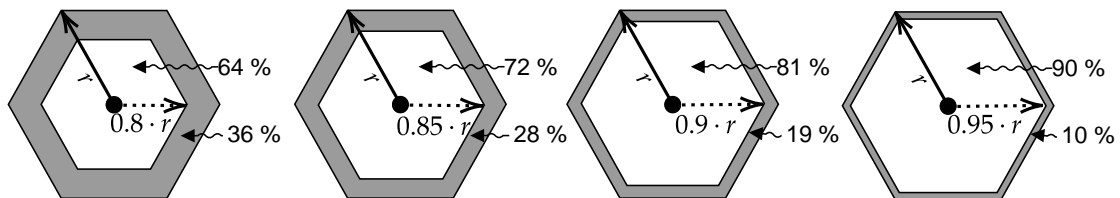

Source: elaborated by the author (2020).

In order to check the discrepancies between cell-center and cell-edge, Table 2 shows the difference in terms of SINR for each combination of E_f and layout. Concerning the values, a subtle change is noted in terms of E_f and layouts. For this reason, a complementary criterion was adopted based on the region of coverage, where it is preferable the case in which the user is located as far as possible from the cell of interest.

This way, $E_f = 0.95$ was chosen in this thesis because it limits the border to a region of only 10% of total coverage, different from $E_f = 0.8$ which has 36%, as illustrated in Figure 25.

Table 2 – SINR discrepancies between cell-center and cell-edge.

Layout	Illustration	Percentile	E_f			
			0.8	0.85	0.9	0.95
4		95	17.79 dB	17.32 dB	16.53 dB	16.40 dB
		50	12.94 dB	12.44 dB	11.28 dB	11.00 dB
		5	9.56 dB	8.77 dB	8.05 dB	7.22 dB
8		95	17.36 dB	16.89 dB	16.18 dB	15.30 dB
		50	13.07 dB	12.11 dB	11.43 dB	10.81 dB
		5	10.17 dB	8.82 dB	8.27 dB	7.72 dB
12		95	16.31 dB	15.43 dB	15.18 dB	14.07 dB
		50	13.29 dB	12.82 dB	11.64 dB	11.24 dB
		5	11.56 dB	10.49 dB	9.88 dB	9.48 dB

Source: elaborated by the author (2020).

Figure 25 – Division of the coverage area between the cell-center and the cell-edge for each E_f.

Source: elaborated by the author (2020).

3.2 Problem Formulation and Reference ABS e-ICIC Algorithms

This section discusses about problem formulation and reference ABS e-ICIC algorithms. Initially, the analytical formulation of the ABS problem adopted in this thesis is presented. Then, reference ABS e-ICIC algorithms are described for performance comparison with the proposed solutions.

3.2.1 Problem Formulation

In general, the goal of the e-ICIC is to improve the system performance through sharing radio resources in the time domain. Concerning this thesis, the problem formulation is

based on system capacity. Then, the e-ICIC problem formulation can be stated as follows.

$$
\begin{aligned}
\underset{x_k^{\text{abs}},\, x_k^{\text{non}-\text{abs}}}{\text{maximize}} \quad & \sum_{k=1}^{N_{sf}} \sum_{u=1}^{U} C_{u,k}^{\text{macro}} \cdot x_k^{\text{non}-\text{abs}} + \sum_{o=1}^{O} \sum_{k=1}^{N_{sf}} \left(\sum_{m=1}^{M} C_{m,k}^{(o),\text{small}} \cdot x_k^{\text{non}-\text{abs}} + \sum_{l=1}^{L} C_{l,k}^{(o),\text{small}} \cdot x_k^{\text{abs}} \right) \\
\text{subject to} \quad & x_k^{\text{abs}} + x_k^{\text{non}-\text{abs}} = 1 : \forall k \in \left\{ 1, \cdots, N_{sf} \right\}, \\
& x_k^{\text{abs}},\, x_k^{\text{non}-\text{abs}} \in \{0,1\}.
\end{aligned}
$$

$$(3.19)$$

The formulation can be separated into three terms. The first is related to macro cell capacity, while the second and third terms are responsible for the small cell's capacity in the center and edge, respectively.

Furthermore, it is necessary to add an association constraint due to exclusive transmission of the UE at small cell's edge during ABS and simultaneous transmission to UE at macro cell and small cell's center areas during non-ABS. To this end, binary variables (i.e., x_k^{abs} and $x_k^{\text{non}-\text{abs}}$) are used, where $x_k^{\text{abs}} = 1$ and $x_k^{\text{non}-\text{abs}} = 0$ when the system uses ABS in the subframe k. Otherwise, $x_k^{\text{abs}} = 0$ and $x_k^{\text{non}-\text{abs}} = 1$.

The problem addressed in this thesis presents some difficulties in the search for the optimal solution:

- The HetNet is unaware of the consequences of ABS and non-ABS during a subframe, that is, it is not omniscient. As a result, (3.19) has $C_{u,k}^{\text{macro}}/C_{m,k}^{(o),\text{small}}$ or $C_{l,k}^{(o),\text{small}}$, but not all capacities simultaneously;

- Another difficulty is due to a large number of solutions, which causes an increase in the computational cost (i.e., time). For example, it is necessary to check more than 1 trillion combinations adopting 40 subframes. However, 40 subframes do not provide reliable results. Taking this into account, the number of combinations would increase to $2^{1000} = 10^{301}$ adopting 1000 subframes. To reinforce such arguments, Deb *et al.* (2014) showed that the ABS formulation problem is NP-hard even with a single small cell and macro cell.

3.2.2 Reference ABS e-ICIC Algorithms

In order to evaluate the added value of the proposed solutions, four strategies were chosen:

1. **Baseline**: is the reference algorithm because it does not use ABS e-ICIC. Therefore, it is useful to compare whether ABS e-ICIC really provides gains for HetNets;

2. **Random ABS e-ICIC**: a random ABS ratio is raffled for each duty-cycle. This is another reference strategy, now, in terms of dynamic ABS ratio setting;

3. **Fixed ABS e-ICIC**: based on 3GPP Rel.10 (3GPP, 2013b). The Fixed ABS e-ICIC approach defines an ABS ratio to control interference between macro and small cells. For instance, an ABS ratio of 40% means that the macro cell gates off 40% of the duty-cycle time (40 ms) and transmits in the rest (simultaneously with small cell's center area);

4. **Efficient Coordination of ABS with Coupling Macro Cells (ECO)**: was proposed by Wang e Huang (2019). The ECO algorithm computes the ABS ratio based on multiple factors such as data rate and traffic demand. Basically, ECO has five steps that evaluate channel quality, assess network condition, classify the DL data, set ABS ratios, and decide ABS placement. It is important to highlight that the addition of ABS depends on three policies. In the first policy, it is checked whether each small cell can satisfy the traffic demands of its UEs in a period. If it is true, ABS ratio is set to 0. If false, ECO will check the necessity to increase or decrease the ABS ratio through an inequality, which is formulated from the difference between theoretical data rate supported by each small cell with and without ABS, and traffic supported by the macro cell.

3.3 Algorithm Proposal: MAC for the ABS

The inspiration for the proposed algorithm can be exposed by two questions. The first question is **"What moves stock prices?"**. According to the literature, there are some factors that move stock prices. In other words, the stock prices influencers are:

- **Political situation:** Negotiations between countries, war, product breakthroughs, mergers, acquisitions, and other unforeseen events impact stock prices (SOON, 2010);

- **News:** News impacts companies and industries, consequently affecting stock prices. Usually, positive news (e.g., good earnings reports, new product, and corporate acquisition) will cause individuals to buy stocks. On the other hand, negative news (e.g., bad earnings report and lapse in corporate governance) will normally cause people to sell stocks (SOON, 2010);

- **Market sentiment:** It refers to the psychology of market participants, individually and collectively (SOON, 2010).

The second question is **"What moves user capacity in a wireless communication network?"**. It is possible to list:

- **Traffic pattern:** Different transport protocols can impact user capacity. For example, full buffer is a simplified version of the traffic received/transmitted by a user in a data session in which the buffers of the users' data flows always have an unlimited amount of data to transmit (LUO, 2020);

- **User location:** The user's receiving power takes into account its position in the coverage area. For example, users away from base stations usually have low reception power, which reduces the SINR and impacts the user capacity (LUO, 2020);

- **Scheduling:** It is a fundamental component in the process of resource management for mobile communication networks, becoming an influencer of the user capacity. For example, RR is a scheduler that provides equal radio resource distribution, while Proportional Fair (PF) tries to balance capacity and fairness among all the users (DONG *et al.*, 2015);

- **Channel:** Many effects, such as free-space loss, refraction, diffraction, reflection, and absorption impact the user capacity (DONG *et al.*, 2015).

In both areas of knowledge, such characteristics can be represented through time series, which is a collection of observations made sequentially in time. All in all, it is important to emphasize that news/market sentiment are some factors responsible for the downtrend/uptrend of stock prices in the economy. Similarly, one or more of the previously mentioned factors that influence the user capacity can provide uptrend or downtrend, which can be extracted through MAC.

Among all financial tools, MAC is considered simple and powerful in several financial scenarios (KOEHLER *et al.*, 2008). However, it is necessary to adapt the finance framework for telecommunications. So, ABS e-ICIC based on MAC considers that:

- the **time** (independent variable) is defined as **subframe** k instead of minutes, hours or years and, consequently, the window size n is measured in number of subframes;

- the **price**, which is used to provide crossover in trading, is replaced by **macro cell capacity**;

- the **trading operation interval** is defined as N_{sf}, which must be a multiple of forty.

The MAC acts as ABS manager, that is, it increases or decreases the number of ABSs. Initially, the MAC collects information about the macro cell capacity to perform ABS management. The second step is the decision, in which the MAC defines ABS when a downward trend occurs in macro cell capacity; otherwise, it does not define ABS. Making an analogy with finance, one can imagine that the macro cell, when perceiving a downward trend, sells its

subframes to the small cell, ending when it notices an upward trend. In the last step, the macro cell communicates its decision to the small cell through the X2 interface. As a consequence of the last step, the system capacity is affected, as illustrated in Figure 26. It is worth mentioning that ABS directly affects the system capacity, so the allocation of ABSs must be opportunistic, avoiding impairing the system capacity.

Figure 26 – Diagram of the financial process applied to ABS e-ICIC.
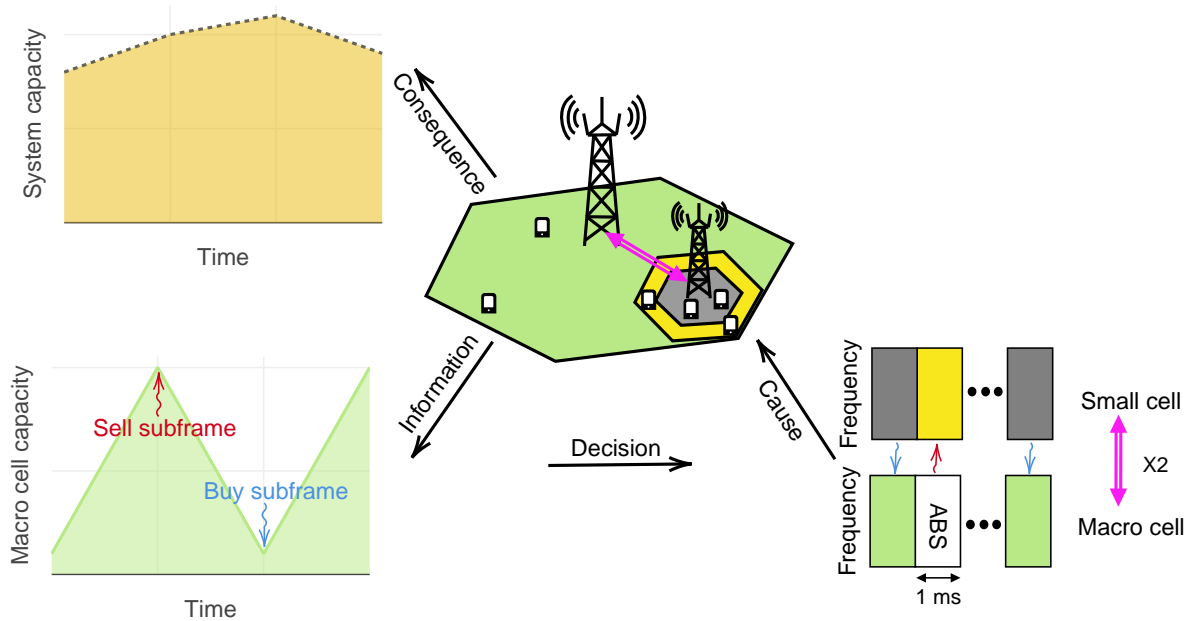
Source: elaborated by the author (2020).

The MAC works properly and opportunistically when well parameterized. However, as in finance, an appropriate parameterization varies from scenario to scenario. After MAC parameterization, the second step is to store the capacity of the macro user u allocated in subframe k, that is, $C_k^{\text{macro}} = C_{u,k}^{\text{macro}}$. Then, the algorithm verifies if the window size $n \geq k$, because it is necessary to have an adequate amount of data before calculating the MAC. If the amount of data is sufficient, the calculation of EMA and SMA begins, as shown below:

$$EMA_k(n) = \left(1 - \frac{n-1}{n+1}\right) \sum_{i=1}^{\infty} \left(\frac{n-1}{n+1}\right)^{i-1} C_{k-i+1}^{\text{macro}}, \tag{3.20}$$

and

$$SMA_k(n) = \frac{\sum_{i=1}^{n} C_{k-i+1}^{\text{macro}}}{n}, \tag{3.21}$$

followed by the calculation of MAC in subframe k:

$$MAC_k(n) = EMA_k(n) - SMA_k(n), \tag{3.22}$$

and the final step is to manage ABS based on the trading signal that can be expressed as:

$$TS_{k+1} = \begin{cases} \text{Non} - \text{ABS}, & \text{if } MAC_k(n) > 0, \\ \text{ABS}, & \text{if } MAC_k(n) \leq 0. \end{cases} \tag{3.23}$$

Algorithm 1 shows the pseudo-code of the proposed MAC ABS e-ICIC algorithm.

Algorithm 1: Proposed MAC ABS e-ICIC Algorithm.

Ensure: Set window size n
    for $k \leftarrow 1$ **to** N_{sf} **do**
      $C_k^{\text{macro}} \leftarrow C_{u,k}^{\text{macro}}$
      if $k \geq n$ **then**
        Compute $SMA_k(n)$ and $EMA_k(n)$
        if $MAC_k(n) \leq 0$ **then**
          Sell signal: set next subframes as ABS
        end if
        if $MAC_k(n) > 0$ **then**
          Buy signal: set next subframes as Non-ABS
        end if
      end if
    end for

In view of Algorithm 1, it is possible to notice that the sell signal has a significant impact on the time series. This also occurs in the economy, originated by the so-called Big Players. They are market participants who can influence prices with just one transaction (KOPPL, 2002).

3.4 Results

3.4.1 MAC ABS e-ICIC General Behavior

MAC ABS e-ICIC numerical simulations provided a mass of data by means of the Monte Carlo method with 1000 random samples, when $n \in [5, 30]$ and $N_{sf} = 1000$ for all layouts. This mass of data presents a **MAC ABS e-ICIC** broad view because it shows the best and worst settings for each layout, as illustrated in Figure 27a. From the mass of data, the best mean system capacity was selected in order to understand the **MAC ABS e-ICIC** behavior, as shown in Figure 27b. At first glance, it is noted a relation between the number of small cells and n since low values of n provided a higher mean system capacity in layouts with few small cells, while high values of n performed better in layouts with more small cells. It is worth mentioning that this is due to the pullbacks, which are detailed in the next subsection. In terms of distance between macro cell and small cell transmitter, it was noted that fixing one small cell, the **MAC**

ABS e-ICIC using $n = 5$ provided the best performance for any distance value. In contrast, fixing four small cells, $n = 20$ provided the best result for 1300 and 326 meters, while $n = 30$ for 726 meters.

Figure 27 – Mass of data and selection of the best results.

(a) Mass of data through parameter sweeping n.

(b) The best values of MAC ABS e-ICIC in terms of distance and number of small cells.
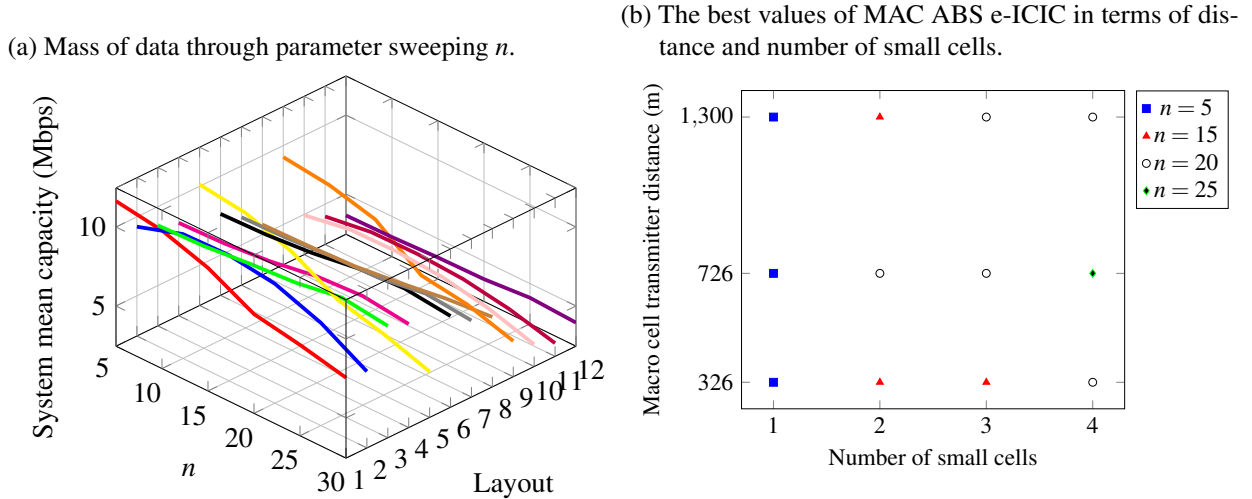
Source: elaborated by the author (2020).

Regarding the results above, it might seem at first sight as a meaningless behavior; however, a quantitative study of pullbacks using the **Baseline** reference algorithm showed the opposite. Figure 28 shows the mean number of pullbacks per subframe for each layout. The increase in the number of small cells causes an increase in the number of pullbacks, which can be controlled through high values of n. In terms of distance, it was noted an increase in the number of pullbacks when the distance changes from 1300 to 726 meters, followed by a subtle drop when it varies to 326 meters, thus the variation in the distance with n does not show a monotonic behavior. Besides that, this explains why n increases from 20 to 25 and then decreases to 20 for layouts with four small cells.

By the way, Figure 28 does not explain the reason for the number of pullbacks for each layout. In order to answer this question, a scatter plot was used to show the layout influence on the pullback, that is, it shows pullbacks in terms of position for each layout, as illustrated in Figure 29. Regarding the creation of Figure 29, it was necessary to find pullbacks in **Baseline** reference algorithm through Algorithms 4 and 5 then the UE location was collected based on the instant the pullback occurred. In general, a concentration of pullbacks can be seen not only close to the macro cell transmitter, but also near to the small cell edge. With this in mind, it was noted an SINR discrepancy between macro UEs of these locations and others, that is, UEs with quality

Figure 28 – Pullback per subframe using the Baseline.
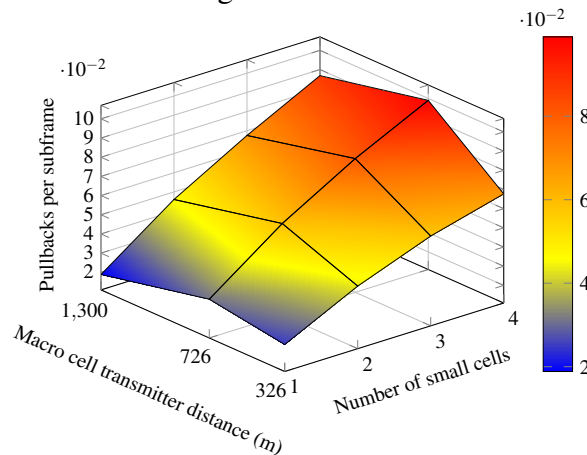
Source: elaborated by the author (2020).

well above or below the average cause a significant disturbance in the capacity time series.

3.4.2 *MAC ABS e-ICIC Algorithms Comparison*

Henceforth, the algorithms will be compared. This way, the system capacity was calculated considering a 95% confidence interval. The following bar plots show the capacity labeled as: **Macro**, for macro cell mean capacity; **Small**, for small cells mean capacity; **System**, for system aggregated mean capacity.

Initially, Figure 30 shows the simulation results for Layout 1. It is noted that **Baseline** provided a system mean capacity of 10.35 Mbps - the performance without interference management. Regarding **Fixed ABS e-ICIC**, it decreased the system capacity when the ABS ratio increases due to a significant drop in macro cell capacity. In addition, it can be noted a variation of the small cell capacity, when the ABS ratio varies from 0.025 up to 0.9. The **Random ABS e-ICIC** kept the small cell capacity within an acceptable level; however, the fact of adding ABSs at random made the macro mean capacity be reduced to 2.9 Mbps. Finally, the **ECO** and **MAC** achieved good results, with **MAC** surpassing **ECO** by approximately 7.5%.

Concerning Layout 2, the mean capacity is illustrated in Figure 30b. As expected, the system mean capacity is reduced compared to Layout 1 due to the increase of interference caused by adding another small cell. This way, **Baseline** provided a system mean capacity of 9.2 Mbps. From the standpoint of the **Fixed ABS e-ICIC**, it provided a system mean capacity of 10.4 Mbps, when the ABS ratio is equal to 0.025. In addition, it can be noted that **Random ABS e-ICIC** obtained a system mean capacity equal to 8.70 Mbps, surpassing **Fixed ABS e-ICIC** performance for ABS ratios above 0.6. At last, the **MAC** presented the best result, however not

significantly - it exceeded **Fixed ABS e-ICIC** by only 0.08% using $n = 15$.

Figure 30c shows the performance for Layout 3. As a consequence of the interference level, **Baseline** provided a system mean capacity of 8.71 Mbps, while **Fixed ABS e-ICIC**
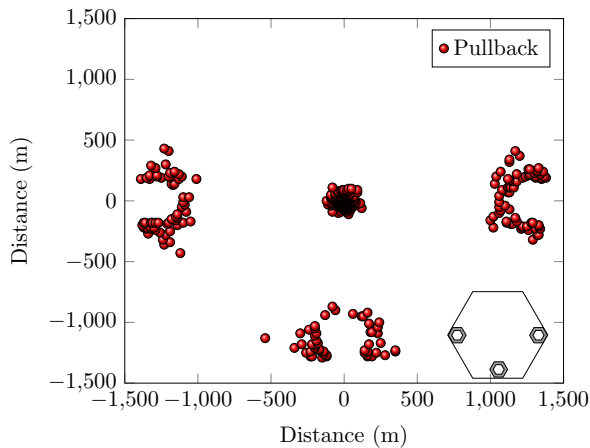
Figure 29 – Pullback mapping for each layout.
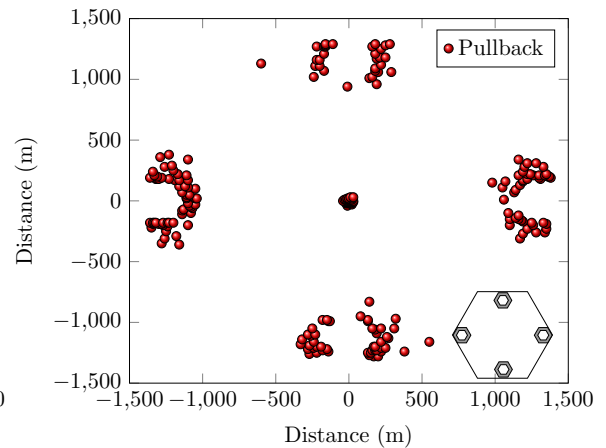
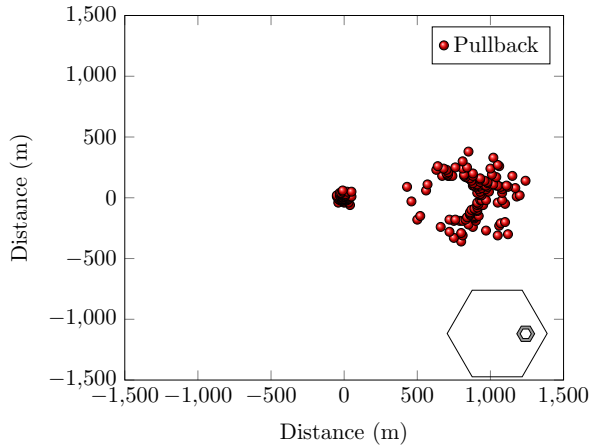(a) Pullbacks for Layout 1.
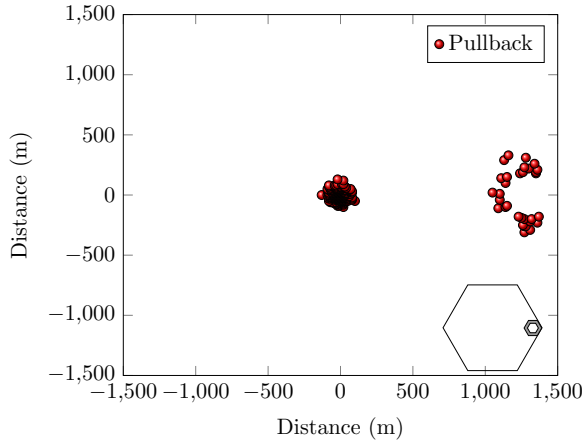
(b) Pullbacks for Layout 2.
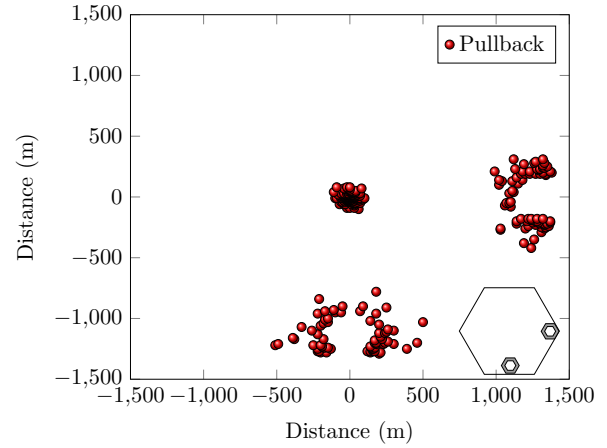
(c) Pullbacks for Layout 3.

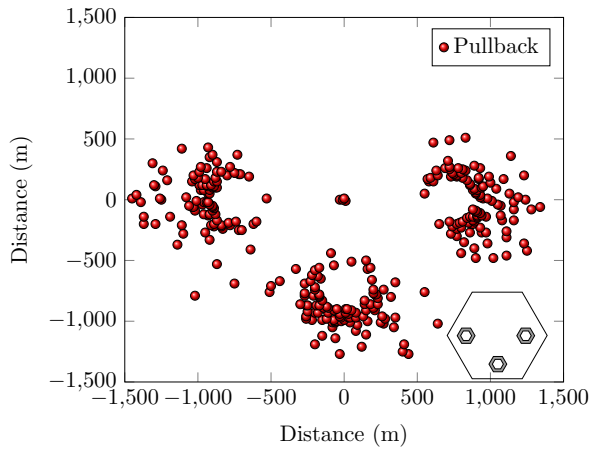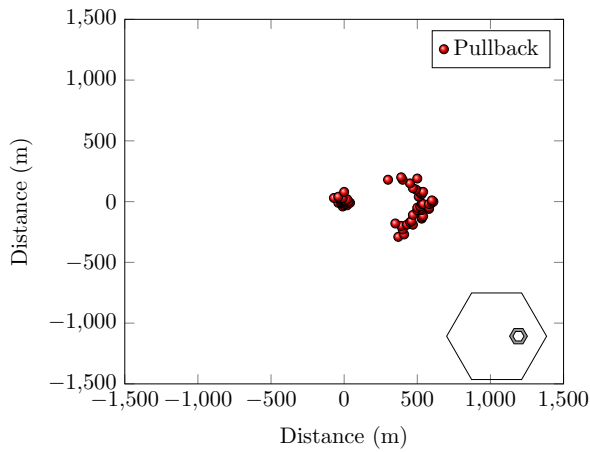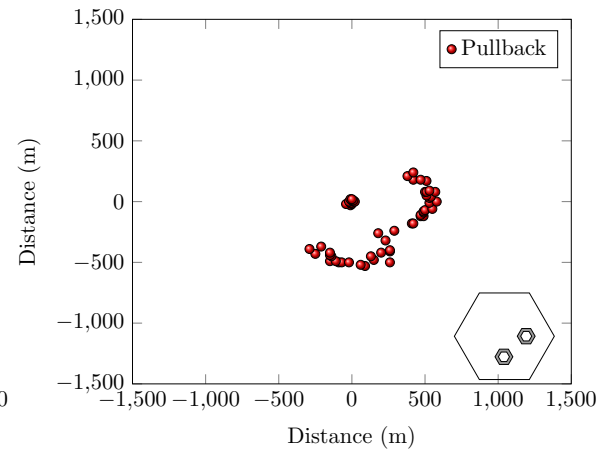
(d) Pullbacks for Layout 4.

(e) Pullbacks for Layout 5.

(f) Pullbacks for Layout 6.
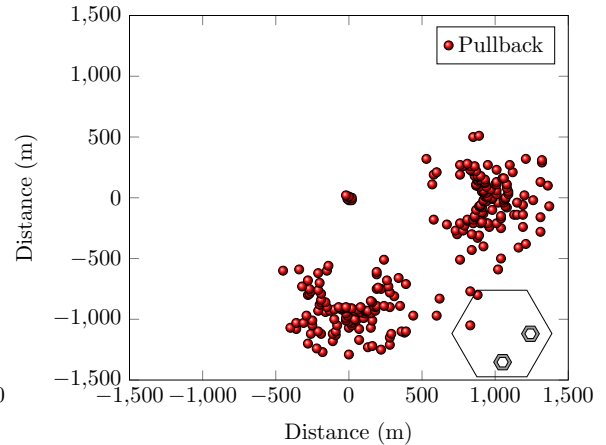
Continues on the next page.

Figure 29 – Pullback mapping for each layout.

(g) Pullbacks for Layout 7.

(h) Pullbacks for Layout 8.
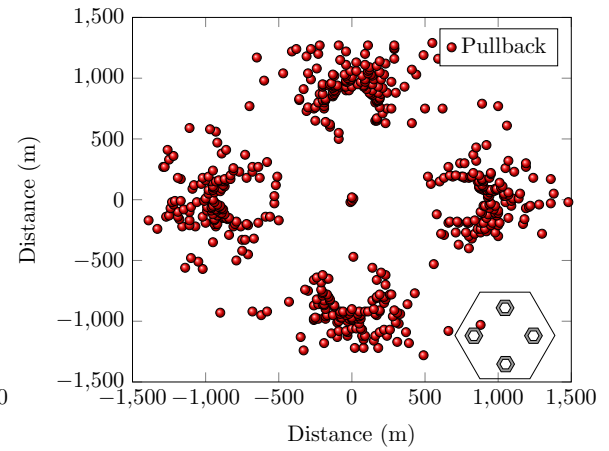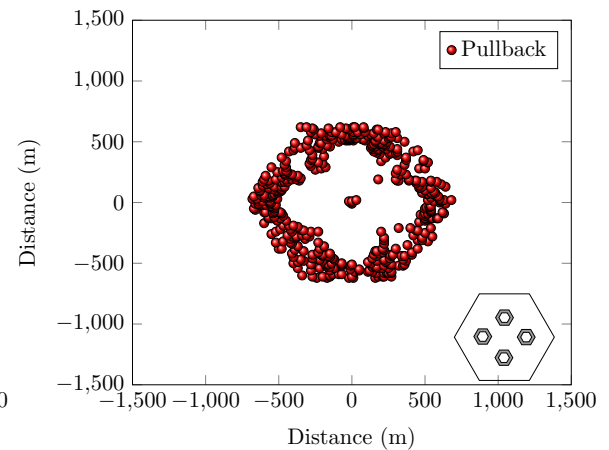

(i) Pullbacks for Layout 9.

(j) Pullbacks for Layout 10.

(k) Pullbacks for Layout 11.
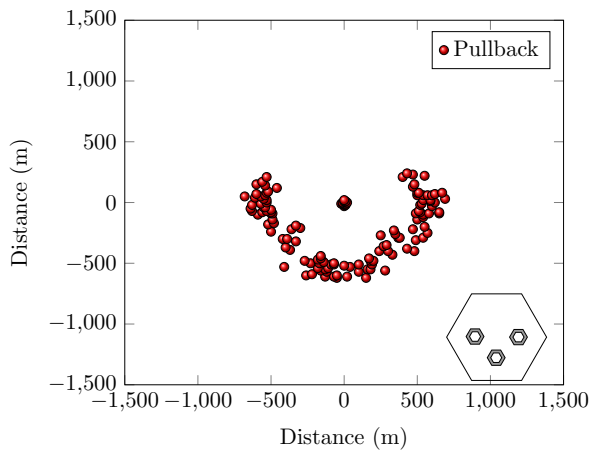
(l) Pullbacks for Layout 12.
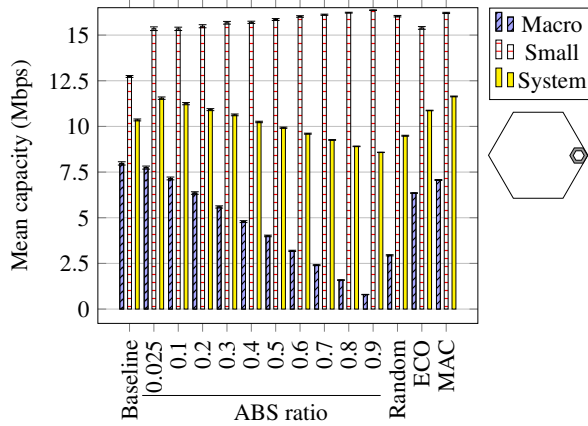

Source: elaborated by the author (2020).

achieved 9.8 Mbps using 0.025. Among the dynamic algorithms, **MAC** outperformed **Random ABS e-ICIC** and **ECO** by approximately 18% and 13%, respectively.

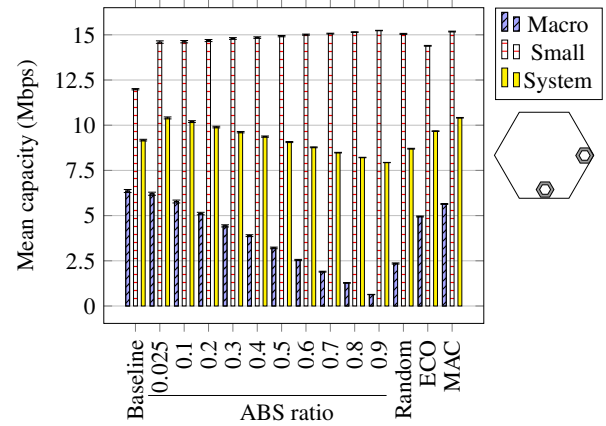Figure 30d illustrates the mean capacity for Layout 4. It can be seen that the

system mean capacity of **Baseline** reached 8.12 Mbps. **Fixed ABS e-ICIC** obtained the best performance using the ABS ratio equal to 0.025. Again, **MAC ABS e-ICIC** established itself as the best strategy, however not significantly - it exceeded **Fixed ABS e-ICIC** by only 0.09%.

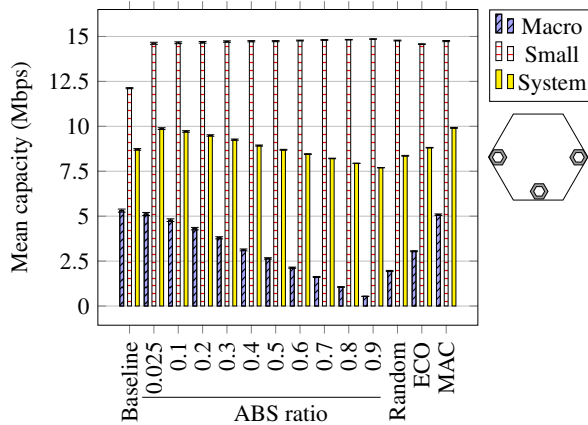Figure 30 – Results for Layouts 1, 2, 3 and 4.
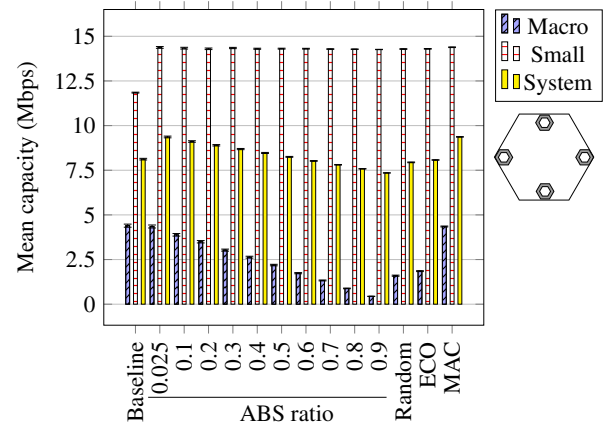
(a) Results for Layout 1.

(b) Results for Layout 2.

(c) Results for Layout 3.

(d) Results for Layout 4.

Source: elaborated by the author (2020).

From now on, a value of 726 meters is adopted as the distance between the macro cell and small cell transmitter. This way, Figure 31 shows the mean capacity for Layout 5 in which **Baseline** achieved a system mean capacity equal to 7.7 Mbps. This performance is overcome by all **Fixed ABS e-ICIC** settings, that is, this layout favors ABS e-ICIC gains. In addition, **Fixed ABS e-ICIC** showed a subtle performance variation regardless of the ABS ratio, providing only a capacity transfer between macro and small cells. For instance, the higher the ABS ratio, the higher the performance gain of the small cell with proportional performance loss of the macro cell, keeping the system capacity unchanged. At last, **MAC** reached the best result using $n = 5$, it overcame the **Fixed ABS e-ICIC** and **ECO** by 14% and 16%, respectively.

Figure 31b shows the simulation results for Layout 6 in which **Baseline** provided a system mean capacity of 6.76 Mbps. Looking at the **Fixed ABS e-ICIC** results, it is noted that the small cell mean capacity variation for Layout 6 is 11% less than in Layout 5 due to the inclusion of another small cell in the central ring. Concerning **MAC**, it overcomes the **Fixed ABS e-ICIC**, **Random ABS e-ICIC**, and **ECO** by 9%, 21%, and 18%, respectively.

Regarding Layout 7, Figure 31c shows that **Baseline** decreased system mean capacity to 6.06 Mbps due to not only the proximity of the small cell to the macro cell transmitter but also the proximity of the small cells to each other. For **Fixed ABS e-ICIC**, it can be noted that the gain provided by the small cell does not support the significant loss of the macro cell by adopting high ABS ratios, resulting in the worst performance when using 0.9. From dynamic algorithms standpoint, **MAC ABS e-ICIC** had a gain of 15% and 14% when compared to **Random ABS e-ICIC** and **ECO**, respectively.

Figure 31d shows the performance of strategies for Layout 8, that is, the macro cell transmitter is surrounded by interference. In this situation, **Baseline** achieved a system mean capacity of 5.60 Mbps. For **Fixed ABS e-ICIC**, it is noted that the small cell mean capacity variation for Layout 8 is 25% less than in Layout 5 due to the inclusion of three small cells in the central ring. Concerning **MAC ABS e-ICIC**, it overcame the **Random ABS e-ICIC** and **ECO** by 16% and 8%, respectively.

The following figures are specific for layouts where the small cells are located in the macro cell inner ring. The performance evaluation for Layout 9 is shown in Figure 32. Regarding **Baseline**, it can be seen as the worst strategy to be applied in the system because it provided only 4.98 Mbps. For **Fixed ABS e-ICIC**, it can be seen a new behavior in which the system mean capacity increases for a higher ABS ratio. The reason for this behavior is the small cell capacity discrepancy between edge and center users, that is, edge users have high capacity. Again, **MAC ABS e-ICIC** provided the best result, reaching a gain of 17%, 26%, and 23% when compared to **Fixed ABS e-ICIC**, **Random ABS e-ICIC** and **ECO**, respectively.

Figure 32b shows the mean capacity for Layout 10. It is noted that **Baseline** provided the lowest result, reaching a system mean capacity of 4.09 Mbps. Looking at the **Fixed ABS e-ICIC** results, it is noted a system mean capacity of 4.4 Mbps using a ABS ratio equals to 0.025. Concerning **MAC ABS e-ICIC**, it overcame the **Fixed ABS e-ICIC**, **Random ABS e-ICIC**, and **ECO** by 12%, 28%, and 25%, respectively.
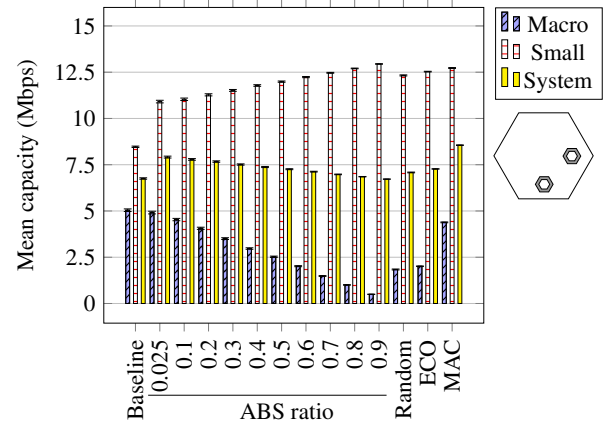
According to the Figure 32c, **Baseline** obtained 3.60 Mbps in Layout 11. For **Fixed**
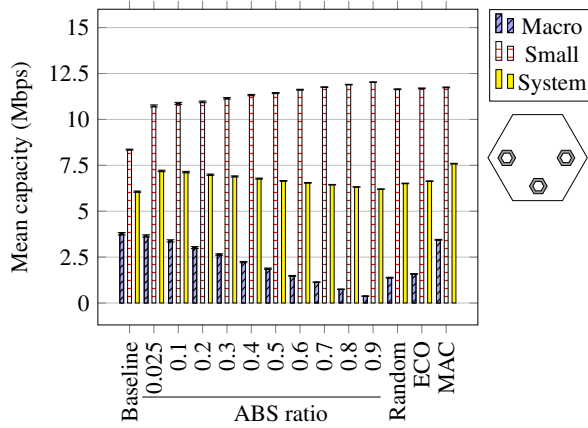
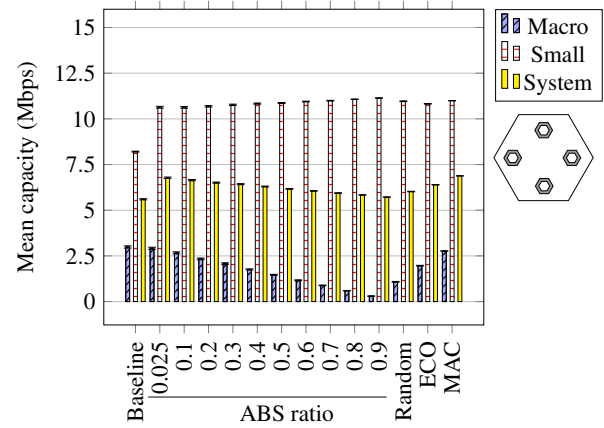Figure 31 – Results for Layouts 5, 6, 7 and 8.

(a) Results for Layout 5.
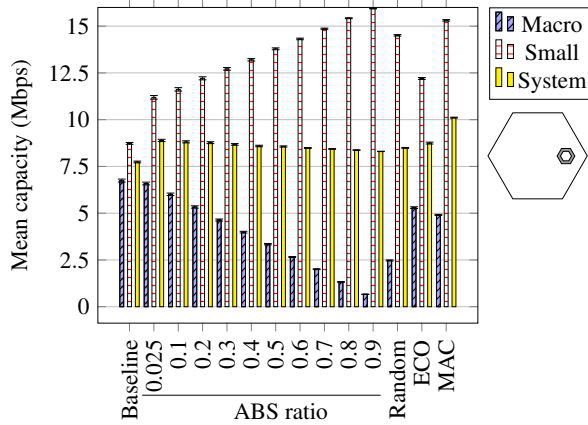
(b) Results for Layout 6.

(c) Results for Layout 7.

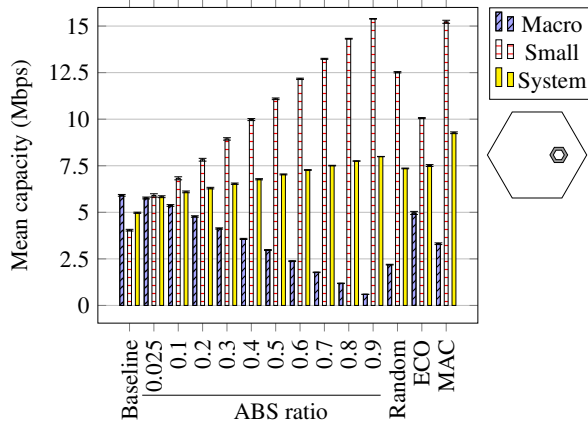(d) Results for Layout 8.

Source: elaborated by the author (2020).

ABS e-ICIC, it is noted that the small cell mean capacity variation for Layout 11 is 92% less than in Layout 9 due to the inclusion of three small cells in the inner ring. With regard to **MAC**, it overcame the **Fixed ABS e-ICIC**, **Random ABS e-ICIC**, and **ECO** by 7%, 27%, and 26%, respectively. Figure 32d shows the performance of strategies for Layout 12. It can be seen that **Baseline** reached a system average capacity of 3.24 Mbps. In this challenging layout, **MAC** had a gain of 3%, 28% and 21% when compared to **Fixed ABS e-ICIC**, **Random ABS e-ICIC**, and **ECO**, respectively.

3.5   Chapter Summary

In this chapter, it was noted that there exists a relationship between the layouts, pullbacks and **MAC ABS e-ICIC** parametrization. For example, at a distance of 726 meters between the macro cell transmitter and small cell transmitters, a scattering of pullbacks were

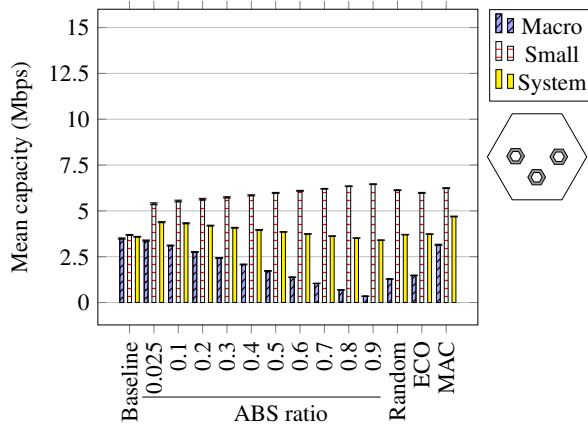Figure 32 – Results for Layouts 9, 10, 11 and 12.

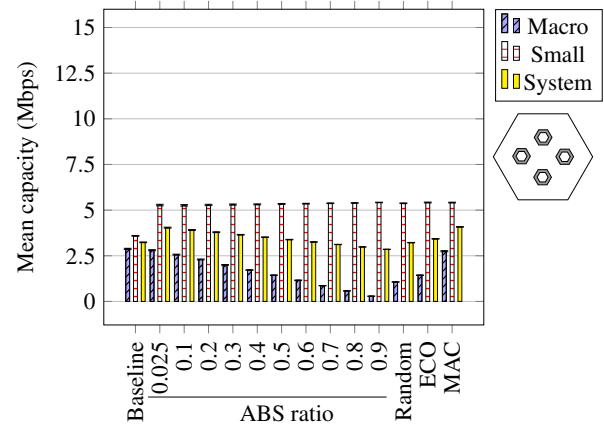(a) Results for Layout 9.

(b) Results for Layout 10.
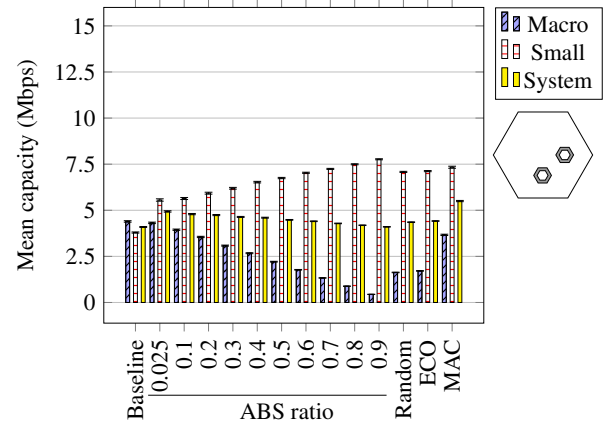
(c) Results for Layout 11.

(d) Results for Layout 12.

Source: elaborated by the author (2020).

verified in the macro cell area. As a result, the macro cell capacity disturbance is high. In order to overcome this situation, it is necessary to use the **MAC ABS e-ICIC** with higher window size values.

Besides, the results show evidence that the **MAC ABS e-ICIC** provides performance gains in all tested layouts. In general, the gains are more expressive in layouts where the small cell is closer to the macro cell transmitter. The largest gain provided by **MAC ABS e-ICIC** was 86% on Layout 9, while the lowest gain was 12% on Layout 1.

It is important to highlight that ABS does not guarantee performance gains. For instance, **Random ABS e-ICIC** showed a loss in Layouts 1, 2, 3, 4, and 12 of 8%, 5%, 4%, 2%, and 0.5%, respectively.

4 DYNAMIC E-ICIC USING MACD

In view of the results obtained by **MAC ABS e-ICIC**, this chapter aims to answer **"Does a strategy considering the historical volatility bring additional gain?"**. With this in mind, the **MACD ABS e-ICIC** algorithm is proposed followed by its parameterization and achieved capacity. In addition, some questions are discussed about behavior and performance of all proposed and tested algorithms.

4.1 Algorithm proposal: MACD for the ABS

In order to keep a fair basis between **MAC ABS e-ICIC** and **MACD ABS e-ICIC** results, the same methodology is used, that is, **time** t is defined as **subframe** k. Thus, the window size n is measured in the number of subframes; the **price** is the **macro cell capacity**, and $N_{sf} = 1000$.

Similarly to **MAC ABS e-ICIC**, the **MACD ABS e-ICIC** works properly when well parameterized. Thus, the first step is to set n_1, n_2, and n_{sig}, observing that $n_1 < n_2$. After **MACD ABS e-ICIC** parameterization, the second step is to store the capacity reached by the user u allocated in subframe k, that is, $C_k^{macro} = C_{u,k}^{macro}$. Then, the algorithm checks if $k \geq n_2 + n_{sig} - 1$, because it is necessary to have a sufficient amount of capacity values before calculating the MACD. If the amount of data is sufficient, $EMA_k(n_1)$ and $EMA_k(n_2)$ are calculated as:

$$EMA_k(n_1) = \left(1 - \frac{n_1 - 1}{n_1 + 1}\right) \sum_{i=1}^{\infty} \left(\frac{n_1 - 1}{n_1 + 1}\right)^{i-1} C_{k-i+1}^{macro}, \tag{4.1}$$

and

$$EMA_k(n_2) = \left(1 - \frac{n_2 - 1}{n_2 + 1}\right) \sum_{i=1}^{\infty} \left(\frac{n_2 - 1}{n_2 + 1}\right)^{i-1} C_{k-i+1}^{macro}. \tag{4.2}$$

Then, assuming $t = k$, $MAC_k(n_1, n_2)$, $Signal_k(n_{sig})$, and $MACD_k(n_1, n_2, n_{sig})$ are calculated according to (2.26), (2.27), and (2.28), respectively. The final step of the proposed algorithm is to define ABSs based on the trading signal that can be expressed as:

$$TS_{k+1}(n_1, n_2, n_{sig}) = \begin{cases} \text{Non} - \text{ABS}, & \text{if } MACD_k(n_1, n_2, n_{sig}) > 0, \\ \text{ABS}, & \text{if } MACD_k(n_1, n_2, n_{sig}) \leq 0. \end{cases} \tag{4.3}$$

Algorithm 2 shows the pseudo-code of the proposed **MACD ABS e-ICIC** method.

Algorithm 2: Proposed MACD ABS e-ICIC Algorithm.

   Ensure: Set n_1, n_2 and n_{sig}

     for $k \leftarrow 1$ **to** N_{sf} **do**

       $C_k^{\text{macro}} \leftarrow C_{u,k}^{\text{macro}}$

       if $k \geq n_2 + n_{\text{sig}} - 1$ **then**

         Compute $MACD_k(n_1, n_2, n_{sig})$ of C_k^{macro}

         if $MACD_k(n_1, n_2, n_{\text{sig}}) \leq 0$ **then**

           Sell signal: set next subframes as ABS

         else

           if $MACD_k(n_1, n_2, n_{\text{sig}}) > 0$ **then**

             Buy signal: set next subframes as non-ABS

           end if

         end if

       end if

     end for

4.2 Parametrization of MACD ABS e-ICIC

First of all, n_1, n_2, and n_{sig} parameterization strategy is performed through parameter sweeping. It is important to mention that the axes of Figures 34 and 35 referring to Layouts with 2 to 4 small cells are standardized for better visualization and comparison of the curves. The parameter sweeping in Layout 1 shows that high values of n_1, n_2, and n_{sig} cause a decrease in terms of capacity, as shown in Figure 33a. The main reason for this behavior is the excessive elimination of C_k^{macro} fluctuations caused by the high values of n_1, n_2, and n_{sig}. In these configurations, the **MACD ABS e-ICIC** is highly smooth (insensitive), producing long buy and sell signals that impair the algorithm's performance. In order to avoid long trading signals in Layout 1, it is necessary to use parameters with low values, keeping **MACD ABS e-ICIC** less smooth (i.e., more reactive) to offer good trading signals. So, the best configuration occurs to $n_1 = 5$, $n_2 = 10$, and $n_{sig} = 5$. The parameter sweeping for Layout 2 shows that the best system mean capacity is achieved to $n_1 = 15$, $n_2 = 20$, and $n_{sig} = 5$, as illustrated in Figure 33b. A capacity loss due to increased pullbacks is avoided when n_1 and n_2 increase. Regarding the Layout 3, the best system mean capacity is achieved to $n_1 = 5$, $n_2 = 15$, and $n_{sig} = 25$, as shown in Figure 33c. At last, among the layouts at a distance of 1300 meters, Layout 4 has the largest number of pullbacks, which can be reduced using $n_1 = 10$, $n_2 = 25$, and $n_{sig} = 15$, as illustrated in Figure 33d.

Similar to financial problems, the parameterization of **MACD ABS e-ICIC** is a crucial point because there is a difference between the best and worst results equal to 67%, 53%, 39%, and 32% for Layouts 1 to 4, respectively.

Figure 33 – System mean capacity for Layouts 1, 2, 3, and 4 through parameter sweeping.

(a) Layout 1.

(b) Layout 2.
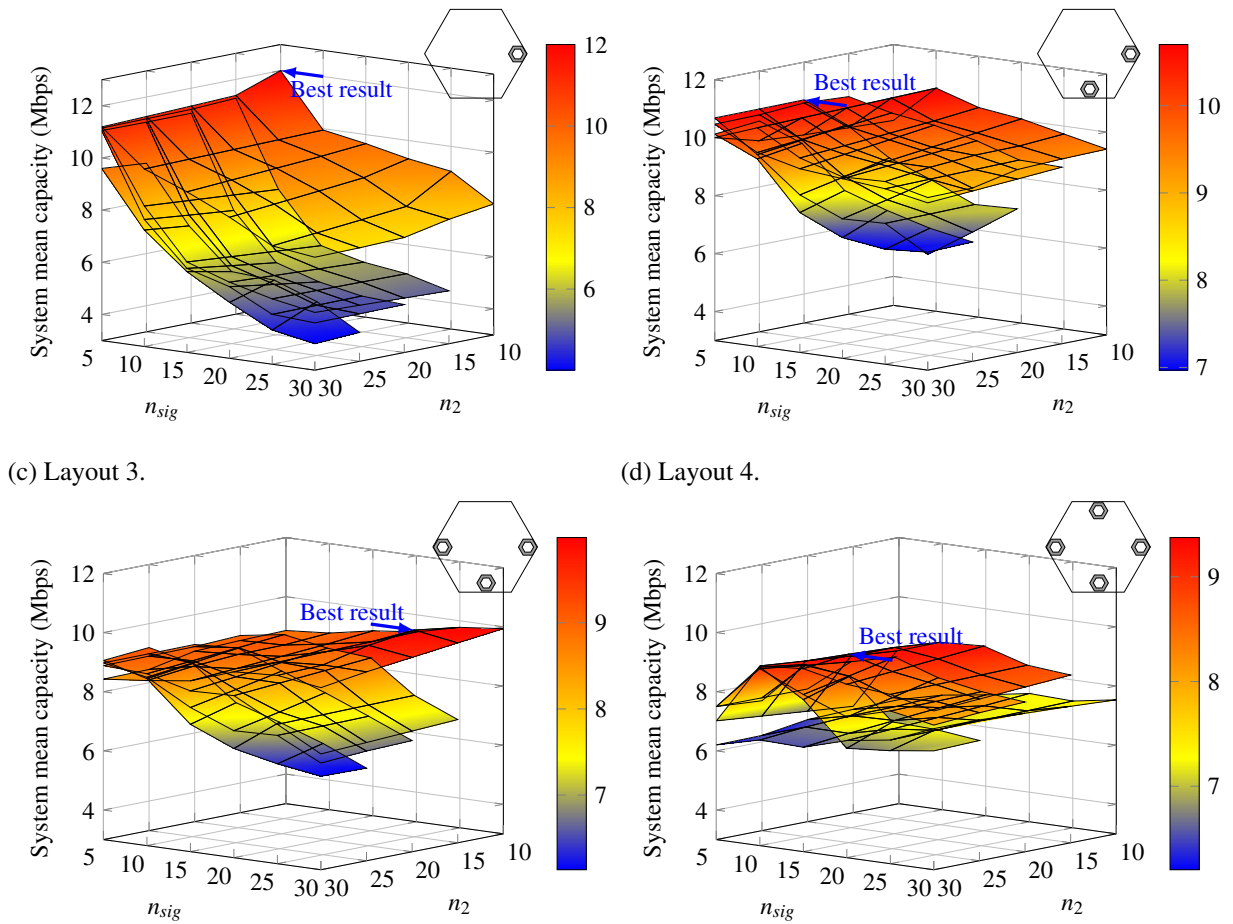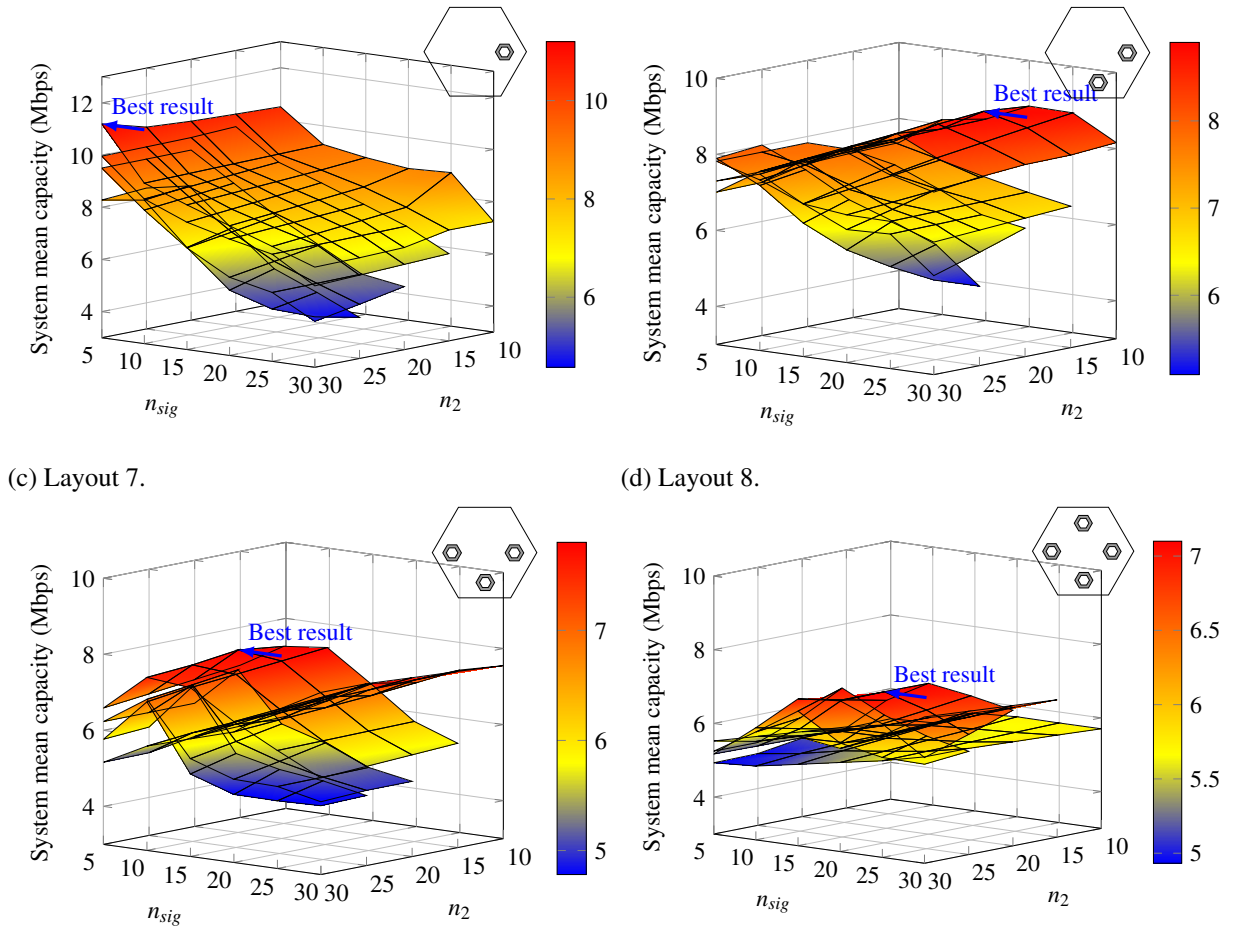

(c) Layout 3.

(d) Layout 4.

Source: elaborated by the author (2020).

The next analysis refers to the small cells at 726 meters from the macro cell transmitter. In Layout 5, the best system mean capacity occurs in configuration $n_1 = 5$, $n_2 = 30$, and $n_{sig} = 5$ because the level of pullbacks is low, as illustrated in Figure 34a. The worst results are within the quadrant formed by values of n_2 and n_{sig} above 20. From Layout 5 to Layout 6, the best performance is achieved by maintaining the value of n_1, decreasing n_2, and increasing n_{sig}, as shown in Figure 34b. With regard to the Layout 7, the good settings occur on the surface center, with $n_1 = 10$, $n_2 = 20$, and $n_{sig} = 10$ as the best parameters. For Layout 8, the location and number of small cells boost the disturbance in the system, which is the main reason for the highest number of pullbacks (0.55 pullbacks per subframe). However, this disturbance is controlled using $n_1 = 15$, $n_2 = 25$, and $n_{sig} = 20$, as illustrated in Figure 34d.

The analysis of the small cell at the inner ring is started by Layout 9, where the best result occurred for $n_1 = 5$, $n_2 = 25$, and $n_{sig} = 5$, as illustrated in Figure 35a. It is worth mentioning that when analyzing layouts with only one cell, the best results are obtained with

Figure 34 – System mean capacity for Layouts 5, 6, 7, and 8 through parameter sweeping.

(a) Layout 5.

(b) Layout 6.

(c) Layout 7.

(d) Layout 8.

Source: elaborated by the author (2020).

the same value of n_1 and n_{sig}, while n_2 is modified. So, n_2 acts as a fine adjustment since the difference of pullbacks between these layouts are subtle. The result for Layout 10 is illustrated in Figure 35b. The best system mean capacity is 6.04 Mbps using $n_1 = 10$, $n_2 = 20$, and $n_{sig} = 5$. The parameter sweeping for Layout 11 shows that the best performance is achieved for $n_1 = 5$, $n_2 = 25$, and $n_{sig} = 10$, while the worst is achieved to $n_1 = 20$, $n_2 = 30$, and $n_{sig} = 30$, as illustrated in Figure 35c. Finally, Figure 35d shows the results for Layout 12 in which the best system mean capacity occurred to $n_1 = 10$, $n_2 = 15$, and $n_{sig} = 10$. In order to highlight the effects of parameterization, it is noted that inadequate parameters can cause a capacity loss equal to 74%, 56%, 43%, and 41% for Layouts 9 to 12, respectively.

Figure 35 – System mean capacity for Layouts 9, 10, 11, and 12 through parameter sweeping.

(a) Layout 9.   (b) Layout 10.

(c) Layout 11.   (d) Layout 12.
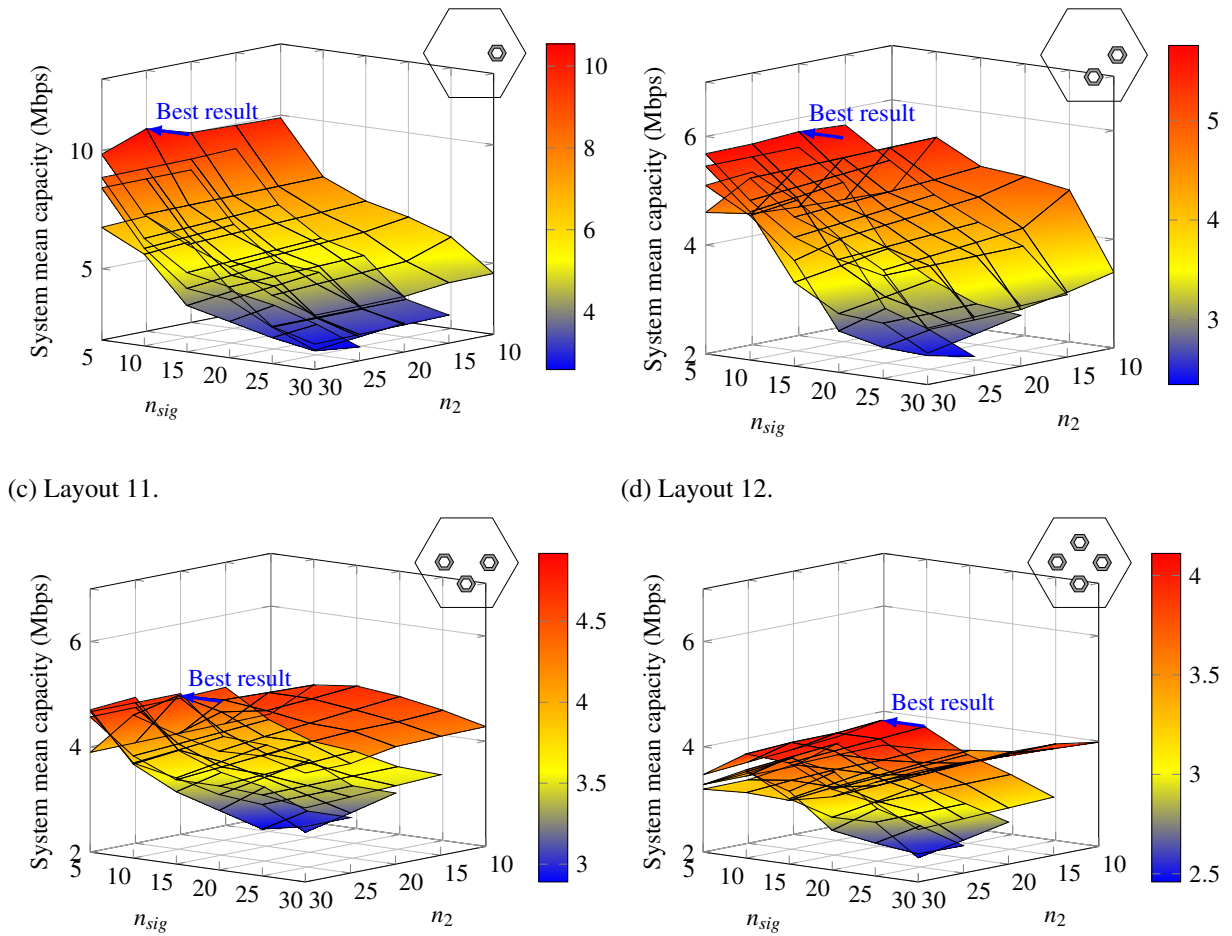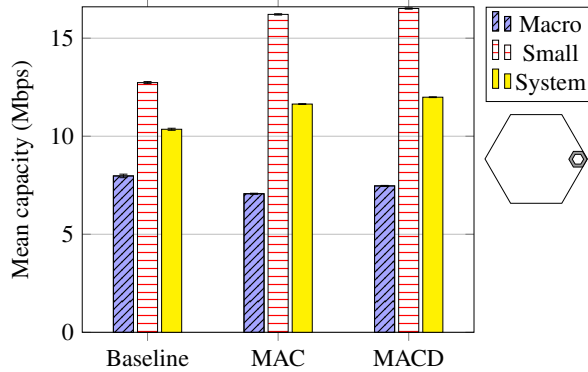

Source: elaborated by the author (2020).

4.3 Results

Henceforth, the best **MACD ABS e-ICIC** results are compared with **Baseline** and **MAC ABS e-ICIC** without the result of **Fixed ABS e-ICIC**, since **MAC ABS e-ICIC** surpassed all results obtained by **Fixed ABS e-ICIC**. Figure 36a shows the mean capacity for Layout 1. The **MACD ABS e-ICIC** surpassed all other strategies, reaching a system mean capacity of 11.99 Mbps. When adding another small cell, the **MACD ABS e-ICIC** provided a capacity of 10.70 Mbps - the best result among all the strategies - using the $n_1 = 15$, $n_2 = 25$, and $n_{sig} = 5$, as shown in Figure 36b. Furthermore, it is worth mentioning that the capacity gain between **MACD ABS e-ICIC** and **MAC ABS e-ICIC** in Layout 1 is 3%, while in Layout 2 it was 2.9%. The results for Layout 3 and 4 are illustrated in Figures 36c and 36d. **MACD ABS e-ICIC** obtained system mean capacity of 9.99 and 9.38 Mbps, respectively. Besides, it can be confirmed by Layout 3 and 4 a downward trend of ABS gain, since the capacity gain between **MACD ABS**
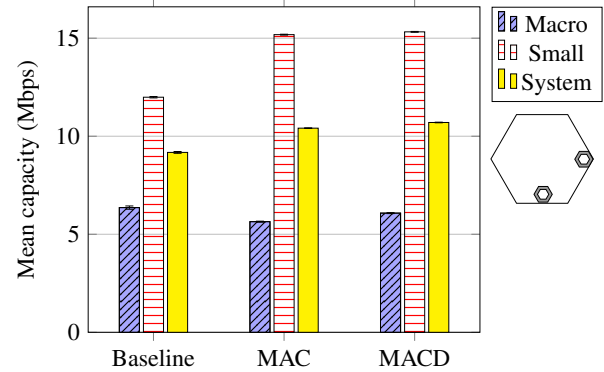
e-ICIC and **MAC ABS e-ICIC** decreased to 0.8% and 0.1%.

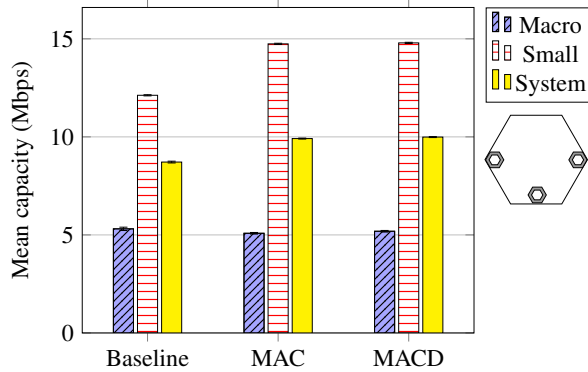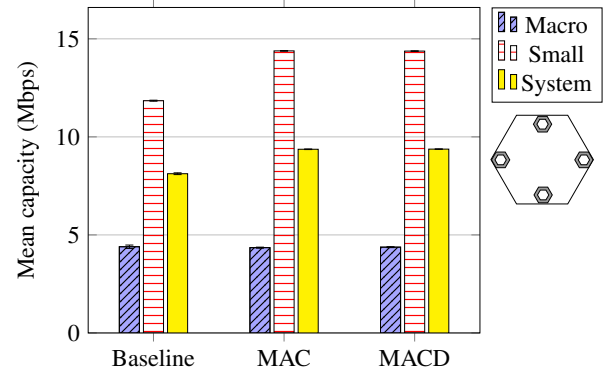Figure 36 – MACD results for Layouts 1, 2, 3, and 4.

(a) Layout 1.

(b) Layout 2.
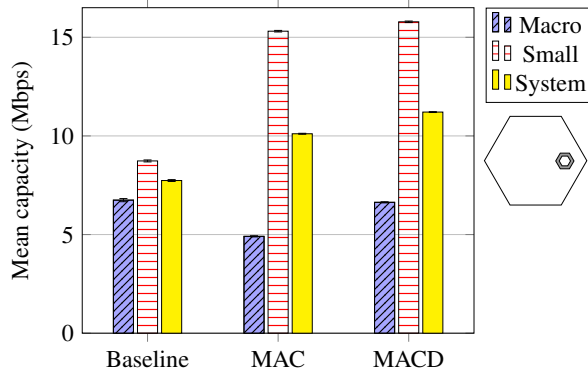

(c) Layout 3.

(d) Layout 4.

Source: elaborated by the author (2020).

From now on, Figure 37 illustrates the results obtained by **Baseline**, **MACD ABS e-ICIC**, and **MACD ABS e-ICIC**, when the distance between the macro cell and small cell transmitter is 726 meters. In Layout 5, **Baseline** achieves a system mean capacity of 7.7 Mbps, that is, the worst performance, while **MACD ABS e-ICIC** reached the best result because it overcomes the **Baseline** and **MAC ABS e-ICIC** by 46% and 11%, respectively. The numerical simulations of Layout 6 showed that **Baseline** provided a system mean capacity of 6.76 Mbps, which is overtaken by 34% when adopting **MACD ABS e-ICIC**. Besides, **MACD ABS e-ICIC** overcomes **MAC ABS e-ICIC** by 6%. Regarding Layout 7, Figure 37c shows that **Baseline** decreased system mean capacity to 6.06 Mbps. From dynamic algorithms standpoint, **MACD ABS e-ICIC** has a gain of 4% when compared to **MAC ABS e-ICIC**. In Layout 8, **Baseline** achieves a system mean capacity of 5.60 Mbps. Concerning **MACD ABS e-ICIC**, it overcomes the **Baseline** and **MAC ABS e-ICIC** by 27% and 3%, as shown in Figure 37d.
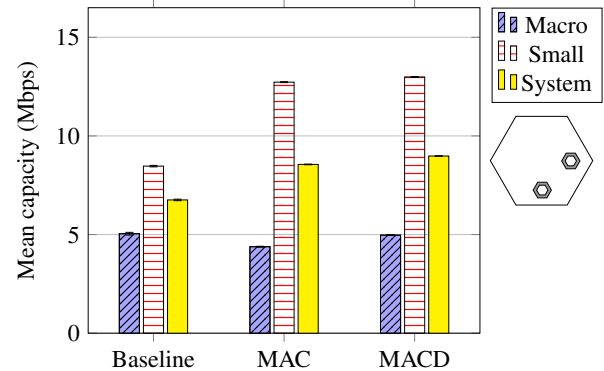
Figure 38a shows the results for Layout 9. As analyzed in other layouts, the ABS

Figure 37 – MACD results for Layouts 5, 6, 7, and 8.
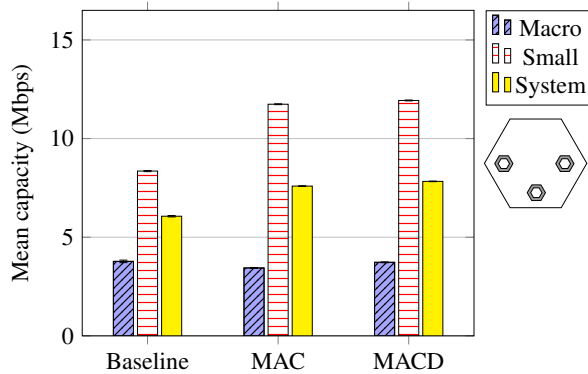
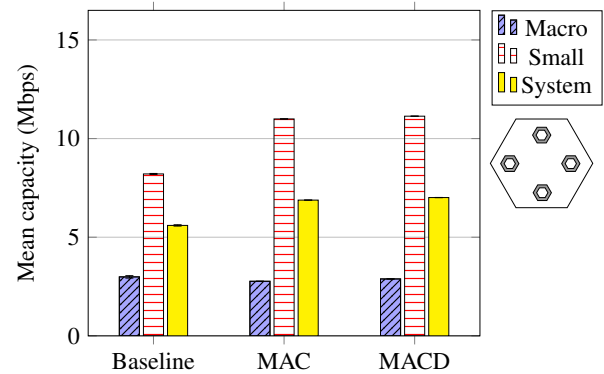(a) Layout 5.   (b) Layout 6.

(c) Layout 7.   (d) Layout 8.

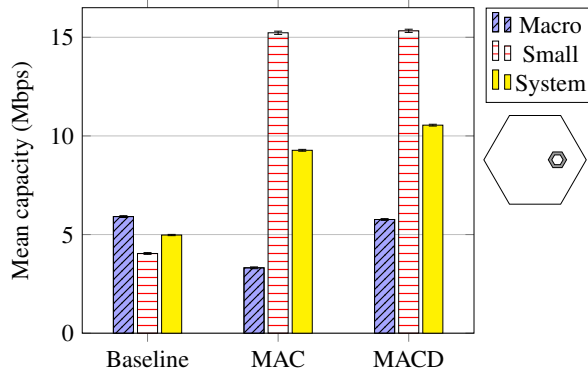Source: elaborated by the author (2020).

remains essential, since all algorithms that use ABS properly surpass the **Baseline** capacity. Again, **MACD ABS e-ICIC** provides the best result, with high performance for both macro and small cells, reaching a system mean capacity of 10.60 Mbps using $n_1 = 5$, $n_2 = 25$, and $n_{sig} = 5$. At this moment, it is possible to perceive a significant drop when modifying a layout from one to two small cells. It is caused by the addition of interference to the small cell edge users. Even so, **MACD ABS e-ICIC** performance is expressive, obtaining a system mean capacity of 6.04 Mbps, as illustrated in Figure 38b. At last, the **MACD ABS e-ICIC** keeps the best system mean capacity for Layout 11 and 12, achieving 4.93 and 4.11 Mbps, respectively.

In order to highlight the results, Figure 39 shows relative gains (in terms of mean capacity) of ABS e-ICIC strategies compared to **Baseline**. Among all the strategies and layouts, the worst performance is for **Random ABS e-ICIC**, achieving a loss of 8.4% in Layout 1. This is evidence that the ABS ratio cannot be defined by chance. On the opposite side, the **MACD ABS e-ICIC** provides a gain of 112% in Layout 9.
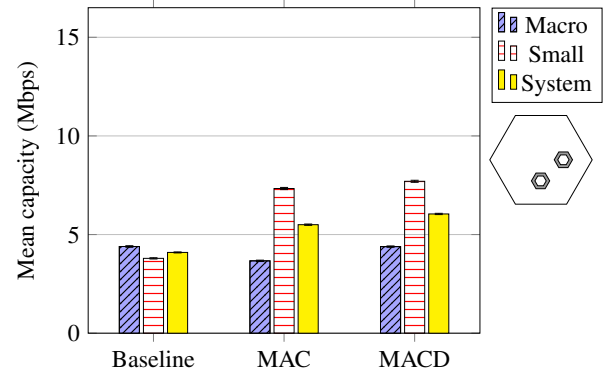
By the way, Table 3 groups all the relative gains obtained during the numerical simulations and computes the mean for each algorithm. **Random ABS e-ICIC** has the worst

Figure 38 – MACD results for Layouts 9, 10, 11, and 12.

(a) Layout 9.   (b) Layout 10.
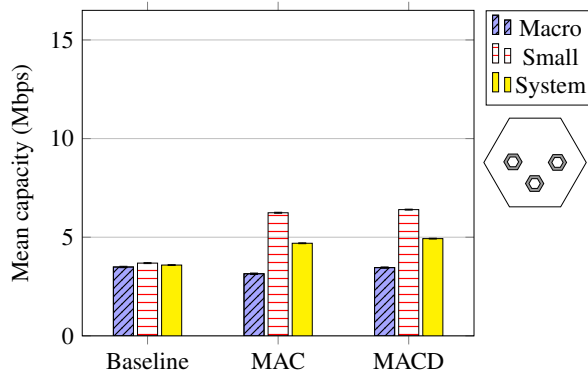
(c) Layout 11.   (d) Layout 12.
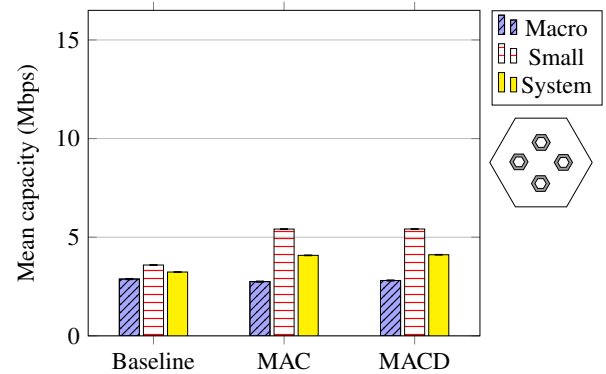
Source: elaborated by the author (2020).

performance because it obtains a mean relative gain of 5.55%. In the penultimate and the third position are **ECO** and **Fixed ABS e-ICIC** with gains of 10.31% and 21.11%, respectively. Finally, the two best results were obtained by **MAC ABS e-ICIC** and **MACD ABS e-ICIC**, reaching 28.16% and 34.88%, respectively. This way, the use of three RAMAs, specifically the **MACD ABS e-ICIC**, improve the results, since it provides a variety of parameterization for different scenarios.

From now on, some questions that arose during the development of this thesis are discussed. For instance:

1. Why is there an upward trend in Figure 39 when the distance between macro and small cells decreases?

   Distance has a direct relation with the interference level suffered by macro and small cell users. In other words, the decrease of distance causes an increase of interference suffered by small cell users due to the proximity of the macro cell transmitter. Similarly, the best macro users raise the level of interference due to the proximity of the small cell

Figure 39 – Relative capacity gain of the different ABS approaches in each tested layout.

(a) Layouts with one small cell.
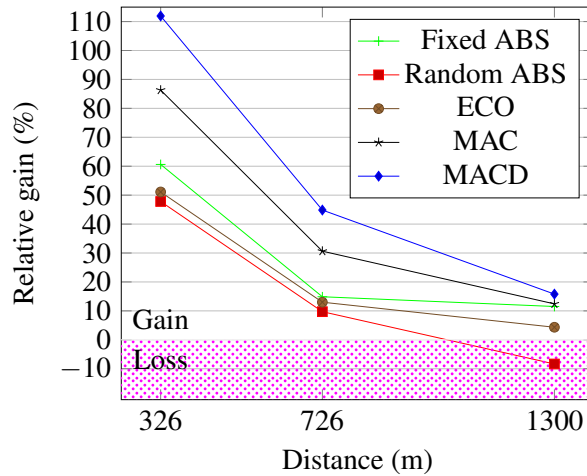
(b) Layouts with two small cells.
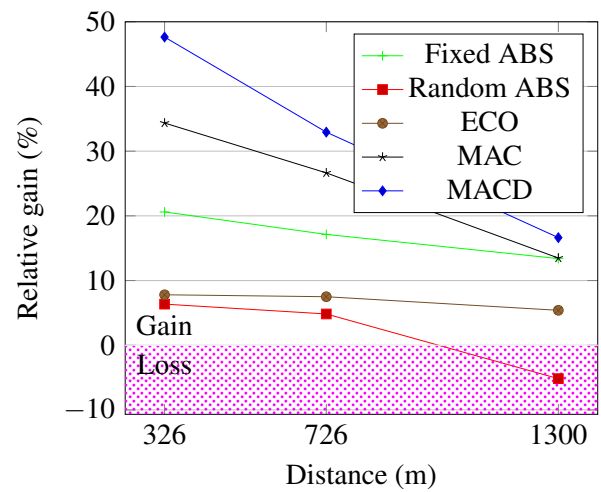
(c) Layouts with three small cells.
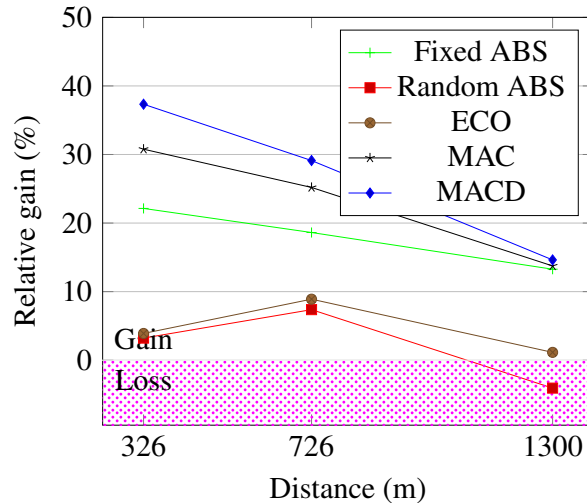
(d) Layouts with four small cells.
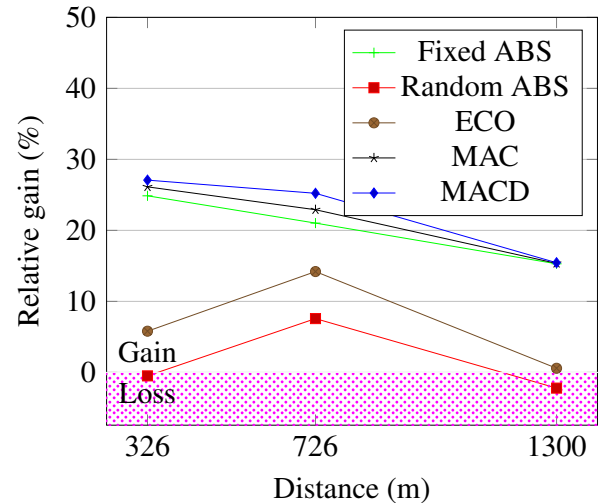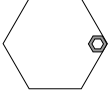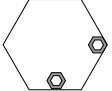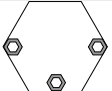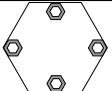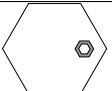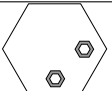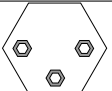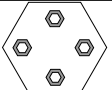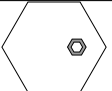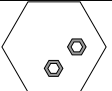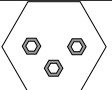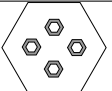
Source: elaborated by the author (2020).

transmitter. So, the good performance of interference management techniques combined with underperforming **Baseline** contributes to the increase in relative gain.

2. Why does a higher number of small cells cause the approximation of performances among **Fixed ABS e-ICIC**, **MAC ABS e-ICIC**, and **MACD ABS e-ICIC**?

In order to understand this behavior, the link quality of edge and center users for Layouts 9, 10, 11, and 12 are analyzed, as illustrated in Figure 40. Looking at Layout 9, it can be seen a difference of 26.7 dB between edge and center users in terms of SINR, allowing more significant ABS gains. However, this variation decreases to 3.8 dB in Layout 12, limiting the gain provided by ABS. So, the increase of small cells equalize the link quality of edge and center users, reducing the gain offered by ABS.

Table 3 – Mean relative gain (%) for each layout.

Layout	Illustration	Fixed	Random	ECO	MAC	MACD
1		11.51	-8.35	4.34	12.41	15.79
2		13.39	-5.16	5.40	13.47	16.63
3		13.26	-4.07	1.14	13.74	14.62
4		15.29	-2.21	0.58	15.35	15.44
5		14.87	9.72	13.00	30.63	44.84
6		17.13	4.83	7.50	26.64	32.94
7		18.62	7.37	8.90	25.19	29.11
8		21.02	7.57	14.2	22.91	25.22
9		60.61	47.80	51.10	86.31	111.92
10		20.60	6.35	7.80	34.35	47.63
11		22.13	3.22	3.90	30.77	37.33
12		24.86	-0.49	5.80	26.13	27.07
Mean		21.11	5.55	10.31	28.16	34.88

Source: elaborated by the author (2020).

3. Why does the **Random ABS e-ICIC** gain reduce with the increased number of small cells at 326 meters?

Two factors can explain this behavior; the first is related to link quality because ABS provides a more significant gain in Layout 9 than Layout 12, as explained earlier. The second factor that contributes to this falling behavior can be understood through a region that contains the possible capacity values in a subframe, as illustrated in Figure 41. It was modeled from maximum and minimum capacity values obtained through numerical simulations.

The ABS problem divides this region into three parts:

- Gain: Part of the region in which ABS provides gain;
- Neutral: Part of the region in which ABS does not provide either gain or loss;
- Loss: Part of the region in which ABS provides loss.

Figures 41a shows the capacity region of Layout 9. ABS provides gain, neutral, and loss corresponding to 25.73%, 0.67%, and 73.60% of the region, respectively. In contrast, Figure 41b shows the capacity region of Layout 12, where it is verified that ABS provides gain, neutralized, and loss corresponds to 5.81%, 0.39%, and 93.80% of the region, respectively. It is worth emphasizing that **Random ABS e-ICIC** does not have logic in choosing ABS; that is, it risks a solution. So, the probability of loss in Layout 12 is higher than in Layout 9, causing a drop in relative gain. It is important to emphasize that this analysis is an estimate because the capacity has continuous features, resulting in infinite values.

Figure 40 – Communication link quality of edge and center users for Layouts 9, 10, 11, and 12.
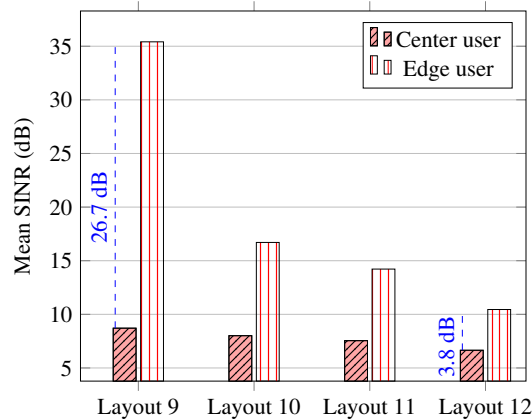
Source: elaborated by the author (2020).

Figure 41 – Possible capacity values in a subframe.
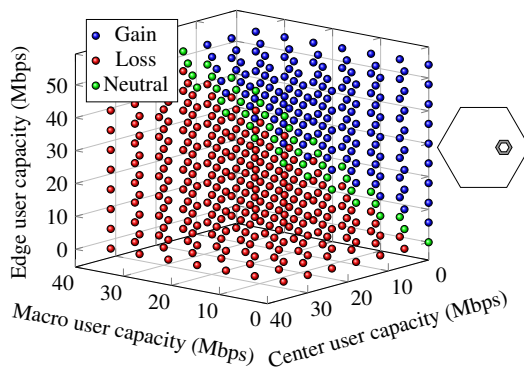
(a) Layout 9.   (b) Layout 12.
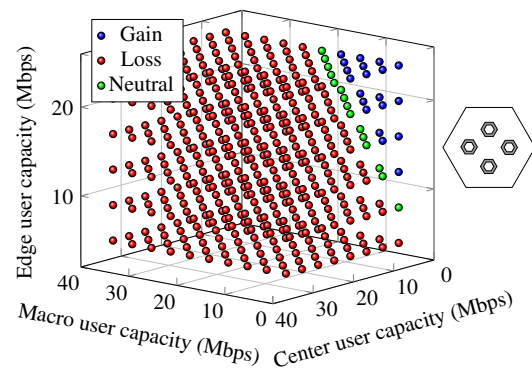
Source: elaborated by the author (2020).

4.4   Chapter Summary

In this chapter, the good results obtained by **MACD ABS e-ICIC** were presented. Such results surpassed all the comparison strategies mentioned in the thesis. The main reason for the good result of **MACD ABS e-ICIC** is due to the fact that the strategy allocates ABS in an opportunistic way when the capacity of the macro cell is in a downward trend. In addition, the signal causes the **MACD ABS e-ICIC** to become more cautious in the allocation of ABS, that is, the allocation is made when a downward trend becomes more evident. Regarding the relative gain, it was found that **MAC ABS e-ICIC** and **MACD ABS e-ICIC** obtained a mean gain of 28.16% and 34.88%, respectively.

5 CONCLUSION

This thesis presented solutions for the ABS allocation problem using trading know-how as a real-time strategy to dynamically define the ABS ratio and improve the performance of HetNet systems. By the way, they achieved the best performance in all layouts using a proper parameter setting. Furthermore, it is important to be highlighted that position and distance of small cells influence the gains provided by ABS. In addition, it is noted that the segregation of users into two groups harms the SINR of edge users. This way, ABS can be used to provide an adequate SINR level.

From now on, a discussion about the RQs that guided the development of this thesis is presented.

- **RQ 1:** What is the sensitivity of the system gain to the use of ABS in different layouts?

  - This thesis analyzed twelve layouts to validate some factors that influence the ABS gain. In order to be fair with results, it was necessary to use a reference algorithm, that is, **Fixed ABS e-ICIC**. This way, the analysis does not contain the gain provided by algorithms. In doing so, the ABS gain tends to increase in view of the interference levels from HetNets. This conclusion can be confirmed by the number of small cells or proximity between small cell and macro cell. Generally:

    * Number of small cells: ABS gain increased with number of small cells, because ABS can protect small cell edge users from macro cell transmitter. For example, at 726 m, the **Fixed ABS e-ICIC** provided gains of 14.87%, 17.13%, 18.62%, and 21.02% when the number of small cells increases;

    * Proximity between small cell and macro cell: proximity increases the interference level of the small cell users and the best macro users, that is, the majority of users are harmed. For this reason, ABS is used to protect small cell's edge users, promoting an improvement in system capacity. For example, **Fixed ABS e-ICIC** provided gains of 15.29%, 21.02%, 24.86% when proximity increases in layouts with four small cells.

  Therefore, the results obtained by the thesis confirm hypothesis related to **RQ 1** (Section 1.1).

- **RQ 2:** Is there any circumstance in which the use of ABS impairs the system capacity?

  - The results showed that ABS does not impair the capacity of the system, on the contrary, it improves the performance of HetNet. However, the way ABS is managed

can harm HetNet. This became evident using **Random ABS e-ICIC**, where gains of -8.35%, -5.10%, -4.07%, and -2.21% were obtained for Layouts 1 to 4. So, this conclusion confirms the hypothesis related to **RQ 2**, where some algorithms are not able to provide good results or even harm the system in layouts where the interference of the edge and center small cell users are similar. In this case, the opportunity to allocate ABS is not only rare but also extremely damaging if it is assigned inappropriately.

- **RQ 3:** Is it feasible to develop a real-time dynamic ABS Ratio algorithm using financial strategies?

    - Financial strategies can improve HetNet in the ABS e-ICIC problem because both **MAC ABS e-ICIC** and **MACD ABS e-ICIC** achieved good results in interference management. Basically, the algorithms replace users of the macro cell that have low capacity with users of the small cell that have a lower interference level. By the way, the satisfactory result is only possible through a precise and well-parameterized adaptation for wireless communication systems. Therefore, this conclusion confirms the hypothesis related to **RQ 3**, where the real-time financial strategies used to buy and sell stocks can be migrated to recognize good opportunities to allocate ABS, thus improving the system's capacity. However, feasibility depends on a precise merge of the financial know-how and the wireless communication system.

5.1 Perspectives

For future works, it is interesting to investigate how to automate the ABS ratio setting in order to avoid the parameter sweeping. Besides that, other research fronts can be performed in more realistic scenarios, adopting penetration loss in indoor environments or a real outdoor layout. In technological terms, the effect of Multiple-Input Multiple-Output (MIMO) with ABS using trading know-how is another possible approach.

BIBLIOGRAPHY

3GPP. *Physical Layer Aspects for Evolved Universal Terrestrial Radio Access (UTRA)*. [S.l.], 2006.

3GPP. *Further Advancements for E-UTRA Physical Layer Aspects*. [S.l.], 2009.

3GPP. *Evolved Universal Terrestrial Radio Access Network (E-UTRAN); X2 Application Protocol (X2AP)*. [S.l.], 2011. Disponível em: <http://www.3gpp.org/ftp/Specs/html-info/36423.htm>.

3GPP. *Coordinated Multi-Point Operation for LTE Physical Layer Aspects* . [S.l.], 2013.

3GPP. *Evolved Universal Terrestrial Radio Access (E-UTRA) and Evolved Universal Terrestrial Radio Access Network (E-UTRAN); Overall description; Stage 2*. [S.l.], 2013. Disponível em: <http://www.3gpp.org/ftp/Specs/html-info/36300.htm>.

3GPP. *FDD Repeater Radio Transmission and Reception*. [S.l.], 2018.

3GPP. *LTE; Evolved Universal Terrestrial Radio Access Network (E-UTRAN); X2 Application Protocol (X2AP) (3GPP TS 36.423 version 15.3.0 Release 15)*. [S.l.], 2018.

3GPP. *Radio Frequency (RF) System Scenarios*. [S.l.], 2018.

3GPP. *Radio Network Planning Aspects*. [S.l.], 2018.

3GPP. *Vocabulary for 3GPP Specifications*. [S.l.], 2018. Disponível em: <http://www.3gpp.org/ftp/Specs/html-info/21905.htm>.

ACTON, Q. **Issues in Global Environment—Biology and Geoscience: 2012 Edition**. ScholarlyEditions, 2013. ISBN 9781481647502. Disponível em: <https://books.google.com.br/books?id=8jiiV4BQQroC>.

ALEXANDROV, T. A Method Of Trend Extraction Using Singular Spectrum Analysis. **Statistical Journal**, v. 7, abr. 2009.

ALEXANDROV, T.; BIANCONCINI, S.; DAGUM, E. B.; MAASS, P.; MCELROY, T. **A Review of Some Modern Approaches to the Problem of Trend Extraction**. [S.l.], 2008.

ASIF, S. **5G Mobile Communications: Concepts and Technologies**. CRC Press, 2018. ISBN 9780429881343. Disponível em: <https://books.google.com.br/books?id=yg1mDwAAQBAJ>.

BAJRACHARYA, R.; SHRESTHA, R.; KIM, S. W. Q-Learning Based Fair and Efficient Coexistence of LTE in Unlicensed Band. **Sensors**, v. 19, n. 13, p. 2875, 2019.

BOURDENA, A.; PALLIS, E.; KORMENTZAS, G.; MASTORAKIS, G. Efficient radio resource management algorithms in opportunistic cognitive radio networks. **Transactions on Emerging Telecommunications Technologies**, v. 25, n. 8, p. 785–797, 2014. Disponível em: <https://onlinelibrary.wiley.com/doi/abs/10.1002/ett.2687>.

BOVIK, A. **The Essential Guide to Image Processing**. Elsevier Science, 2009. ISBN 9780080922515. Disponível em: <https://books.google.com.br/books?id=6TOUgytafmQC>.

BOX-STEFFENSMEIER, J. M.; FREEMAN, J. R.; HITT, M. P. **Time Series Analysis for the Social Sciences**. Cambridge University Press, 2015. ISBN 0521871166. Disponível em: <https://www.ebook.de/de/product/23186399/janet_m_box_steffensmeier_john_r_freeman_matthew_p_hitt_time_series_analysis_for_the_social_sciences.html>.

BULKOWSKI, T. N. **Trading Classic Chart Pattern**. [S.l.]: John Wiley & Sons, 2002.

CASPEELE, R.; TAERWE, L.; FRANGOPOL, D. **Life Cycle Analysis and Assessment in Civil Engineering: Towards an Integrated Vision: Proceedings of the Sixth International Symposium on Life-Cycle Civil Engineering (IALCCE 2018), 28-31 October 2018, Ghent, Belgium**. CRC Press, 2018. (Life-Cycle of Civil Engineering Systems). ISBN 9781351857574. Disponível em: <https://books.google.com.br/books?id=yMfADwAAQBAJ>.

CHATFIELD, C. **The Analysis of Time Series: Theory and Practice**. [S.l.]: Springer US, 1975.

CHATTERJEE, S.; ABDEL-RAHMAN, M. J.; MACKENZIE, A. B. Optimal distributed allocation of almost blank subframes for LTE/WiFi coexistence. In: **2017 15th International Symposium on Modeling and Optimization in Mobile, Ad Hoc, and Wireless Networks (WiOpt)**. [S.l.: s.n.], 2017. p. 1–6.

CHO, Y. S.; KIM, J.; YANG, W. Y. **MIMO-OFDM Wireless Communications with MATLAB**. [S.l.]: John Wiley & Sons, 2010.

CISCO. **Cisco Visual Networking Index: Forecast and Trends, 2017–2022**. [S.l.], 2019.

CLAUSSEN, H.; LOPEZ-PEREZ, D.; HO, L.; RAZAVI, R.; KUCERA, S. **Small Cell Networks: Deployment, Management, and Optimization**. [S.l.]: JOHN WILEY & SONS INC, 2016. ISBN 1118854349.

CLEVELAND, R. B.; CLEVELAND, W. S.; TERPENNING, I. STL: A Seasonal-Trend Decomposition Procedure Based on Loess. **Journal of Official Statistics**, v. 6, mar. 1990.

CRYER, K.-S. C. J. D. **Time series analysis with applications in r**. Springer-Verlag GmbH, 2009. ISBN 0387759581. Disponível em: <https://www.ebook.de/de/product/7043936/jonathan_d_cryer_kung_sik_chan_time_series_analysis_with_applications_in_r.html>.

CULLEN, C.; CANTOR, L. **The Mobile Internet Phenomena Report**. [S.l.], 2019.

DAEINABI, A.; SANDRASEGARAN, K.; BARUA, S. A dynamic almost blank subframe scheme for video streaming traffic model in heterogeneous networks. In: **2015 12th International Conference on Electrical Engineering/Electronics, Computer, Telecommunications and Information Technology (ECTI-CON)**. [S.l.: s.n.], 2015. p. 1–6.

DAHLMAN, E.; PARKVALL, S.; SKOLD, J. **4G: LTE/LTE-Advanced for Mobile Broadband**. Academic Press, 2013. ISBN 0124199976. Disponível em: <https://www.amazon.com/4G-LTE-LTE-Advanced-Mobile-Broadband-ebook/dp/B00G4N7K1Y?SubscriptionId=AKIAIOBINVZYXZQZ2U3A&tag=chimbori05-20&linkCode=xm2&camp=2025&creative=165953&creativeASIN=B00G4N7K1Y>.

DEB, S.; MONOGIOUDIS, P.; MIERNIK, J.; SEYMOUR, J. P. Algorithms for Enhanced Inter-Cell Interference Coordination (eICIC) in LTE HetNets. **IEEE/ACM Transactions on Networking**, v. 22, n. 1, p. 137–150, 2014.

DHILLON, H. S.; GANTI, R. K.; BACCELLI, F.; ANDREWS, J. G. Modeling and Analysis of K-Tier Downlink Heterogeneous Cellular Networks. **IEEE Journal on Selected Areas in Communications**, v. 30, n. 3, p. 550–560, April 2012. ISSN 1558-0008.

DONG, X.; FAN, W.; GU, J. Predicting LTE Throughput Using Traffic Time Series. **ZTE Communications**, v. 13, n. 4, p. 61–64, 2015. Disponível em: <https://res-www.zte.com.cn/mediares/magazine/publication/com_en/article/201504/446840/P020151222314374147525.pdf>.

DORIGO, M.; DORIGO, D. M.; STUTZLE, T.; STUTZLE, T. **Ant Colony Optimization**. BRADFORD BOOK, 2004. (A Bradford book). ISBN 9780262042192. Disponível em: <https://books.google.com.br/books?id=_aefcpY8GiEC>.

DöTTLING, M.; MOHR, W.; OSSEIRAN, A. **Radio Technologies and Concepts for IMT-Advanced**. John Wiley & Sons, 2009. ISBN 9780470748084. Disponível em: <https://www.ebook.de/de/product/15194951/radio_technologies_and_concepts_for_imt_advanced.html>.

DURANT, T.; SCHULZ, W.; EL-KHOURY, J. Moving averages: Real-time data monitoring in the clinical chemistry laboratory. **American Journal of Clinical Pathology**, Oxford University Press (OUP), v. 147, n. suppl_2, p. S163–S164, mar 2017.

GARTLEY, H. M. **Profits in the Stock Market/With Charts**. [S.l.]: Lambert Gann Publishing, 1935. ISBN 9780939093076.

GHOSH, A.; ZHANG, J.; ANDREWS, J.; MUHAMED, R. **Fundamentals of LTE**. Pearson Education, 2010. (Communications Engineering & Emerging Technology Series from Ted Rappaport). ISBN 9780137033898. Disponível em: <https://books.google.com.br/books?id=HjxmKq5MABcC>.

GHYSELS, M. M. E. **Applied Economic Forecasting using Time Series Methods**. Oxford University Press, 2018. Disponível em: <https://www.ebook.de/de/product/33604339/eric_ghysels_massimiliano_marcellino_applied_economic_forecasting_using_time_series_methods.html>.

GORSHE, S.; RAGHAVAN, A.; STARR, T.; GALLI, S. **Broadband Access: Wireline and Wireless - Alternatives for Internet Services**. Wiley, 2014. (No Longer used). ISBN 9781118878798. Disponível em: <https://books.google.com.br/books?id=XzsKAwAAQBAJ>.

GRIMES, A. **The Art and Science of Technical Analysis: Market Structure, Price Action, and Trading Strategies**. Wiley, 2012. (Wiley Trading). ISBN 9781118115121. Disponível em: <https://books.google.com.br/books?id=MtE565quU_gC>.

HODGES, G. J.; MALLETTE, M. M.; CHEUNG, S. S. Cutaneous neural activity and endothelial involvement in cold-induced vasodilatation. **European Journal of Applied Physiology**, Springer Science and Business Media LLC, v. 118, n. 5, p. 971–978, mar 2018.

HOLMA, H.; TOSKALA, A. **LTE-Advanced: 3GPP Solution for IMT-Advanced**. John Wiley & Sons, 2012. ISBN 1119974054. Disponível em: <https://www.ebook.de/de/product/18118427/lte_advanced.html>.

HOSSAIN, E.; RASTI, M.; LE, L. B. Cell Association in Cellular Networks. In: ____.
Radio Resource Management in Wireless Networks: An Engineering Approach. [S.l.]:
Cambridge University Press, 2017. p. 276–288.

HOSSAIN, M. R.; REAL, A. Z. M. A. H.; RAHMAN, A. Handover management in
heterogeneous network. In: **2015 18th International Conference on Computer and
Information Technology (ICCIT)**. [S.l.: s.n.], 2015. p. 87–92.

HU, Y. Q. R. Q. **Heterogeneous Cellular Networks**. John Wiley & Sons, 2013. ISBN
111999912X. Disponível em: <https://www.ebook.de/de/product/20056422/heterogeneous_
cellular_networks.html>.

HUANG, J.; LI, J.; CHEN, Z.; PAN, H. HICIC: Hybrid Inter-Cell Interference Coordination
for Two-Tier Heterogeneous Networks With Non-Uniform Topologies. **IEEE Access**,
Institute of Electrical and Electronics Engineers (IEEE), v. 6, p. 34707–34723, 2018.
Doi:10.1109/access.2018.2841194.

HUQ, K.; RODRIGUEZ, J. **Backhauling / Fronthauling for Future Wireless Systems**.
Wiley, 2016. ISBN 9781119170341. Disponível em: <https://books.google.com.br/books?id=
p8E0DQAAQBAJ>.

HYNDMAN, R.; ATHANASOPOULOS, G. **Forecasting: principles and practice**. [S.l.]:
OTexts, 2018.

JIANG, L.; CHE, H.; SUN, W.; LIU, J. Resource Allocation Method for Inter-Cell Interference
Coordination in Heterogeneous Networks with Almost Blank Subframe. In: **2019 5th
International Conference on Transportation Information and Safety (ICTIS)**. [S.l.: s.n.],
2019. p. 875–879.

JUNGNICKEL, D. **Graphs, Networks and Algorithms**. Springer Berlin Heidelberg, 2007.
(Algorithms and Computation in Mathematics). ISBN 9783540727804. Disponível em:
<https://books.google.com.br/books?id=NvuFAglxaJkC>.

KALMAN, R. E. A New Approach to Linear Filtering and Prediction Problems. **Transactions
of the ASME–Journal of Basic Engineering**, v. 32, p. 34–45, 1960.

KHAN, F. **LTE for 4G Mobile Broadband**. Cambridge University Press, 2009. ISBN
0521882214. Disponível em: <https://www.ebook.de/de/product/8217206/farooq_khan_lte_for_
4g_mobile_broadband.html>.

KOEHLER, A.; ORD, K.; SNYDER, R.; HYNDMAN, R. **Forecasting with Exponential
Smoothing**. Springer-Verlag GmbH, 2008. Disponível em: <https://www.ebook.de/de/
product/8897174/anne_koehler_keith_ord_ralph_snyder_rob_hyndman_forecasting_with_
exponential_smoothing.html>.

KOLKOVA, A. Indicators of Technical Analysis on the Basis of Moving Averages as Prognostic
Methods in the Food Industry. **Journal of Competitiveness**, Tomas Bata University in Zlin,
v. 10, n. 4, p. 102–119, dec 2018.

KOPPL, R. **Big Players and the Economic Theory of Expectations**. [S.l.]: Palgrave
Macmillan UK, 2002. ISBN 9780230629240.

LEE, N.; LIN, X.; ANDREWS, J. G.; HEATH, R. W. Power Control for D2D Underlaid Cellular Networks: Modeling, Algorithms, and Analysis. **IEEE Journal on Selected Areas in Communications**, v. 33, n. 1, p. 1–13, 2015.

LEE, Y. L.; TAN, W. L.; LAU, S. B. Y.; CHUAH, T. C.; EL-SALEH, A. A.; QIN, D. Joint Cell Activation and User Association for Backhaul Load Balancing in Green HetNets. **IEEE Wireless Communications Letters**, p. 1–1, 2020.

LESCUYER, P. **Evolved Packet System (EPS)**. Wiley-Blackwell, 2008. ISBN 0470059761. Disponível em: <https://www.ebook.de/de/product/6857115/pierre_lescuyer_evolved_packet_system_eps.html>.

LI, L.; ZHOU, Z.; HU, Y.; JIANG, T.; WEI, M. Pricing framework for almost blank subframe scheme in two-tier heterogeneous networks. **International Journal of Communication Systems**, v. 31, n. 3, p. e3454, 2018. E3454 dac.3454. Disponível em: <https://onlinelibrary.wiley.com/doi/abs/10.1002/dac.3454>.

LI, Q.; XIA, H.; ZENG, Z.; ZHANG, T. Dynamic enhanced inter-cell interference coordination using reinforcement learning approach in heterogeneous network. In: **2013 15th IEEE International Conference on Communication Technology**. [S.l.: s.n.], 2013. p. 239–243.

LIANG, Q.; MU, J.; JIA, M.; WANG, W.; FENG, X.; ZHANG, B. **Communications, Signal Processing, and Systems: Proceedings of the 2017 International Conference on Communications, Signal Processing, and Systems**. Springer Singapore, 2018. (Lecture Notes in Electrical Engineering). ISBN 9789811065712. Disponível em: <https://books.google.com.br/books?id=OfZeDwAAQBAJ>.

LOPES-DIAS, C.; SBURLEA, A. I.; MüLLER-PUTZ, G. R. Online asynchronous decoding of error-related potentials during the continuous control of a robot. **Scientific Reports**, Springer Science and Business Media LLC, v. 9, n. 1, nov 2019.

LUO, F. **Machine Learning for Future Wireless Communications**. Wiley, 2020. (Wiley - IEEE). ISBN 9781119562252. Disponível em: <https://books.google.com.br/books?id=GFTGDwAAQBAJ>.

LV, L.; CHEN, M.; LIU, Y.; YU, X. A plane moving average algorithm for short-term traffic flow prediction. In: **Advances in Knowledge Discovery and Data Mining**. [S.l.]: Springer International Publishing, 2015. p. 357–369.

MAGLOGIANNIS, V.; NAUDTS, D.; SHAHID, A.; MOERMAN, I. A Q-Learning Scheme for Fair Coexistence between LTE and Wi-Fi in Unlicensed Spectrum. **IEEE Access**, IEEE, v. 6, p. 27278–27293, 2018. ISSN 21693536.

MAKRIDAKIS, S. G.; WHEELWRIGHT, S. C. **Forecasting: Methods and Applications**. [S.l.]: Wiley, 1997.

MELO, Y. V. L. de; BATISTA, R. L.; SILVA, C. F. M. e; MACIEL, T. F.; SILVA, J. M. B. da; CAVALCANTI, F. R. P. Uplink Power Control with Variable Target SINR for D2D Communications Underlying Cellular Networks. In: **2015 IEEE 81st Vehicular Technology Conference (VTC Spring)**. [S.l.: s.n.], 2015. p. 1–5.

MISHRA, S.; RANGINENI, S.; MURTHY, C. S. R. Exploiting an optimal user association strategy for interference management in hetnets. **IEEE Communications Letters**, v. 18, n. 10, p. 1799–1802, 2014.

MOREIRA, J.; SILVA, E. da; GUARDIERO, P. eICIC Optimization Improvements in Downlink Resource Allocation in LTE-A HetNets. **Journal of Communication and Information Systems**, v. 35, n. 1, p. 15–24, Jan. 2020. Disponível em: <https://jcis.sbrt.org.br/jcis/article/view/680>.

MUHAMMAD, B.; MOHAMMED, A. Uplink closed loop power control for LTE system. In: **2010 6th International Conference on Emerging Technologies (ICET)**. [S.l.: s.n.], 2010. p. 88–93.

NIELSEN, A. **Practical Time Series Analysis**. O'Reilly UK Ltd., 2019. ISBN 1492041653. Disponível em: <https://www.ebook.de/de/product/34950876/aileen_nielsen_practical_time_series_analysis.html>.

OMHENI, N.; GHARSALLAH, A.; ZARAI, F.; OBAIDAT, M. S. Call admission control and adaptive bandwidth management approach for HWNs. In: **2014 IEEE Global Communications Conference**. [S.l.: s.n.], 2014. p. 112–117.

RUMNEY, M. **LTE and the Evolution to 4G Wireless**. John Wiley & Sons, 2013. Disponível em: <https://www.ebook.de/de/product/21165166/lte_and_the_evolution_to_4g_wireless.html>.

SAALASTI, S. **Neural Networks for Heart Rate Time Series Analysis**. Dissertação (Mestrado) — University of Jyvaskyla, 2003.

SADIQ, B.; MADAN, R.; SAMPATH, A. Downlink Scheduling for Multiclass Traffic in LTE. **EURASIP Journal on Wireless Communications and Networking**, 2009.

SANTANA, P. M. de; JR., V. A. de S.; ABINADER, F. M.; NETO, J. M. de C. DM-CSAT: a LTE-U/Wi-Fi coexistence solution based on reinforcement learning. **Telecommunication Systems**, 2019.

SARAYDAR, C. U.; MANDAYAM, N. B.; GOODMAN, D. J. Efficient power control via pricing in wireless data networks. **IEEE Transactions on Communications**, v. 50, n. 2, p. 291–303, 2002.

SAUTER, M. **From GSM to LTE-Advanced Pro and 5G**. John Wiley and Sons Ltd, 2017. ISBN 111934686X. Disponível em: <https://www.ebook.de/de/product/29865944/martin_sauter_from_gsm_to_lte_advanced_pro_and_5g.html>.

SHIN, Y. **Time Series Analysis in the Social Sciences**. University of California Press, 2017. Disponível em: <https://www.ebook.de/de/product/28021111/youseop_shin_time_series_analysis_in_the_social_sciences.html>.

SIMSEK, M.; BENNIS, M.; CZYLWIK, A. Dynamic inter-cell interference coordination in hetnets: A reinforcement learning approach. In: **2012 IEEE Global Communications Conference (GLOBECOM)**. [S.l.: s.n.], 2012. p. 5446–5450. Doi:10.1109/GLOCOM.2012.6503987.

SOON, Y. C. **News which Moves the Market: Assessing the Impact of Published Financial News on the Stock Market**. Tese (Doutorado) — Singapore Management University, 2010.

TURNER, T. **Short-Term Trading in the New Stock Market**. St. Martin's Publishing Group, 2006. ISBN 9781429969123. Disponível em: <https://books.google.com.br/books?id=zLfxpidUSnIC>.

WANG, J.; KIM, J. Predicting stock price trend using macd optimized by historical volatility. **Mathematical Problems in Engineering**, p. 12, dez. 2018.

WANG, Y.-C.; HUANG, B.-J. Efficient coordination of almost blank subframes with coupling macro cells in heterogeneous networks. **International Journal of Communication Systems**, v. 33, 2019.

WICKLIN, R. **Using finite differences to estimate the maximum of a time series**. 2013. Disponível em: <https://blogs.sas.com/content/iml/2013/08/28/finite-diff-estimate-maxi.html>.

XIAO, D.; YU, X.; YANG, D. A Novel Downlink ICIC Method Based on User Position in LTE-Advanced Systems. In: **2012 IEEE Vehicular Technology Conference (VTC Fall)**. [S.l.: s.n.], 2012. p. 1–5. ISSN 1090-3038.

YAFFEE, R.; MCGEE, M. **An Introduction to Time Series Analysis and Forecasting: With Applications of SAS and SPSS**. [S.l.]: Academic Press, 2000. ISBN 9780127678702.

YANG, G.; XIAO, M.; ALAM, M.; HUANG, Y. Low-latency heterogeneous networks with millimeter-wave communications. **IEEE Communications Magazine**, v. 56, n. 6, p. 124–129, 2018.

YANG, Y.; LUO, X.; CHU, X.; ZHOU, M. **Fog-Enabled Intelligent IoT Systems**. Springer International Publishing, 2019. ISBN 9783030231859. Disponível em: <https://books.google.com.br/books?id=dCK3DwAAQBAJ>.

YEH, S.; TALWAR, S.; WU, G.; HIMAYAT, N.; JOHNSSON, K. Capacity and coverage enhancement in heterogeneous networks. **IEEE Wireless Communications**, v. 18, n. 3, p. 32–38, June 2011. ISSN 1558-0687.

YIN, R.; YU, G.; ZHANG, H.; ZHANG, Z.; LI, G. Y. Pricing-Based Interference Coordination for D2D Communications in Cellular Networks. **IEEE Transactions on Wireless Communications**, v. 14, n. 3, p. 1519–1532, 2015.

ZAKAMULIN, V. **Market Timing with Moving Averages: The Anatomy and Performance of Trading Rules**. [S.l.]: Springer International Publishing, 2017. Doi:10.1007/978-3-319-60970-6.

APPENDIX A –   FRAMEWORK TO DETECT PIVOT POINTS

The peaks and valleys of prices that arise in the dynamics of the financial market are called pivot points. It can be used to find a pullback; for this purpose, it is necessary to classify them as pivot high and pivot low (GRIMES, 2012). A pivot high is a price that is higher than the price that came before it and the price that comes after it. On the other hand, a pivot low is the same concept inverted, that is, a price that is lower than the price that came before it and the price that comes after it. It is worth mentioning that the pivot points mentioned above are called first-order pivots; however, there are also second-order pivots (GRIMES, 2012).

The second-order pivot highs are first-order pivot highs that are preceded and followed by lower first-order pivot highs; again, this structure is inverted for second-order pivot lows. It is interesting to use second-order pivot because it provides more significant structural points, that is, important turning points (GRIMES, 2012).

In order to find the pivot highs, a sequence called DIF-SIGN-DIF was used in Algorithm 3, which is a sequence that works for most time series that arise in practice (WICKLIN, 2013).

Initially, Algorithm 3 requires the time series to be loaded. Then, the finite differences of the time series are performed, and the result is assigned to **dif** vector, which approximates the derivative of a function. The next step is to produce the **sign** vector from the values of the **dif** vector, that is, the values +1, 0, -1 are assigned for a set of positive, zero, or negative slopes, respectively. The penultimate step is to compute the finite differences of **sign** vector and store the result in the **difsign** vector. Finally, the last step is to find the pivot highs, which is always followed by a –2 in the **difsign** vector.

Algorithm 3: Pivot points detector.

Require: Load time series $Y(t), t \in \{1, \ldots, T\}$

  for $t \leftarrow 2$ **to** T **do**
    $\text{dif}(t) \leftarrow Y(t) - Y(t-1)$
  end for
  for $t \leftarrow 2$ **to** T **do**
    if $\text{dif}(t) > 0$ **then**
      $\text{sign}(t) \leftarrow 1$
    else if $\text{dif}(t) < 0$ **then**
      $\text{sign}(t) \leftarrow -1$
    else
      $\text{sign}(t) \leftarrow 0$
    end if
  end for
  for $t \leftarrow 3$ **to** T **do**
    $\text{difsign}(t) \leftarrow \text{sign}(t) - \text{sign}(t-1)$
  end for
  for $t \leftarrow 3$ **to** T **do**
    if $\text{difsign}(t) = -2$ **then**
      $\text{pivot}(t-1) \leftarrow Y(t-1)$
    end if
  end for

APPENDIX B – FRAMEWORK TO DETECT PULLBACK

Algorithms were developed to detect pullback in uptrend and downtrend. It is worth mentioning that the frameworks are based on the explanation in Section 2.5.3. Algorithm 4 was created to detect pullback in the uptrend. Initially, the time series $Y(t)$ is loaded, then Algorithm 3 acts to provides first-order and second-order pivots. It is worth highlighting that the pivot lows are found by inverting the time series. After finding all the pivot points, the next step is to enter control variables such as **FlagPointC**, **FlagPointD**, and **CountPullback**. The algorithm defines the first value of the series as **Point A**. The next step is to define **Point B**; for this, it is verified if the second-order pivot high is located on the right and higher than **Point A**. If there is no second-order pivot high that meets these conditions, a first-order pivot high will be searched. In the latter case, the algorithm modifies **Point A**, if there is not yet a pivot point that satisfies the conditions. In contrast, if **Point B** is found, the algorithm defines the **FlagPointC** variable as true, allowing to search for **Point C**.

The following step is to define **Point C**, which must be a second-order or first-order pivot low. It must be situated on the right of **Point B**, and between **Points A** and **B**. It is worth mentioning that between **Points B** and **C**, it should be ensured that the values are lower than **Point B** and higher than **Point C**. If the pivot point is not found, the algorithm modifies **Points A** and **B**. In contrast if **Point C** is found, the algorithm defines the **FlagPointD** variable as true, enabling the search for **Point D**.

The penultimate is to find **Point D**, which must be located on the right of **Point C** and higher than **Point B**. If there is no second-order or first-order pivot high that satisfies the conditions, the algorithm changes **Points A**, **B**, and **C**.

The last step is to check if all points were found using variables **FlagPointC** and **FlagPointD**. If they are true, one will be added to the counter and false will be assigned to **FlagPointC** and **FlagPointD**.

Algorithm 4: Pullback detector to uptrend.

Require: Load time series $Y(t), t \in \{1, \ldots, T\}$
To obtain PivotHighFirst(t) running Algorithm 3 with input $Y(t)$
To obtain PivotLowFirst(t) running Algorithm 3 with input $-1 * Y(t)$
To obtain PivotHighSecond(t) running Algorithm 3 with input PivotHighFirst(t)
To obtain PivotLowSecond(t) running Algorithm 3 with input $-1 * $PivotLowFirst$(t)$
FlagPointC $\leftarrow$ False
FlagPointD $\leftarrow$ False
CountPullback $\leftarrow$ 0
for $t \leftarrow 1$ **to** T **do**
    if $t \leq T$ **then**
        PointAIndex $\leftarrow t$
        PointAValue $\leftarrow Y(t)$
    else
        print "Limit data"
    end if
    if $(t >$ PointAIndex$) \wedge ($PivotHighSecond$(t) >$ PointAValue$)$ **then**
        PointBIndex $\leftarrow t$
        PointBValue $\leftarrow Y(t)$
        FlagPointC $\leftarrow$ True
        print "Point B is a pivot of Second Order"
    else if $(t >$ PointAIndex$) \wedge ($PivotHighFist$(t) >$ PointAValue$)$ **then**
        PointBIndex $\leftarrow t$
        PointBValue $\leftarrow Y(t)$
        FlagPointC $\leftarrow$ True
        print "Point B is a pivot of First Order"
    else
        FlagPointC $\leftarrow$ False
        print "No Point B"
    end if
    if FlagPointC $\wedge (t >$ PointBIndex$) \wedge ($PivotLowSecond$(t) >$ PointAValue$) \wedge ($PivotLowSecond$(t) <$ PointBValue$)$ **then**
        PointCIndex $\leftarrow t$
        PointCValue $\leftarrow Y(t)$
        FlagPointD $\leftarrow$ True
        print "Point C is a pivot of Second Order"
    else if FlagPointC $\wedge (t >$ PointBIndex$) \wedge ($PivotLowFirst$(t) >$ PointAValue$) \wedge ($PivotLowFirst$(t) <$ PointBValue$)$ **then**
        PointBIndex $\leftarrow t$
        PointBValue $\leftarrow Y(t)$
        FlagPointD $\leftarrow$ True
        print "Point C is a pivot of First Order"
    else
        FlagPointD $\leftarrow$ False
        print "No Point C"
    end if
    if FlagPointD $\wedge (t >$ PointCIndex$) \wedge ($PivotHighSecond$(t) >$ PointBValue$)$ **then**
        PointDIndex $\leftarrow t$
        PointDValue $\leftarrow Y(t)$
        print "Point D is a pivot of Second Order"
    else if FlagPointD $\wedge (t >$ PointCIndex$) \wedge ($PivotHighFirst$(t) >$ PointBValue$)$ **then**
        PointDIndex $\leftarrow t$
        PointDValue $\leftarrow Y(t)$
        print "Point D is a pivot of First Order"
    else
        FlagPointC $\leftarrow$ False
        FlagPointD $\leftarrow$ False
        print "No Point D"
    end if
    if FlagPointC $\wedge$ FlagPointD **then**
        CountPullback $\leftarrow$ CountPullback $+ 1$
        FlagPointC $\leftarrow$ False
        FlagPointD $\leftarrow$ False
        print "Pullback"
    end if
end for

Algorithm 5 was created to detect pullback in the downtrend. Initially, the time series $Y(t)$ is loaded, then Algorithm 3 acts to provide first-order and second-order pivots. The pivot lows are found by inverting the time series.

After finding all the pivot points, the next step is to enter control variables such as **FlagPointC**, **FlagPointD**, and **CountPullback**. The algorithm defines the first value of the series as **Point A**. The next step is to define **Point B**; for this, it is verified if the second-order pivot low is located on the right and lower than **Point A**. If there is no second-order pivot low that meets these conditions, a first-order pivot low will be searched. In the latter case, the algorithm modifies **Point A**, if there is not yet a pivot point that satisfies the conditions. In contrast, if **Point B** is found, the algorithm defines the **FlagPointC** variable as true, allowing to search for **Point C**.

The following step is to define **Point C**, which must be a second-order or first-order pivot high. It must be situated on the right of **Point B**, and between **Points A** and **B**. It is worth mentioning that between **Points B** and **C**, it should be ensured that the values are higher than **Point B** and lower than **Point C**. If the pivot point is not found, the algorithm modifies **Points A** and **B**. In contrast if **Point C** is found, the algorithm defines the **FlagPointD** variable as true, enabling the search for **Point D**.

The penultimate is to find **Point D**, which must be located on the right of **Point C** and lower than **Point B**. If there is no second-order or first-order pivot low that satisfies the conditions, the algorithm changes **Points A**, **B**, and **C**.

The last step is to check if all points were found using variables **FlagPointC** and **FlagPointD**. If they are true, one will be added to the counter and false will be assigned to **FlagPointC** and **FlagPointD**.

Algorithm 5: Pullback detector to downtrend.

Require: Load time series $Y(t)$, $t \in \{1, \ldots, T\}$
To obtain PivotHighFirst(t) running Algorithm 3 with input $Y(t)$
To obtain PivotLowFirst(t) running Algorithm 3 with input $-1 * Y(t)$
To obtain PivotHighSecond(t) running Algorithm 3 with input PivotHighFirst(t)
To obtain PivotLowSecond(t) running Algorithm 3 with input $-1 *$ PivotLowFirst(t)
FlagPointC $\leftarrow$ False
FlagPointD $\leftarrow$ False
CountPullback $\leftarrow$ 0
for $t \leftarrow 1$ **to** T **do**
    if $t \leq T$ **then**
        PointAIndex $\leftarrow t$
        PointAValue $\leftarrow Y(t)$
    else
        print "Limit data"
    end if
    if $(t > \text{PointAIndex}) \wedge (\text{PivotLowSecond(t)} < \text{PointAValue})$ **then**
        PointBIndex $\leftarrow t$
        PointBValue $\leftarrow Y(t)$
        FlagPointC $\leftarrow$ True
        print "Point B is a pivot of Second Order"
    else if $(t > \text{PointAIndex}) \wedge (\text{PivotLowFist(t)} < \text{PointAValue})$ **then**
        PointBIndex $\leftarrow t$
        PointBValue $\leftarrow Y(t)$
        FlagPointC $\leftarrow$ True
        print "Point B is a pivot of First Order"
    else
        FlagPointC $\leftarrow$ False
        print "No Point B"
    end if
    if FlagPointC $\wedge (t > \text{PointBIndex}) \wedge (\text{PivotHighSecond(t)} < \text{PointAValue}) \wedge (\text{PivotHighSecond(t)} > \text{PointBValue})$ **then**
        PointCIndex $\leftarrow t$
        PointCValue $\leftarrow Y(t)$
        FlagPointD $\leftarrow$ True
        print "Point C is a pivot of Second Order"
    else if FlagPointC $\wedge (t > \text{PointBIndex}) \wedge (\text{PivotHighFirst(t)} < \text{PointAValue}) \wedge (\text{PivotHighFirst(t)} > \text{PointBValue})$ **then**
        PointBIndex $\leftarrow t$
        PointBValue $\leftarrow Y(t)$
        FlagPointD $\leftarrow$ True
        print "Point C is a pivot of First Order"
    else
        FlagPointD $\leftarrow$ False
        print "No Point C"
    end if
    if FlagPointD $\wedge (t > \text{PointCIndex}) \wedge (\text{PivotLowSecond(t)} < \text{PointBValue})$ **then**
        PointDIndex $\leftarrow t$
        PointDValue $\leftarrow Y(t)$
        print "Point D is a pivot of Second Order"
    else if FlagPointD $\wedge (t > \text{PointCIndex}) \wedge (\text{PivotLowFirst(t)} < \text{PointBValue})$ **then**
        PointDIndex $\leftarrow t$
        PointDValue $\leftarrow Y(t)$
        print "Point D is a pivot of First Order"
    else
        FlagPointC $\leftarrow$ False
        FlagPointD $\leftarrow$ False
        print "No Point D"
    end if
    if FlagPointC $\wedge$ FlagPointD **then**
        CountPullback $\leftarrow$ CountPullback $+ 1$
        FlagPointC $\leftarrow$ False
        FlagPointD $\leftarrow$ False
        print "Pullback"
    end if
end for